SIMULATING SURFACE WATER–GROUNDWATER INTERACTION IN THE BERTRAND CREEK WATERSHED, B.C.

by

Cynthia Ann Starzyk

B.A.Sc., The University of British Columbia, 2000

A THESIS SUBMITTED IN PARTIAL FULFILLMENT OF

THE REQUIREMENTS FOR THE DEGREE OF

DOCTOR OF PHILOSOPHY

in

THE FACULTY OF GRADUATE STUDIES

(Geological Engineering)

THE UNIVERSITY OF BRITISH COLUMBIA

(Vancouver)

June 2012

Abstract

This research investigates the nature and controls of surface water–groundwater interaction at the watershed scale, and investigates how mechanisms which control this interaction during baseflow conditions might best be represented within an integrated surface-subsurface numerical model. The study site is the 46 km^2 Bertrand Creek Watershed, which is situated in a glaciated landscape in southern western British Columbia.

A conceptual model of surface water–groundwater interaction along Bertrand Creek is developed based on a field data collection program conducted during the dry seasons of 2006 and 2007. The investigation relies on a suite of field techniques to characterize the nature of the interaction, including hydrologic measurements, stream water chemistry, and point-based measurements of streambed flux. These measurements are complemented by an assessment of topographic slope over the alluvial aquifer to infer the groundwater flow direction. Results indicate that topography adjacent to the stream is a principal control on water exchange between Bertrand Creek and the underlying aquifer. Topography influences the direction of groundwater flow adjacent to the stream and determines the persistence and magnitude of groundwater discharge along the channel.

The conceptual model is used to develop an integrated numerical model of Bertrand Creek Watershed using HydroGeoSphere. HydroGeoSphere is a three-dimensional physics-based model that simulates overland flow, unsaturated flow, and groundwater flow in a fully integrated manner. The watershed model is calibrated using field data collected in 2007, including measured streamflows, groundwater contributions to streamflow, hydraulic heads,

soil moisture contents, and change in surface water height in a pond. The calibrated watershed model is then evaluated against, and suitably represents, hydrologic data collected in 2006. Simulating baseflows and the seasonal hydrologic response requires that features controlling the spatial distribution of recharge, such as surficial soils and topography, are adequately characterized and represented within the model. Model results further demonstrate that evapotranspiration, particularly transpiration within the riparian zone, is a significant control of baseflows in Bertrand Creek. Finally, the calibrated model is used as a predictive tool to assess the impact of groundwater withdrawals on streamflow depletion.

Table of Contents

List of Tables

List of Figures

List of Symbols and Abbreviations

ET_{act} – actual evapotranspiration

ET_o – reference evapotranspiration

ET_p – potential evapotranspiration

GLF – glaciofluvial (deposit of the unconfined Abbotsford aquifer)

K_h – horizontal hydraulic conductivity

K_{sat} – saturated hydraulic conductivity

LAI – leaf area index

masl – metres above sea level

OP – outwash plain (deposit of the unconfined Abbotsford aquifer)

SHOP – South of Hopington (aquifer)

TOL – Township of Langley

USGS – U.S. Geological Survey

WALD – West of Aldergrove (aquifer)

WSC – Water Survey of Canada

Acknowledgements

I would like to extend my deepest gratitude to the people that have supported me through this work. First and foremost, a huge thank-you to Dr. Leslie Smith for serving as my supervisor, providing me with guidance (and much needed bits of humour!), and ultimately helping me see this project through to completion – it has truly been an honour. I would also like to extend a most sincere thank-you to my committee members Dr. Roger Beckie and Dr. Mark Johnson for their guidance, support, and critiques, and to past committee member, Dr. Markus Weiler, who was an instrumental resource during the field program. I am also grateful to Dr. Uli Mayer, Dr. Diana Allen, and Dr. Dan Moore for maintaining an open door for questions. I would also like to thank Rob McLaren for the HydroGeoSphere and Grid Builder codes, the prompt assistance with questions and requests, and the technical support during a visit to Waterloo.

Research was funded by scholarships awarded to myself from the Natural Sciences and Engineering Research Council (NSERC) and a UBC University Graduate Fellowship. Funding was also provided by an NSERC grant to L. Smith. Thank-you to the kind donors of the McPhail Memorial Bursary of Birdtail River School Division, the UBC Lorntzsen and MacKay Scholarship, UBC George E. Winkler Memorial Scholarship, and the CWRA Dillon Engineering Scholarship, which I was awarded during several years of my studies.

A large thank-you to all of the residents surrounding Bertrand Creek that allowed me access to their property and groundwater well, and made me feel welcome in their neighbourhood and creek. Particular mention to Beverley, Ravi Cheema, and the Lechner, Knott, Paar,

Kratzenberg, Dyck, Esdale, and Schofield residences, whom could find me at least weekly on their property dressed in hip waders. Thanks also to the Township of Langley and City of Abbotsford for providing data used in this analysis. Also, a thank-you to Joern Unger for help machining field equipment, and to Pamela Hinshaw and Richard So for assistance in the field.

I am gratefully endeavored to an amazing support team in my life, almost all of whom have made a trip out to 'the creek' to assist me in collecting data or installing equipment. A very special thank-you to Cathy Safadi, Jordin Barclay, and Morgan Garett for help in the field and for our water talks and beloved planning sessions. I am indebted with gratitude to Holly Peterson, Heather Narynski, and Colette Wabnitz for editing draft sections of this manuscript and providing me with moral support to believe an end was near. Thanks also to other past and present members of the hydro group, with particular mention to Tom Gleeson, Rich Amos, Trevor Hirsche, Matthew Neuner, Jessica Doyle, Natasha Sihota, Yaming Chen, Mario Bianchin, Cassandra Koenig, Sergi Molins, and Jason McAllister. Thanks also go to friends and colleagues Ryan Donohoe, Alexi Zawadzki, Adrianne Gilbride, Mark Baumann, Bev Soriano, and Kim and Kent Devlin for their time spent in hip waders in the creek. Thanks also go to Kim Devlin for help drafting figures 3.1 and 3.14. Finally, thanks to Angela Blanchard for help compiling references and for relocating me to a beautiful destination to write the introduction and conclusions.

To my family, thank-you for the love, patience, and support in helping me to achieve my goal.

Dedication

For Mervin and Cathy Starzyk

and Baba

Chapter 1: Introduction

"The creek this summer is the lowest I've ever seen. There used to be lots of very cold water even in the summer."

-Resident, Bertrand Creek Watershed, 2006

1.1 Motivation and Context

The connection between a stream and underlying aquifer determines the extent of water exchanged between the two domains and understanding the nature of this connection is fundamental when assessing management strategies. Although the need for integrated management of streams and aquifers is widely recognized (Sophocleous, 2002; Council of Canadian Academies, 2009), the methodology and tools currently in use to assess and predict the dynamics of surface water–groundwater interactions are not well suited either for watershed-scale investigations or in addressing groundwater and surface water as a single resource. In this thesis, I present a framework for assessing the exchange of water between a stream and aquifer at the scale of a moderate-size watershed (i.e., 46 km^2) during baseflow conditions, and investigate how to represent the interaction and key controlling processes using an integrated numerical model.

Groundwater comprises a significant component of the dry season water balance of many streams and provides an essential source of water for the maintenance of stream ecosystems (Standford and Ward, 1993; Brunke and Gonser, 1997). The flow of water between a stream and an underlying unconfined aquifer is dynamic and develops based on the variable

influences of topography, geology, climate, and vegetation (Winter, 1999; Sophocleous, 2002). Streams exchange water with subsurface aquifers across a wide range of spatial and temporal patterns that vary seasonally with water table fluctuations or within hours in response to rainfall events (e.g., Freeze, 1972; Winter et al., 1998; Wroblicky et al., 1998). Characterizing the nature of surface water and groundwater exchange at the scale of a watershed is a comprehensive endeavour, but a necessary first step for developing a hydrologic numerical model.

Considering the interconnected and dynamic nature of streams and aquifers, traditional groundwater models are not well suited for simulating the exchange of water across the surface-subsurface boundary. For example, the widely used groundwater flow model MODFLOW (Harbaugh et al., 2000) requires that flux across the water table and stream water height are defined a-priori, and then handles flux between the surface and subsurface domain as a boundary condition with limited feedback between the two domains. Recently however, there has been significant progress in the development of physics-based numerical models capable of simulating the continuous flow of water between the surface and subsurface domains. A selection of these integrated numerical models, which approximate the three-dimensional movement of water between the saturated, unsaturated, and surface water zones, include: InHm (VanderKwaak, 1999), MODHMS (Panday and Huyakorn, 2004), ParFlow (Kollet and Maxwell, 2006), and HydroGeoSphere (Therrien et al., 2010). By simulating feedback, or exchange of water, between the surface and subsurface domains under the influence of a heterogeneous landscape and variable climate, integrated hydrologic

models may provide a more realistic representation of the interactions between a stream and aquifer than the traditional modelling approach.

Initial applications of integrated surface-subsurface models have primarily been in studies assessing the controls of rainfall-runoff generation in hillslope or small catchment environments (e.g., VanderKwaak and Loague, 2001; Loague et al., 2005; Ebel et al., 2007; James et al., 2010; Mirus et al., 2011). These studies illustrate the importance of a detailed data set for evaluating model performance and assigning parameter values (see discussion by Mirus et al., 2011). They also highlight the sensitivity of simulated hydrologic processes to the spatial resolution of subsurface properties.

The application of integrated surface-subsurface models to evaluate the flow of water at the scale of a watershed is still in its infancy. A few studies have demonstrated the suitability of these models for simulating watershed-scale runoff and water balance (Jones et al., 2008; Li et al., 2008), as well as contaminant transport (Sudicky et al., 2008). However, these studies were limited in their evaluations of hydrologic processes or controls on streamflow generation. Moreover, the performance of these transient models was only evaluated against streamflows and did not include data from the subsurface domain. More recently, Goderniaux et al., (2009) evaluated the performance of a regional-scale (465 km^2) HydroGeoSphere model against hydraulic heads in addition to streamflows. In addition to a more detailed evaluation of model performance, this study also demonstrated the sensitivity of parameters to modelled spatial and temporal resolution. All of these previous studies provide fundamental information on model parameterization, grid resolution, and simulation

run times, which are considered to be among the greatest challenges associated with using physics-based models.

At present, only a few real-world surface water–groundwater studies using integrated hydrologic models explicitly include evapotranspiration as a modelled process (Kollet and Maxwell, 2008; Li et al., 2008; Goderniaux et al., 2009). Although the addition of evapotranspiration increases the number of modelled parameters and adds complexity to a model (Li et al., 2008; Goderniaux et al., 2009), this work has demonstrated that actual evapotranspiration is sensitive to the depth of a shallow water table (Kollet and Maxwell, 2008). Therefore, explicitly including it as a process may have an important influence on simulation of baseflows.

The 46 km^2 Bertrand Creek Watershed, located within the Fraser Valley of British Columbia, provides an ideal setting for investigating stream–aquifer interaction. First, the watershed is considered large enough to display significant heterogeneity in the nature of stream–aquifer interactions, yet small enough that a detailed investigation of the interaction along the stream is possible. Second, Bertrand Creek is situated within a hummocky, glaciated landscape and is hydrologically connected to an underlying aquifer. These characteristics establish favourable conditions for the dynamic flow of water between the surface and subsurface domains. Third, several aquifers, including an unconfined aquifer in connection with the stream, provide the primary source of water for domestic, agricultural, commercial and municipal uses within the watershed. Results of a regional (530 km^2) groundwater modelling study indicate these groundwater withdrawals have reduced the present-day baseflows in

Bertrand Creek 20 percent below historic volumes (Golder, 2005). Given future projections of agricultural intensification and urbanization, future increases in groundwater demand are expected to contribute to further reductions in baseflows (Golder, 2005). Finally, the Bertrand Creek Watershed is an ecologically sensitive area that supports two endangered fish species, the Nooksack Dace and Salish Sucker (Pearson, 2004). A recent draft Action Plan to support the recovery of these two endangered species states that one key approach is to "establish and maintain adequate base flow" (Fisheries and Oceans Canada, 2012). It is therefore essential that a thorough understanding of stream–aquifer interaction be gained so that water management strategies in Bertrand Creek Watershed are proactive in addressing ecosystem needs while planning how to meet future increases in water demand.

In the context of this study, baseflow refers to the persistent or delayed sources of water that sustain streamflow during periods of no rain (Sophocleous, 2002). In addition to groundwater discharge, baseflows can also be fed by other shallow subsurface sources such as soil water, surface sources such as wetlands, and water stored in river banks following rain events (bank storage). As well, anthropogenic activities such as industrial discharge or irrigation returns can modify the baseflow signature.

1.2 Thesis Objective and Research Format

The key research questions addressed in this thesis are:

1. What are the dominant controls of stream–aquifer interaction during baseflow conditions within Bertrand Creek Watershed?

2. Can baseflow within a real-world watershed be reasonably simulated with a physics-based hydrologic model?
3. What are the key hydrologic and landscape data required to simulate observed baseflows?

These questions were addressed by studying the surface water and groundwater interaction within the 46 km^2 Bertrand Creek Watershed.

This thesis follows the paper format style and has been organized into five chapters that present the development of a conceptual model and numerical model. Following the Introduction, Chapter 2 describes the geologic and hydrogeologic setting of the Bertrand Creek Watershed. The next two chapters are separate studies that focus on specific objectives using field methods (Chapter 3) and modelling (Chapter 4):

- Chapter 3 examines controls on surface water–groundwater interaction that operate at the watershed-scale during periods of baseflow. Based on an extensive field data collection program conducted during the dry season, a conceptual model for surface water–groundwater interaction is developed for the watershed. The study evaluates geomorphic controls that govern baseflow generation along Bertrand Creek, such as topography and subsurface permeability. The study identifies a specific measureable feature of topography that can be used to anticipate seasonal development of gaining and losing conditions along Bertrand Creek.

- Chapter 4 examines how to parameterize a physics-based integrated model for use at the watershed-scale with a specific focus on simulating dry season baseflow. Model development is based on the data collection program and conceptual model developed in Chapter 3. The hydrologic model is used to examine the nature of the surface water–groundwater exchange and how mechanisms that control this exchange influence development of the hydrologic model during baseflow conditions. A predictive application of the calibrated Bertrand Creek Watershed model is illustrated.

A summary of these studies is presented in Chapter 5 with implications of the results for assessment of watershed-scale, stream–aquifer interaction during baseflow conditions, and suggestions for future research.

Chapter 2: Study Site, Bertrand Creek Watershed

2.1 Introduction

The Bertrand Creek Watershed is located approximately 60 km east of Vancouver, within the agriculture-rich Fraser Valley in southwestern British Columbia, Canada (49°03'N, 122°29'W; Figure 2.1). Bertrand Creek drains a 46 km^2 area in Canada before flowing south into the United States where it becomes a tributary to the Nooksack River. This geographic border to the United States serves as the southern (outlet) boundary for the study area and is at an elevation of 45 m above sea level (masl). The land surface across the watershed is gently undulating, characterized by rolling hills and 100 m total relief between distinct uplands and lowlands (Luttmerding, 1980). Climate is typical of the Pacific Northwest with wet winters, dry summers, and an average annual temperature of 9.9°C. The average annual precipitation (1,530 mm/yr; Environment Canada, 2009) occurs primarily as rainfall as snowfall is generally limited to a period of a week or two. Approximately 70% of the annual precipitation occurs between the months of October and March (Figure 2.2), providing the primary source of recharge to shallow aquifers (Halstead, 1986). During the summer, potential evapotranspiration is greater than precipitation and a precipitation deficit is generally assumed (Halstead, 1986).

The urban area of Aldergrove (population 12,000) comprises 8% of the watershed area, which spans local municipal boundaries between the Township of Langley (TOL) and the City of Abbotsford. Approximately 18% of the watershed is forested and consists predominantly of alder, maple, poplar, and coniferous species (Douglas fir and red cedar)

within riparian zones and forest groves. The remaining land use is primarily agricultural with a predominance of berry, poultry, and mushroom farms, and pasture grazing areas for small livestock operations (Ministry of Agriculture, Food and Fisheries, 2002). Water supply to the urban area is provided by seven municipal groundwater wells that withdraw groundwater from the semi-confined Aldergrove aquifer. Outside the urban area, water supply to residential, agricultural, and commercial properties is supplied by private wells.

Bertrand Creek originates in a wetland in the northern portion of the watershed (Figure A1) and flows through Aldergrove and surrounding agricultural lands before flowing south into the United States. Stream discharge is reported at a permanent gauging station maintained at the Canada–USA border (Figure A2). Streamflows were previously reported on a seasonal basis (April to October) by the Water Survey of Canada (WSC; 1981-2007), and are now reported annually by the U.S. Geological Survey (USGS; 2007-present). Average annual discharge for the three years with available annual record is 1 m^3/s (2007-2010; USGS, 2010), and the corresponding summer baseflows are on the order of 0.02 m^3/s (Figure 2.2; WSC, 2008). Winter streamflows exceed summer flows by up to three orders of magnitude. In addition to seasonal contrasts in discharge, Bertrand Creek has a flashy hydrologic response to rainfall due to decreased infiltration and increased storm drain conveyance associated with the urban area (Kerr Wood Leidal, 2009). During baseflow conditions, stream water depths range from 0.10 m to 0.75 m, and stream widths range between 2 m and 7 m. During years with low rainfall, especially low spring and summer rainfall, streamflow within the upper portion of the watershed can become stagnant and the streambed mid-watershed can go dry (Figure A3; Johanson, 1988). Most tributaries to Bertrand Creek are

ephemeral, including the upper portion of Howes Creek, which is the largest tributary to Bertrand Creek (Langley Environmental Partners Society, 2006). At present, a detailed account of streamflow generation along Bertrand Creek is lacking. Photos taken throughout the watershed are included within Appendix A.

The Bertrand Creek Watershed is an ecologically sensitive area which supports a diverse population of fish and wildlife. The watershed is home to endangered fish species (e.g., Nooksack Dace and Salish Sucker) (Pearson, 2004), as well as the endangered Oregon Spotted Frog. Under the Species at Risk Act, the Department of Fisheries and Oceans Canada has developed a draft Action Plan to implement measures supporting the recovery strategy for the Nooksack Dace and Salish Sucker species (Fisheries and Oceans Canada, 2012). One of the key recovery approaches outlined within the Plan is to "establish and maintain adequate base flow in all habitats with high potential productivity".

2.2 Regional Geology

The Fraser Lowland is located within a major structural trough bound by the Coast Mountains to the north and the Cascade Mountains to the east and southeast (Mathews, 1972). Sediments eroded from these adjacent mountains infilled the trough and form the Tertiary-age sedimentary bedrock (Clague and Luternauer, 1983). Pleistocene glaciers then shaped and eroded the bedrock surface, which is encountered within the Lowlands at elevations of -100 to -200 metres above sea level (masl; Hamilton and Ricketts, 1994).

A 300 m thick stratigraphic sequence of glacial drift and marine deposits of late-Quaternary age overlies the bedrock surface (Armstrong, 1977). Late-Quaternary time is divisible into three major climatic units defined by glacial and non-glacial periods: the Olympia Interglaciation, the Fraser Glaciation, and the Postglaciation (Figure 2.3; Armstrong, 1981; Clague, 1981). Sediments deposited during the Olympia Interglaciation sit on top of a succession of deposits from the previous glaciation, and consist of a succession of marine, estuarine, and fluvial sediments known as the Cowichan Head Formation (Clague, 1977). During the initial glacial advance, a well-sorted outwash known as the Quadra Sand was deposited up to 100 m thick in advance of the ice sheet (Clague, 1977). This outwash was subsequently eroded by proglacial meltwater and the overriding ice sheet, which dissected the widespread sand unit into isolated permeable units (Clague, 1977).

The near surface stratigraphy primarily consists of sediments deposited during the Fraser Glaciation, and evidences a succession of glacial advance and retreat, isostatic rebound, and eustatic sea level changes (Clague and Luternauer, 1983; Ryder et al., 1991). This glacial period is divisible into three phases based on the extent of the ice sheet advance: the Vashon Stade, the Everson Interstade, and the Sumas Stade (Figure 2.3; Armstrong et al., 1965). The Cordilleran Ice sheet reached its maximum southern extent during the Vashon Stade, during which time a diamicton consisting predominantly of till with interbedded sand and gravel units known as the Vashon Drift was deposited (Armstrong, 1984). Rapid retreat of the ice at the end of the Vashon Stade and a eustatic sea level rise to 200 m above present created a marine transgression onto the isostatically depressed land (Easterbrook, 1963; Armstrong et al., 1965). During this interglacial period, the Everson Interstade, marine sediments were

deposited across the central Lowlands adjacent to a fluctuating ice-margin. Local deposits associated with this Interstade are known as the Fort Langley Formation, and consist of a complex interbedding of diamicton with sand and gravel deposits exceeding 200 m thick (Easterbrook, 1963; Armstrong, 1984). Ice-marginal and proglacial deposits are prevalent within the study area, especially east of Aldergrove where the eastward-retreating ice stabilized (Armstrong, 1981; Clague et al., 1997).

Re-emergence of the lowlands was accompanied by a topographically controlled advance of piedmont glaciers during the Sumas Stade (Armstrong et al., 1965; Clague et al., 1997). Sumas drift was deposited within a combination of glaciofluvial (meltwater channels, raised deltas, and outwash floodplains), ice contact, and morainal environments (Armstrong, 1984). While specific details regarding timing and advance (or standstill) of the Sumas ice are contested (Clague et al., 1997; Kovanen, 2002; Easterbrook et al., 2007), several Sumas-age glaciofluvial deposits constitute important near-surface permeable units within the Bertrand Creek Watershed. Early in the Sumas Stade, southwesterly-flowing meltwater channels developed from a prominent moraine in the southeast portion of the watershed (Armstrong, 1960; Mark and Ojamaa, 1979; Kovanen, 2002; Kovanen and Easterbrook, 2002). A widespread outwash floodplain known as the Sumas outwash was later deposited accompanying readvance of the glacier (Armstrong, 1984). This gravel and sand outwash deposit sits atop the Fort Langley Formation and is up to 50 m thick (Cox and Kahle, 1999).

After the final disappearance of the ice margin, sediments deposited during the Holocene period are limited to Salish sediments of fluvial and lacustrine origin (Armstrong, 1960).

2.3 Local Geology and Hydrostratrigraphy

Within the Bertrand Creek Watershed, heterogeneous surficial geology and distinct topographic uplands and lowlands evidence the area's complex depositional history. The uplands in the north of the watershed are characterized by a glaciomarine stoney clay deposited during the marine transgression of the Everson Interstade (Figure 2.4). The southern lowlands consist of surficial deposits of outwash sands associated with local advances of the Sumas Stade ice. Surficial till deposits of Sumas-age are also found across the eastern and southern portions of the watershed. Sedimentary bedrock is encountered at -210 and -230 masl in boreholes within the watershed (Halstead, 1966; BC MoE, 2008). Little information is available regarding local deposits pre-dating the Olympia Interstade, however, available borehole records show the older deposits are predominantly fine grained (BC MoE, 2008).

Five principal aquifers underlie the footprint of the Bertrand Creek Watershed (Figure 2.4). Each aquifer is associated with deposits from the Fraser Glaciation and is discussed in order of increasing age (and depth) below (Figure 2.3). Descriptions are based on interpretation of over 1,400 borehole logs obtained from the BC Ministry's water well database (BC MoE, 2008) in addition to literature review. Names of the deeper aquifers were adopted from Golder (2005).

The unconfined Abbotsford aquifer is a 200 km^2 regional aquifer that provides an important source of water for agricultural and domestic uses (Cox and Kahle, 1999). The aquifer consists of glaciofluvial meltwater channels and outwash sediments associated with the local

re-advance of the Sumas Stade ice (Figure 2.4). A widespread sand and gravel outwash plain forms the principal portion of the regional, south-sloping aquifer which sits atop glaciomarine sediments (Cox and Kahle, 1999). Several successions of meltwater channels, also associated with the Sumas Stade, traverse the watershed from east to west and are considered to be hydrologically connected to the outwash sands, forming one permeable unit (Mark and Ojamaa, 1979; Golder, 2005). The oldest of the Sumas-age glaciofluvial deposits is a meltwater channel referred to as the Campbell Channel, which accommodated the flow of meltwater from the eastern extent of the watershed to the former Campbell Delta located 7 km west of the watershed (Armstrong, 1960; Mark and Ojamaa, 1979; Clague and Luternauer, 1983). This meltwater channel underlies the westerly flowing portion of Bertrand Creek where it locally forms the northwestern extension to the aquifer's outwash plain (Figure 2.4). Borehole logs within the watershed indicate the aquifer thickness ranges from less than 10 m along its northern and western limits to approximately 30 m within the outwash plain. Groundwater flow direction within the Abbotsford aquifer is primarily toward the south, but is, however, influenced by local groundwater flow systems that discharge to stream valleys (Cox and Kahle, 1999; Golder, 2005; Scibek and Allen, 2005). Depth to groundwater is typically between 2 and 10 m below the ground surface. The aquifer is primarily recharged by precipitation, with corresponding seasonal water table fluctuations up to 3 m that lag monthly precipitation by one to three months (Cox and Kahle, 1999; Graham et al., 2010). Where the Abbotsford aquifer and Bertrand Creek are contiguous, they are considered to be hydrologically connected (Johanson, 1988; Berg and Allen, 2007).

The Aldergrove aquifer is a semi-confined aquifer comprised of glaciomarine outwash (deltaic) sands of the Fort Langley Formation (Golder, 2005). The aquifer becomes unconfined east of Aldergrove and along the south margin of the aquifer where meltwater channels of Sumas drift incise into the top of the aquifer (Piteau, 1991; Golder, 2005). The clinoformal aquifer is approximately 30 m thick; elevation of the aquifer surface is between 80 masl and 100 masl near the center and dips to 60 masl at the northern and southern margins (Golder, 2005). The western portion of the aquifer is overlain by glaciomarine silts and clays while the eastern portion of the aquifer is overlain by till deposits. These heterogeneous overlying sediments were likely the result of erosion by overriding glaciers or meltwater (Golder, 2005), or possibly evidence the extent of a local ice standstill. Overriding ice is also thought to have created breaks within the aquifer center where borehole lithologies reveal the permeable unit is locally absent (Figure 2.4; Golder, 2005). Groundwater flow within the aquifer is radially outward from an area near the aquifer center, adjacent the watershed boundary (Piteau, 1991; Golder, 2005). Groundwater discharge is primarily to creeks beyond the watershed footprint and to a lesser degree Bertrand Creek. The seven municipal wells which supply water to the town of Aldergrove are screened within this aquifer and extract a combined average 6,720 m^3/d. Declining groundwater levels in the northern portion of the aquifer, where most of the municipal wells are located, suggest the aquifer is being overpumped (Golder, 2005; Piteau, 2004).

The West of Aldergrove (WALD) and the South of Hopington (SHOP) confined aquifers are a complex of intertill deposits located beneath the western portion of the watershed (Figure 2.4). These aquifers were deposited during the Vashon Stade and are believed to be

laterally equivalent deposits with limited connectivity (Golder, 2005). The WALD aquifer is composed of two separate westerly-sloping permeable units initially encountered at 80 masl and vertically separated by a unit of till 20 to 40 m thick (Golder, 2005). The northwestern portion of the upper aquifer appears to be an erosional unconformity overlain by glaciomarine silts and clays, but within the watershed limits the aquifer is overlain by till (Golder, 2005). The SHOP aquifer complex similarly consists of two permeable units; the upper permeable unit is initially encountered at 60 masl and is locally incised into the lower permeable unit. Each of the WALD and SHOP aquifers are between 5 and 20 m thick.

The confined Aldergrove Quadra aquifer is the deepest mapped aquifer within the Bertrand Creek Watershed. The aquifer consists of the Quadra Sand outwash and is located between elevations of 20 masl and -20 masl (Armstrong, 1981; Golder, 2005). The Quadra Sand sits on top of a thick succession of silts and clays and underlies glacial till deposited during the Vashon Stade (Halstead, 1966; Clague, 1994). Groundwater from a well completed within this aquifer in the northern portion of the watershed was reported to be brackish (Halstead, 1966).

In addition to the aforementioned aquifers, areally-limited permeable units and water-bearing tills overlie the confining units of the Fort Langley Formation (Piteau, 1991). Borehole lithologies indicate a thin and isolated perched unit is present adjacent to Bertrand Creek south of the town of Aldergrove (Figure 2.4).

2.4 Previous Hydrologic Studies

Hydrologic studies within the Bertrand Creek Watershed and surrounding area have addressed water quality and quantity within the subsurface aquifers (Golder, 2005; Scibek and Allen, 2005; Chan, 2006; Pruneda et al., 2010). Golder (2005) conducted a comprehensive regional (530 km^2) groundwater modeling assessment for the TOL which identified the Bertrand Creek Watershed to have significantly diminished baseflow volumes compared to those 40 years ago, and to be at further risk of baseflow reductions due to future development. Scibek and Allen (2005) developed a 160 km^2 steady-state groundwater model of the principal portion of the Abbotsford aquifer to study effects of climate change on the aquifer water balance. The USA portion of this model, which consists of Bertrand Creek and neighbouring Fishtrap Creek Watersheds, was later refined by Pruneda et al. (2010) to study the impact of replacing surface water use with groundwater use on low-flow stream conditions. All hydrologic models discussed above were developed using the groundwater modelling software MODFLOW (Harbaugh et al., 2000).

The Aldergrove aquifer is an important source of water for the TOL municipal supply wells and several reports have addressed water availability within the aquifer (Piteau, 1991, 2004; Chan, 2006). In a water balance of the Aldergrove aquifer, Piteau (1991) estimated that roughly 500 m^3/d groundwater discharges from the Aldergrove aquifer to Bertrand Creek. They estimated that an additional 11,200 m^3/d discharges beyond the southern boundary of the Bertrand Creek Watershed to Pepin Creek. Piteau (2004) later reported that groundwater levels within the Aldergrove aquifer were declining and attributed the decline to groundwater over-extraction. In a water balance and consumptive water use study for the Aldergrove

aquifer, Chan (2006) similarly found that current water extraction from the aquifer is unsustainable and exceeds recharge rates.

Several local and regional studies address groundwater quality within the aquifers, with a particular focus on elevated nitrate concentrations within the unconfined Abbotsford aquifer (Kohut et al., 1989; Carmichael et al., 1995; Wassenaar, 1995; Cox and Kahle, 1999; Tesoriero et al., 2000). In addition to water quality information, these studies further contribute information regarding aquifer delineation (Cox and Kahle, 1999), permeability of aquifer sediments (Cox and Kahle, 1999; Tesoriero et al., 2000) estimates of groundwater water velocities (Tesoriero et al., 2000), and groundwater ages and travel times (Wassenaar, 1995).

Field studies assessing stream–aquifer interaction suggest the unconfined Abbotsford aquifer is strongly connected to overlying streams (Cox et al., 2005; Berg and Allen, 2007; Pruneda et al., 2010). Previous work within the study site is limited to an assessment of low flow variability at and between four measurement locations on the stream (Berg and Allen, 2007). Farther downstream along the USA portion of Bertrand Creek and tributaries to it, gaining and losing sections of the stream were identified using measurements of streamflow and streambed flux (Cox et al., 2005; Pruneda et al., 2010). All aforementioned studies reported that the steam–aquifer exchange was spatially and temporally variable, and attributed the variable nature of groundwater interaction along the stream to the distribution of permeable sediments.

In summary, Bertrand Creek and neighbouring streams are strongly connected to the unconfined Abbotsford aquifer and it is groundwater discharge from this aquifer that maintains summer low flows. Stresses to this aquifer owing to climate and groundwater extraction place groundwater contribution to these streams at risk of decline. The work herein aims to enhance our understanding of stream–aquifer interaction within these strongly connected hydrologic environments.

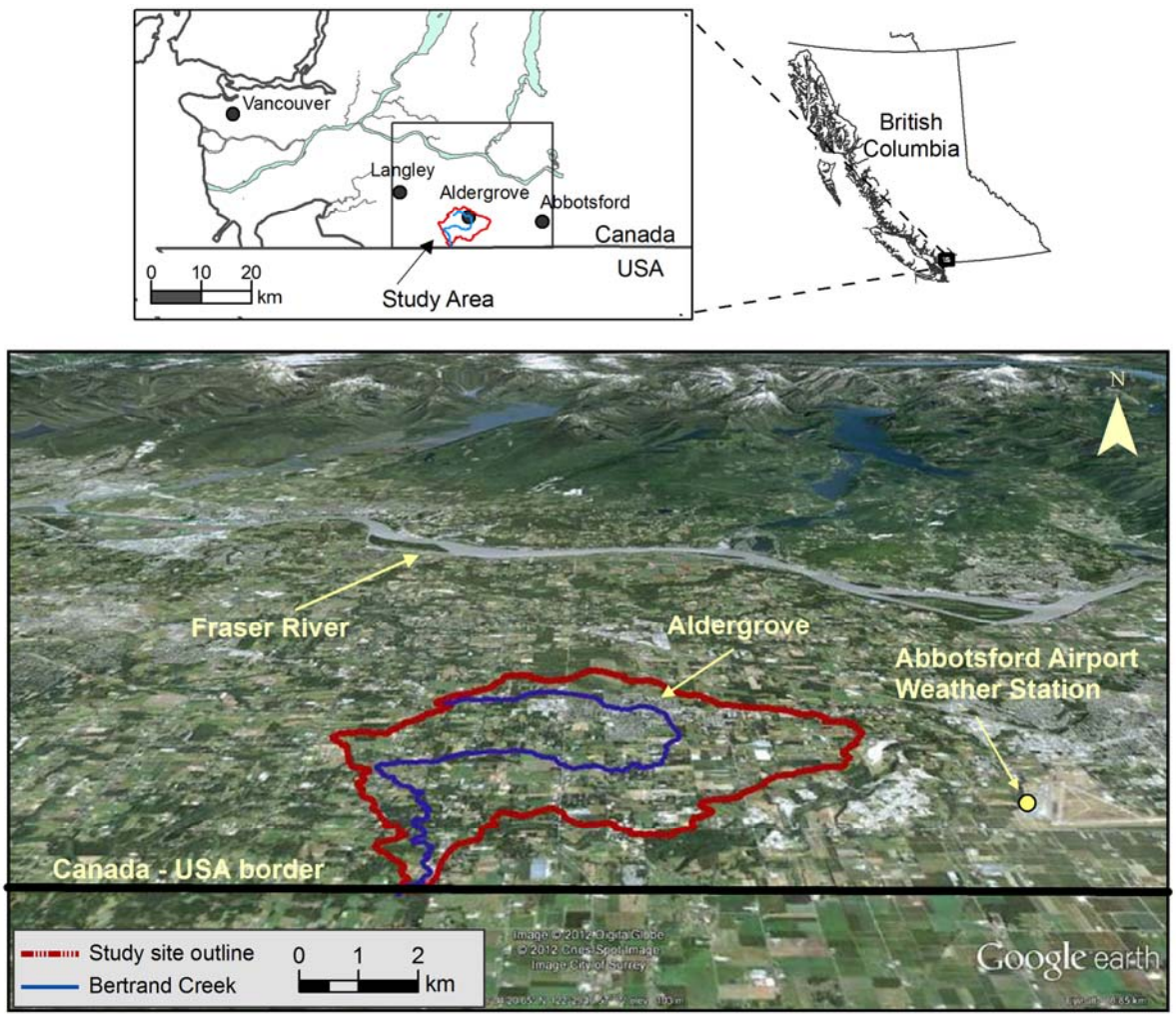

Figure 2.1 Location of the Bertrand Creek Watershed

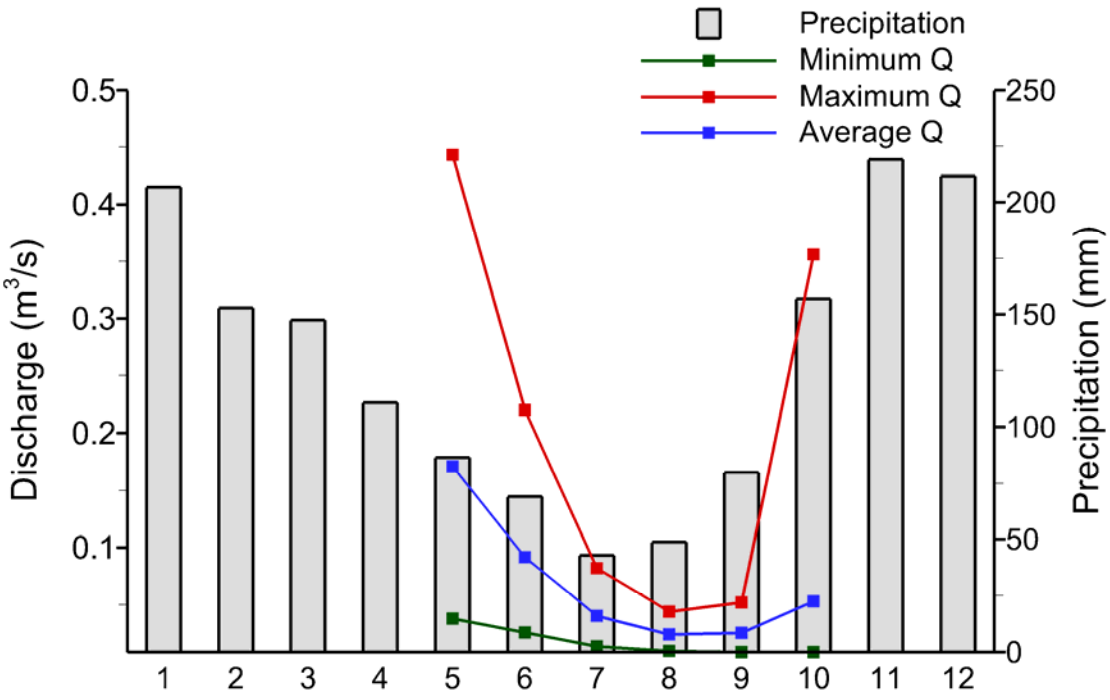

Figure 2.2 Average monthly precipitation for the Abbotsford Airport weather station (1945-2007; Environment Canada, 2009) shown along with minimum, maximum, and average monthly low flows (Q) at the Bertrand Creek gauge during the summer period (1981-2007; WSC, 2008).

Age ka		Geologic Climate Units		Stratigraphic Units	Hydrostratigraphic Units
	Holocene	Postglacial		Salish Sediments	
10	Late Wisconsin	Fraser Glaciation	Sumas Stade	Sumas Drift	Abbotsford aquifer
			Everson Interstade	Fort Langley Formation	Aldergrove aquifer; glaciomarine and till confining units
20			Vashon Stade	Vashon Drift	West of Aldergrove aquifer; South of Hopington aquifer; till confining units
		Olympia Interglacial		Quadra Sands	Quadra Sands aquifer
30				Cowichan Head Formation	
≈ 60					

Figure 2.3 Late-Quaternary events, stratigraphic units and interpreted hydrostratigraphy within the Bertrand Creek Watershed (modified from Armstrong, 1984).

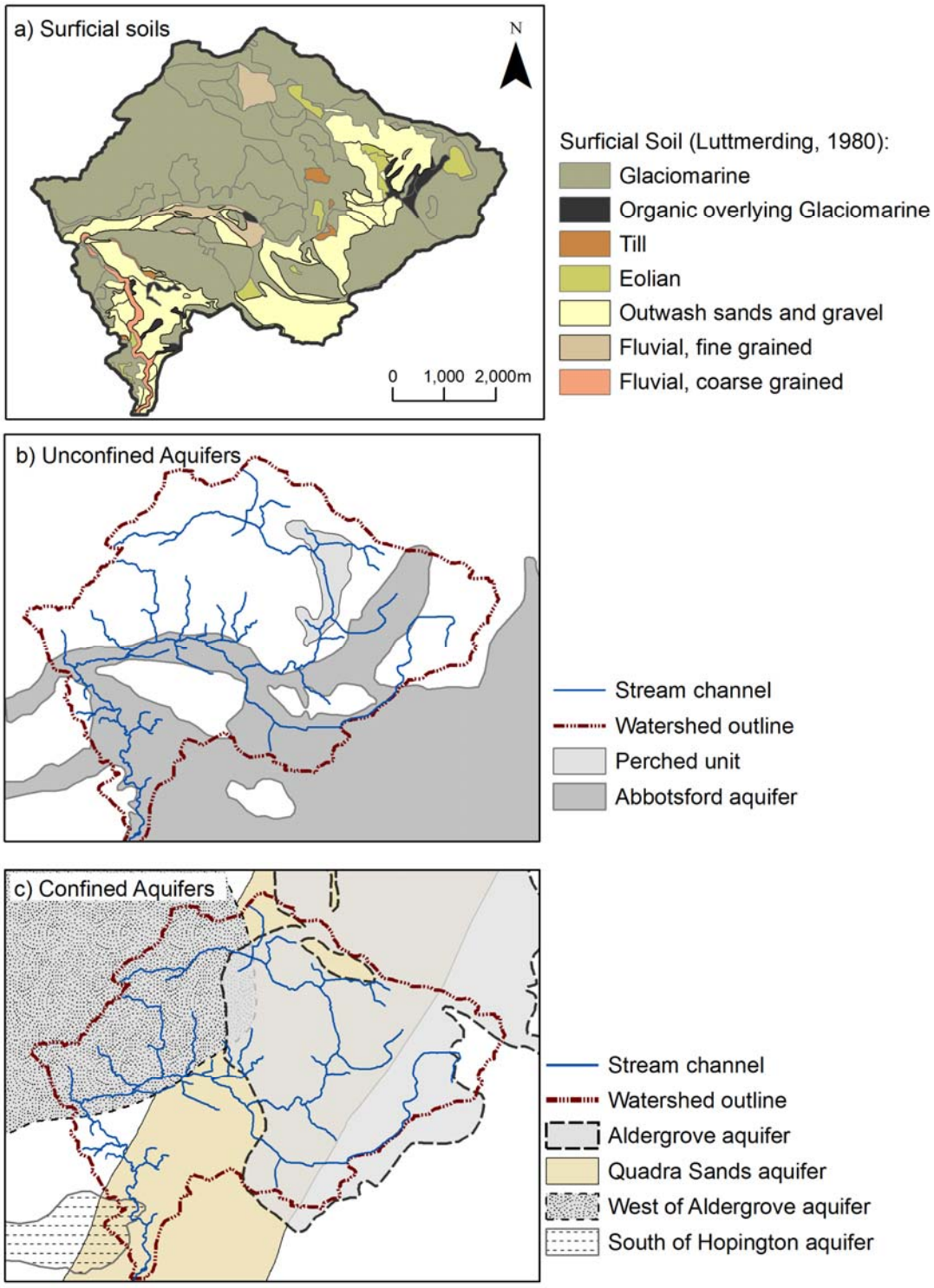

Figure 2.4 a) Distribution of surficial soils, b) outlines of unconfined aquifer and perched water bearing zone, and c) outlines of confined aquifers.

Chapter 3: Geomorphic Controls on Surface Water–Groundwater Interaction in a Glaciated Watershed

3.1 Introduction

Surface water–groundwater interaction has important implications for water resource managers evaluating the impact of water allocations on groundwater-dependent ecosystems. Where a subsurface aquifer is closely connected with a stream, increased stress to groundwater resources can lead to reduced baseflows, which in turn jeopardize stream ecosystems. In the Pacific Northwest, the conflict between water users and ecosystem needs is most evident during summer months, when dry weather combined with greater water demand places increased stress on groundwater resources (Everest et al., 2004). Consequently, water resource managers need to consider the exchange of water between a stream and aquifer when assessing water allocation strategies (Winter, 1999; Sophocleous, 2002). This necessitates a comprehensive understanding of surface water–groundwater interactions, based on field investigation, to determine the nature of the exchange and identify important controls across a watershed.

Assessing stream–aquifer interaction is inherently difficult in low-flow environments. First, stream–aquifer interaction varies spatially and temporally at multiple scales owing to hyporheic flow in addition to exchanges with groundwater. Hyporheic flow constitutes streamflow which enters the subsurface and returns as surface flow a relatively short distance downstream. Hyporheic flow systems create upwelling and downwelling patterns at scales ranging from meters to tens of meters along stream reaches that can be net gaining or losing

at the 10^2 to 10^3 m scale (Woessner, 2000; Ruehl et al., 2006; Krause et al., 2007). Second, the magnitude of error associated with measurement of low flows complicates the comparison of sequential streamflow measurements (e.g., Berg and Allen, 2007). Additionally, the influence of anthropogenic activity on streamflows and water chemistry may be more pronounced in low-flow environments. These challenges necessitate the use of a suite of field techniques in order to develop a well-defined conceptual model of stream–aquifer interaction across a watershed (Kalbus et al., 2006; Andersen and Acworth, 2009).

Catchment-scale studies have demonstrated that the exchange of water between a stream and subsurface aquifer is spatially concentrated along segments of a river associated with specific geologic and geomorphic features (Grapes et al., 2005; Konrad, 2006a; Tetzlaff and Soulsby, 2008). Along several tributaries to the Columbia River for example, the largest groundwater contributions to streamflow occur where the underlying aquifer decreases in thickness or at contrasts in subsurface permeability at the contact of lithologic units (Konrad, 2006a). In other rivers, increased groundwater contribution occurs at the confluence with tributaries (Grapes et al., 2005; Andersen and Acworth, 2009), and at the base of steep slopes (Nelson, 1991). Losing conditions frequently develop when a stream flows over streambed or aquifer sediments with increased permeability, such as onto an alluvial plain from a mountain valley (e.g., Konrad, 2006a; Larned et al., 2008) or over paleochannels (Andersen and Acworth, 2009). Under these conditions, it is not uncommon for streams that flow along their upstream reaches to lose water and become ephemeral along lower reaches (e.g., Konrad, 2006a; Larned et al., 2008; Andersen and Acworth, 2009). While landscape and channel features act as controls of surface water–groundwater interaction, it is their influence on the

convergence and divergence of groundwater flow paths which ultimately governs this interaction (e.g., Kirkby and Chorley, 1967; Winter, 1999).

Groundwater flow is typically assessed using a contour map of the water table based on water level measurements within groundwater wells. However, sufficient water level measurements are not always available. As an alternative, Larkin and Sharp (1992) classified the direction of groundwater flow within an alluvial aquifer underlying a stream according to a river's geomorphic characteristics, such as channel gradient, valley slope, sinuosity, incision, width, and depth. Two end-members of their classification system are the underflow component, which is the portion of groundwater flow that parallels the direction of the stream valley, and the baseflow component, which is the portion of groundwater flow that is perpendicular to streamflow (Figure 3.1). Using this classification, a stream–aquifer system is classified according to its predominant groundwater flow direction as underflow-dominant, baseflow-dominant, or mixed. Mixed-flow systems develop where the longitudinal valley gradient and channel slopes are similar or where the lateral valley slope is negligible. Subsurface flow parallels a stream in both underflow and hyporheic flow systems, and a distinction between the two is made here: hyporheic flow is limited to a zone of meters beneath the stream while underflow characterizes the groundwater flow direction at a larger scale within the unconfined aquifer. Despite the simplicity of Larkin and Sharp's (1992) classification of groundwater flow direction, it has not been employed in studies of stream–aquifer interaction.

Understanding system dynamics at the scale of a watershed requires studies that investigate the nature of the surface water–groundwater exchange at this scale (10^2 to 10^3 km^2; Sophocleous, 2002; Bencala et al., 2011). Despite its importance, characterizing the distributed nature of baseflow and low flow generation at the watershed scale has only recently received increased focus (e.g., Gburek and Folmar, 1999; Tetzlaff and Soulsby, 2008; Andersen and Acworth, 2009; Gleeson et al., 2009; Banks et al., 2011b). Given the diverse range of landscapes, there is still much to be learned about the influence of watershed characteristics on baseflow and the role that geomorphology plays on influencing the dynamics of stream–aquifer exchange (Tetzlaff et al., 2008; Bencala et al., 2011).

The objective of this study is to examine controls on surface water–groundwater interactions that operate at the watershed-scale during periods of baseflow. Relationships are examined between baseflow generation and a watershed's geomorphic characteristics such as topography and subsurface permeability. Hydrometric and tracer-based techniques, in conjunction with an assessment of near-stream topography, are used to examine the exchange of water between a stream and aquifer. The study site, the 46 km^2 Bertrand Creek Watershed in southwestern British Columbia, was monitored for two consecutive dry seasons that each received significantly different amounts of rainfall. Knowledge gained from this study will contribute to our understanding of controls governing gaining and losing stream conditions along a stream that is strongly connected with a subsurface alluvial aquifer.

3.2 Study Setting

The upstream portion of Bertrand Creek overlies sediments forming the confining unit above the Aldergrove aquifer, while the lower 10.8 km of Bertrand Creek overlies the unconfined Abbotsford aquifer (Figure 2.4). A distinction between two portions of the Abbotsford aquifer is made here for easier reference throughout the study: Along the upstream portion of the aquifer (6.1 to 10.8 km upstream of the outlet), the channel flows east to west over sediments deposited by a former glacial meltwater channel. This upper, east-west trending portion of the unconfined aquifer will be referred to as the glaciofluvial (GLF) deposit. The lower 6.1 km of the stream flows over sediments deposited as an outwash plain in addition to former glacial meltwater channels. This lower portion of the aquifer is referred to as the outwash plain (OP) deposit.

Bertrand Creek continues south into the United States, but only the portion of the watershed situated in Canada is included within this study. The downstream limit of the study area was chosen at the border where a permanent streamflow gauge is present and is not at the confluence with another tributary or river. Distances along the stream are referenced from the border and increase upstream (Figure 3.2).

Field work was primarily focused along three reaches in the lower portion of the watershed (Reach A, B, and C; Figure 3.2) where the stream is in hydrologic connection with the unconfined aquifer (Johanson, 1988; Golder, 2005). These reach locations were selected based on the results of a field reconnaissance conducted the previous summer to identify accessible stream locations and stream flow characteristics. Reaches A and B are

approximately 1,200 m in length and overlie the unconfined aquifer. Reach C is a 300 m stream length that overlies the transition zone from confined to unconfined conditions. Daily precipitation records and climate data were obtained from an Environment Canada weather station located at the Abbotsford Airport, approximately 4 km east of the watershed (Figure 2.1). Photos showing the landscape and typical streamflows are included in Appendix A (Figures A1 through A8).

Typical channel geomorphological characteristics differ within the upper and lower portions of the watershed. Within the upper portion of the watershed, streambed material consists primarily of fine grained sediments with well defined and often entrenched stream banks. The lower portion of the stream consists of sand and gravel banks and is characterized by point bars and riffle-pool sequences. Channel width to depth ratios within the lower half of the watershed typically exceed those within the upper watershed, with higher stream water velocities along the lower channel. During baseflow conditions, stream water depths throughout the watershed range from 0.10 m to 0.75 m, and stream widths range between 2 m and 7 m.

3.3 Methods

3.3.1 Groundwater Flow

The groundwater flow direction in the unconfined aquifer is interpreted based on the geomorphic classification of Larkin and Sharp (1992). The Larkin and Sharp (1992) classification uses geomorphic properties of the region surrounding a stream to identify the predominant direction of groundwater flow as either baseflow-dominant or underflow-

dominant (Figure 3.1). This study uses the slope ratio surrounding the stream to characterize the predominant direction of groundwater flow within the unconfined aquifer (Larkin and Sharp, 1992). Topographic slopes along lengths of the stream were analyzed using a 20 m digital elevation model of the Bertrand Creek Watershed obtained from municipal government. The average lateral slope (perpendicular to the stream) and the average longitudinal slope (parallel to the stream valley) were determined along 300 m stream segments where the unconfined aquifer is present beneath Bertrand Creek.

The depth to groundwater within 13 private wells was additionally measured using a water level tape in early June and late September, 2007. All water wells were screened within the unconfined Abbotsford aquifer.

3.3.2 Hydrologic Measurements

In the absence of tributaries or surface water withdrawals, a change in streamflow measured between incremental gauging stations can be attributed to an interaction with groundwater. Streamflows were measured at eight temporary spot gauging stations located within the reaches: four stations were established within each of Reach A (A1 though A4, Figure 3.2) and Reach B (B1 through B4). Distance between successive gauging stations ranged from 180 to 570 m. Gauging locations established at A4b and B1b in 2006 were not suitable locations for weir installations and these stations were re-established at locations A4 and B1 in 2007 (Figure 3.2). Station B3 is located at an elevation unconformity – a road bridge creates a 1.5 m drop in streambed elevation immediately downstream of this station (Figure A8). In addition to the gauging stations established for this study, a permanent

gauging station (Bertrand Creek) is maintained at the outlet of the watershed (Figure 3.2). Prior to 2007, the gauge was maintained by the Water Survey of Canada (WSC), and since 2007 the gauge has been maintained by the U.S. Geological Survey (USGS). The USGS and WSC hydrographs are reported with resolutions of 3.5 L/s and 1 L/s, respectively.

To obtain a continuous record of water height during the 2007 dry season, weirs were installed at stations A1 and A4 within Reach A and at stations B1 and B3 in Reach B (Figure 3.2; Figures A9 to A11). Significant spring rains delayed the installation of weirs and hindered baseflow measurements in the stream. When the high streamflows receded in July, weirs were installed at Stations A1 and B1. These weirs were subsequently damaged by a five-day rain event late in July and were repaired and reinstalled after storm flows receded. Rectangular sharp-crested weirs were installed at A1 and A4, and keyed into natural streambed sediments. V-notch sharp-crested weirs were installed under road bridges at B1 and B3 where the streambed consists of concrete. Sharp crests were constructed from bevelled 1.5 mm steel plates secured to 19 mm marine grade plywood. Plastic sheeting (6 mil vapour barrier) was buried into the streambed 4 m upstream of the weir to reduce subsurface infiltration due to the increased heads along the upstream approach. Stream stage was continuously recorded at each weir using a capacitance datalogger (Dataflow Systems Odyssey capacitance logger) housed in a PVC stilling well. Water heights were referenced to manual recordings at staff gauges installed at each station.

Streamflow at each of the eight gauging stations was measured 8 to 10 times during the dry season using velocity-area surveys (Herschy, 1995) or the salt dilution method (Moore,

2004a,b). For velocity-area surveys, stream velocity was measured at a minimum of 20 verticals using an electromagnetic current meter (Marsh McBirney Model 2000). Errors for each gauging measure were calculated as described by Herschy (1995) and were typically between 5 to 10%. At locations where stream gauging and dilution methods were conducted concurrently, calculated streamflows were generally within 5 to 10%. These gauging measurements were used to establish stage-discharge relationships at each weir, which deviate by less than 1.4 L/s from the theoretical Kindsvater-Carter (1959) and Kindsvater-Shen (ISO, 1980) equations describing flow over sharp-crested weirs. Gauging measurements at all stations and rating curves for stations with a continuous record are provided in Appendix B.

Laboratory testing of the Odyssey capacitance loggers revealed that the water height reported by the loggers is temperature dependent (Appendix C). The loggers employ a Teflon strip as the dielectric medium and it seems that the nature of Teflon's coefficient of thermal expansion is responsible for the temperature dependence: Teflon's coefficient of thermal expansion exhibits a fourfold increase and immediate decrease in value between 10 and 30°C (Kirby, 1956), which is the range of stream water temperature observed during the study period. Since capacitance is inversely proportional to the thickness of the dielectric medium, a change in temperature would influence the thickness of the Teflon and affect the measured capacitance. Differences in air temperature, water temperature, and humidity are expected to affect the Odyssey's reading and thus no correlation could be made to remove the likely temperature dependence from the data record. In addition to temperature, the capacitance loggers are also sensitive to changes in stream water electrical conductivity (EC;

Appendix C; Larson and Runyan, 2009). This sensitivity to EC, however, occurs at values generally below those encountered within the stream where the loggers were deployed. To account for the sensitivity of the Odyssey data logger, the record of stream stage is considered to have an uncertainty of 5 mm, which contributes between 0.2 L/s (station B3; q=0.3 L/s) and 1.5 L/s (station A1; q=20L/s) uncertainty to streamflow records during baseflow conditions late in the summer.

3.3.3 Streambed Seepage

Mini-piezometers were installed within the streambed to measure vertical hydraulic gradients across the streambed and to estimate hydraulic conductivities within streambed sediments (Figures A12 and A13). Mini-piezometers consisted of 0.64 cm inner diameter polyethylene tubing screened with drill holes covered in nylon mesh fabric across the lower 7.6 cm of the tube. The tubes were installed into the subsurface by driving a 1.5 cm diameter hollow steel tube with an inner removable rod into the ground, in a manner similar to Baxter et al. (2003). Mini-piezometers were installed in transects perpendicular to the stream channel along the left and right banks of the creek at nested depths of approximately 0.3 m (A-depth) and 1.0 m (B-depth) below the channel bottom. A total of 95 mini-piezometers were installed along 20 transects and at 15 additional singular locations (Figure 3.2). The naming convention adopted for mini-piezometers includes the site name, the transect number at the site, the cardinal direction of the stream bank, and the designation of A or B to indicate the screen depth. Following this convention, a ‘site’ is considered to consist of adjacent transects located along a stream length of 100 m or less.

Mini-piezometers installed in permeable streambed sediments were developed using a peristaltic pump and pumped until the water was free of sediment. Water level within a mini-piezometer was measured using food-grade dye as a tracer and a measuring tape or alternatively, using a 'dip-stick' constructed from an ohm meter with wire contacts (Moore et al., 2005). The ohm meter registered a reading when the wire contacts encountered the water surface. Water level measurements within a mini-piezometer are considered accurate to ±2 mm when above or slightly below the stream surface and ±1 cm when greater than 5 cm below the stream surface.

Streambed hydraulic conductivities were determined at all mini-piezometers screened in permeable sediments using falling head slug tests. In piezometers with a rapid hydraulic response, falling head slug tests were carried out using a syringe to draw water upward into the mini-piezometer and allowing time for heads to equilibrate prior to conducting the test. Mini-piezometers with a slower equilibration time were tested using a slug of water released into the tubing. Hydraulic conductivity (K_h) was calculated as the average of three successive tests at each mini-piezometer using the Hvorslev (1951) basic time lag method, Case G:

$$K_h = \frac{(r_c^2)\ln(L_s / r_w)}{2L_s T_o} \qquad [1]$$

where r_c is the radius of the casing, L_s the length of the screened interval, r_w is the effective well radius, and T_o is the basic time lag, a value derived from construction of an equilibrium curve. The method of Baxter et al. (2003) was used to calculate hydraulic conductivity when equilibration of the water height was too rapid to record multiple drops in head:

$$K_h = \frac{(0.5)(r_c)}{r_w \Delta t}\left[\ln \frac{h_o}{h}\right] \quad [2]$$

where h_o is the head at t = 0, and h is the head t > 0.

The vertical component of water flux across the streambed in the vicinity of the mini-piezometer can be estimated using Darcy's law:

$$q_v = -K_v \frac{dh}{dl} \quad [3]$$

where K_v is the vertical hydraulic conductivity, dh is the measured difference between head in the mini-piezometer and the stream, and dl is the vertical distance between midpoint of the mini-piezometer screen and the streambed. Hydraulic conductivity of the streambed sediments was assumed to be isotropic. Where the water level inside a mini-piezometer was above the stream water elevation, groundwater was considered to be upwelling to the stream in the presence of a positive (upward) vertical hydraulic gradient. Conversely, a negative (downward) vertical hydraulic gradient indicated downwelling conditions and a stream losing water to groundwater.

In addition to mini-piezometers, a 2.5 cm diameter piezometer capable of accommodating a data logger was installed in the streambed at station B4. The piezometer was constructed of Schedule 40 galvanized steel and screened with 2 mm drill holes along the lower 15 cm of the pipe. A hardened-steel tip was welded to the bottom end of the pipe to facilitate hammering through streambed sands and gravels to a depth of 1.5 m. A PVC stilling well was installed adjacent to the piezometer.

3.3.4 Natural Stream Tracers

3.3.4.1 Geochemical and Isotopic Analysis

Surface water samples were collected monthly at select gauging locations during baseflow conditions between April and August 2007. Water samples were also obtained from select mini-piezometers on August 15 and 16, 2007. Samples were field filtered and preserved with nitric acid; all samples were stored at 4°C until analyzed. Alkalinity was determined using the Gran titration method, major anions were measured by ion chromatography, and metals and trace elements were measured by ICP-OES. Select stream samples were analyzed for stable isotope ratios of ^{2}H and ^{18}O.

3.3.4.2 Electrical Conductivity and Temperature

Change in surface water electrical conductivity (EC) and temperature along a stream length can indicate the presence of upwelling groundwater during baseflow conditions (e.g., Story et al., 2003; Gleeson et al., 2009). Stream water temperature has potential to serve as a natural tracer along Bertrand Creek since the average groundwater temperature within the unconfined Abbotsford Aquifer is 10°C (Cox and Kahle, 1999) and surface water temperatures in the Bertrand Creek can exceed 20°C (unpublished data). On August 15 and August 16, 2007, stream water EC and temperature were recorded along longitudinal profiles at stream sections encompassing Reaches A and B. Stream water EC (corrected to 25ºC) and temperature were measured using a WTW conductivity meter and were related to stream location with a handheld GPS unit. EC and temperature measurements were also obtained from mini-piezometers located along each profile within hours of conducting the

aforementioned profile measurements. EC measurements are considered accurate to ±0.5% of the measured value.

Temperature within streambed deposits can additionally be used to interpret the direction of seepage across a streambed (Constantz, 1998; Stonestrom and Constantz, 2003; Conant, 2004). Temperature profiles within streambed sediments were measured using thermistors installed at three locations along Reach B [T-B1(2), T-B2(1), and T-B4(1); Figure 3.2]. At each location, five thermistors were buried along the left and right banks between 0.2 m and 1.0 m below channel bottom, and one thermistor was placed on top of the streambed. Thermistors were inserted in 1 cm diameter polyethylene tubes installed in the subsurface following the same procedure as mini-piezometer installation (Figure A12). The lower 2 cm of each tube was screened with drill holes and the ends were sealed. Temperatures were recorded every 15 minutes using a Campbell Scientific CR10X logger. Thermistor measurements are considered accurate to within 0.2°C.

3.4 Results and Discussion

3.4.1 Precipitation

The cumulative precipitation record indicates that the 2006 hydrologic year (1,434 mm) was drier than the historic average of 1530 mm (± 220 mm, 1945-2007), while the 2007 hydrologic year was wetter than average (1,843 mm; Figure 3.3; Environment Canada, 2009). The 2007 dry season, June through September, had twice the rainfall as 2006, due in large part to a 5-day, 63 mm rain event late in July. This storm contributed a rainfall amount

exceeding all rainfall recorded during the months of July and August 2006 combined, and resulted in high streamflows that damaged the two weirs (see Section 3.3.2).

3.4.2 Streambed Hydraulic Conductivity

The hydraulic conductivity of streambed sediments is closely related to the location of the confined and unconfined aquifers underlying the stream (Figure 3.4). Within the upper portion of the Bertrand Creek Watershed, where the stream overlies the confined aquifer, the streambed consists of silt and clay sediments with hydraulic conductivities too low to measure by slug test (a site specific estimate of $8x10^{-9}$m/s, Table 3.1). The surficial soils map indicates that local sand deposits may be present beneath the low hydraulic conductivity streambed within the upper portion of the watershed (Luttmerding, 1980); however, they were not encountered within the mini-piezometers installed along this segment (Figure 3.4). At the transition between the confined and unconfined aquifer, which is situated at the upstream extent of Reach C (10.8 km), the clay unit pinches-out over the sandy unconfined aquifer over a distance of approximately 200 m (Figure 3.4).

In the lower portion of the watershed, where Bertrand Creek overlies the unconfined aquifer, the streambed consists predominantly of high hydraulic conductivity sands and gravels with pockets of clay found both at the surface and beneath sandy surficial deposits. Hydraulic conductivities of streambed sediments are generally on the order of 10^{-5} and 10^{-4} m/s, but a few deposits are outside this range and one additionally exceeds the range that could be measured using a slug test (>$8x10^{-4}$ m/s, Table 3.1). The hydraulic conductivity values of streambed sediments at A- and B-depths are similar within the GLF deposit and 1 km

downstream of GLF deposit (between km 5 and km 10.8; Figure 3.4). In contrast, hydraulic conductivity values at the two depths vary considerably farther downstream within the OP deposit, with higher hydraulic conductivity generally measured in shallow deposits. The range of conductivities determined for the permeable sediments spans the values determined by Pruneda et al. (2010) for the portion of Bertrand Creek located downstream in the United States ($9x10^{-6}$ m/s to $1x10^{-3}$ m/s).

3.4.3 Streamflow

Discharge reported at the watershed outlet Bertrand Creek gauge is shown in Figure 3.3. Discharge was highest following winter rains and decreased through the summer. Minimum annual streamflows reported for each year demonstrate a dependence on precipitation. The minimum daily-average streamflow reported at the Bertrand Creek gauge was 15 L/s in 2006 (WSC, 2009) and increased to 21 L/s in 2007 (USGS, 2010) accompanying the increase in precipitation.

Streamflow measurements at the gauging stations are presented in Figure 3.5. Streamflow measurements indicate that all discharge at the watershed outlet during baseflow conditions late in the summer of 2006 and 2007 entered the stream channel between gauging stations A1 and B3 (Figure 3.5b). Between these gauging stations, streamflows measured at successive stations increased with distance downstream. There was no measureable change in streamflow between station A1 and the outlet located 2 km downstream. At station B3, streamflows late in the dry season either ceased or were negligible: streamflows ceased from early July to September, 2006, and the streambed was dry upstream of station B3 along a

stream length exceeding 500 m. The upstream extent of the dry channel was not mapped, but it did not extend more than 1.7 km upstream of station B3. Upstream of this point, water was present in the channel to the headwater. In 2007, a stream water height only centimeters high sustained very low flows at stations B3 and B4 (approximately 0.2 L/s; Figure 3.5b). Streamflows at station B2, which is located only 180 m downstream of station B3 and the (near) dry streambed, were sustained at or above 6 L/s during both years (shown in Figure 3.5a for 2006).

Baseflow contribution to Bertrand Creek, interpreted from incremental streamflow measurements at gauging stations along Reaches A and B, is spatially and temporally variable (Figure 3.6). For example, the seasonal-low baseflow contributions measured across Reaches A and B in 2006 were 5 and 7 L/s, respectively, which are equivalent to contributions of 5 and 13 L/s normalized over a 1 km stream length. Accompanying increased precipitation and streamflow in 2007, the seasonal-low baseflow contributions increased to 7 and 10 L/s across Reaches A and B, respectively (equivalent to 6[1] and 14 L/s/km). The spatiotemporally variable nature of the baseflow contribution is further demonstrated in incremental streamflow measurements at stations within each reach, especially within Reach B (Figure 3.6). At the upstream segment of Reach B, between stations B3 and B4, incremental streamflow measurements indicate that the direction of vertical seepage reversed with time into the dry season, and the stream segment transitioned from gaining to losing at flows around 20 L/s. All other stream segments downstream of station B3 remained gaining. The increment B2-B3 had the highest measured gains

[1] The distance across Reach A differed between 2006 and 2007 (Section 3.3.2)

(>40 L/s/km) while B1-B2 and all increments along Reach A were moderately gaining (<20 L/s/km).

Measurement error associated with the calculation of baseflow contribution between most incremental gauging stations was significant even though the quality of streamflow measurement was considered 'good'. As an example, measurement error exceeded the calculated change in baseflow between most stations in lower Reach A (Figure 3.6).

Runoff generation in the upper portion of the watershed appears to be delayed from runoff generated in the lower watershed late in the dry season. For example, rain events on August 26 and during September, 2007, failed to generate runoff at the B3 weir, but generated increased runoff at all downstream stations (Figure 3.5b). A peak in the B3 hydrograph was subsequently generated one to two days following the August 26 rain event and streamflow records at downstream weirs show each peak continued to travel as an isolated pulse through to the watershed outlet. A similar 'double-peak' hydrograph was created following a rain event on August 19, 2007. This earlier rain event also generated an initial streamflow peak at the B3 hydrograph. Rainfall that could be attributed with generating these hydrograph peaks was not recorded at three additional rain gauges located within and surrounding the watershed, including one gauge centrally located within the urban area. The second peaks could be unrelated to rainfall (e.g., beaver dam removal) but are interpreted to be the delayed arrival of runoff generated within the upstream urban area. The second peak arrived at the watershed outlet between 50 and 70 hours following the first. The absence of increased streamflow at station B3 immediately following rain events late in August and during most of September suggests these events failed to locally increase the

water table upstream of station B3 a sufficient amount to connect it with the stream, thereby increasing streamflow via saturated overland flow or increased subsurface flow. In addition, Horton overland flow to the channel was either insignificant, ponded, or infiltrated through downstream portions of the streambed prior to arriving at station B3. The double-peak hydrograph behaviour was not evident in 2006 or at other times in 2007, which suggests specific hydrologic conditions (such as antecedent wetness of the watershed and rainfall magnitude) are required to generate the phenomenon. If the peaks are not delayed responses to rainfall, all runoff generated upstream of station B3 late in the dry season must either be captured within surface storage zones or infiltrate the streambed prior to arriving at station B3. Unfortunately, a comparison of discharge between successive weirs could not be made since the weirs were not calibrated at the magnitude of streamflow associated with the pulses.

The continuous records of streamflow show diurnal variation up to 3.7 L/s and 1.5 L/s at the Bertrand Creek gauge and weirs, respectively. In addition to direct evaporation from open water, stream withdrawals, and near-stream groundwater withdrawals, diurnal variation in flow can be attributed to evapotranspiration by riparian vegetation (Troxell, 1936; Bren, 1997; Bond et al., 2002), change in streambed fluxes due to dependence of hydraulic conductivity on temperature (Constantz, 1998; Constantz et al., 1994; Ronan et al., 1998), or temperature dependence of data loggers (Appendix C). Part of the diurnal variation at the Bertrand Creek gauge is attributed to scheduled stream or groundwater withdrawals, evidenced by a consistent diurnal decrease in discharge mid-summer on days without rain. In contrast, discharge at the weirs did not display any consistent patterns in the diurnal variation to ascribe a cause. The diurnal variation and interpreted delayed response to

rainfall discussed above highlight the importance of establishing a reference gauge or maintaining a continuous stage record at stream gauging locations, especially when comparing incremental streamflow measurements within a developed watershed. These variations in flow likely contributed to the high streamflow variability and measurement uncertainty that Berg and Allen (2007) previously found when measuring low flows in Bertrand Creek.

3.4.4 Evolution of Surface Water Chemistry

During the dry season, the chemical composition of water in Bertrand Creek is predominantly influenced by the chemistry of influent groundwater. The unconfined Abbotsford aquifer and shallow confined aquifers contain a predominantly calcium carbonate water, which increases in total dissolved solids with increased residence time (Carmichael et al., 1995). Groundwater in the confined aquifers evolves toward a sodium-bicarbonate type water with depth and is brackish at elevations below sea level (Halstead, 1966; Piteau, 1991; Carmichael et al., 1995). In addition, elevated nitrate concentrations are commonly encountered within the unconfined Abbotsford aquifer and are attributed to agricultural activity and possible contribution by septic systems (Liebscher et al., 1992; Carmichael et al., 1995; Wassenaar, 1995). Sulphur-containing fertilizers, which are used locally to create favourable growing conditions for berry crops by lowering the soil pH, may also contribute increased sulphate concentrations within near surface groundwater.

The variation in stream water chemistry along Bertrand Creek can be illustrated in terms of both a variation in EC (at 25°C, Figure 3.7) and the composition of major ions (Figure 3.8).

EC values within Bertrand Creek decreased with distance downstream (Figure 3.7), which is counter to the natural evolution of a stream fed by groundwater (Livingstone, 1963). The trend became more pronounced through the 2007 dry season (Figure 3.7). In July and August, stream water EC values locally decreased between stations B4 and B3. Results of synoptic chemical sampling indicate bicarbonate and sodium ions dominated the chemical composition of baseflow along Bertrand Creek (Figure 3.8). Dissolved ion concentrations behaved in agreement to EC values, decreasing with time into the dry season (not shown) with a pronounced local decrease in the vicinity of station B3 (Figure 3.8). Dissolved ion concentrations are reported in Appendix D, including dissolved silicon concentrations.

At the headwater, stream water chemical composition is a Na-Cl-HCO_3 type water similar to deep groundwater (Figure 3.8), which suggests that significant surface discharge from a deep groundwater well in the area influences headwater streamflow and chemistry (Envirowest, 2000). Discharge from the well is estimated at 8 L/s (Schmidt, 2011). Further details about the well were unavailable. As water flowed downstream through the urban area of Aldergrove and nearby farmlands toward km.11, dissolved constituents originating from the deep groundwater source became diluted, while calcium, sulphate, silicon, and nitrate concentrations increased. Dilution of the stream water is partly attributed to mixing with fresh water within surface storage zones and from the urban storm drain system. The increased calcium, sulphate, and silicon concentrations suggest that a perched groundwater bearing zone in the vicinity of the urban area (Figure 2.4) contributes to baseflow. These near-stream perched zones can be important sources of water for sustaining baseflows (e.g., Niswonger and Fogg, 2008; Banks et al., 2011b); unfortunately, streamflow

measurements are unavailable within this area. Considering the low hydraulic conductivity within near-surface streambed sediments along this reach (Figure 3.4), hyporheic flow is not considered to play a significant role in moderating stream water chemistry.

Dissolved concentrations of most major ions and EC values in stream water decreased as the creek flowed downstream over the GLF portion of the unconfined aquifer between km.11 and km.6.3 (Figure 3.8). EC measurements indicate that the change in stream water chemistry occurs primarily at the downstream end of the GLF deposits, between stations B4 and B3 (Figure 3.7b). Along this stream length, tributary contributions to streamflow are absent, and chemistry and isotopic results suggest that groundwater recharged by recent winter precipitation discharges from the GLF deposit and maintains streamflow between stations B2 and B4. The chemical composition and concentration of stream water at station B3 was similar to groundwater sampled previously from a shallow well installed within the GLF deposit (Carmichael et al., 1995). Furthermore, the stream water had an isotopic composition lighter than the annual weighted mean precipitation for the nearest isotopic station at Victoria, B.C. (Canadian Network for Isotopes in Precipitation, 2009), which suggests that the water originated from winter rainfall.

In the vicinity of station B2 (km.6.1), stream water EC and aqueous concentrations associated with weathering dissolution (Ca, Mg, Na, K, Si, and SO_4) increased considerably (Figure 3.8). The chemical composition of surface water at station B2 was different from upstream waters, which suggests a different and chemically distinct source water contributes to streamflow. The increase in stream water EC value was accompanied by elevated EC

values within mini-piezometers (up to 477 µS/cm, Figure 3.7b) and within a surface spring at this location. The spring contributed approximately 0.05 L/s to the stream during the study period. Spring water EC values ranged from 360 to 400 µS/cm; spring water temperatures ranged from 12.5 to 13.5°C and were cooler than stream water. There are two possible explanations for the increase in dissolved concentrations at station B2: (1) groundwater from the shallow unconfined aquifer was anthropogenically impacted, or (2) groundwater with increased residence time was contributing to streamflow. Chloride concentrations did not increase at B2, which challenges the interpretation of a direct anthropogenic influence on the source water chemistry since increased chloride concentrations typically accompany anthropogenic impacts associated with fertilizers, manure, and septic systems (Kohut et al., 1989; Ritter and Chirnside, 1990; Robertson et al., 1991). However, a mini-piezometer sampled at this location had measurable concentrations of phosphate (0.5 mg/L) and nitrate (6 mg/L as N), which suggests an anthropogenic influence. The presence of the surface spring and the dog-leg turn in the channel hint that a change in subsurface geology may contribute the change in chemistry and increased groundwater discharge, especially since a confined aquifer is present beneath the stream at station B2. Unfortunately, no borehole records are available in this area to interpret the potential for hydrologic connection between the deeper confined (WALD) and unconfined Abbotsford aquifer (Figure 2.4). Further investigation is warranted in this area to determine the source of increased ionic concentrations.

Downstream of station B2, EC values and aqueous concentrations decrease attributed to an influx of groundwater (Figure 3.8). EC values decreased from 204 to 186 µS/cm within the

upstream 700 m of the EC profile along Reach A, then stabilized along the downstream portion of the profile (Figure 3.7a). Most of the EC drop (10 μS/cm) notably occurred coincident with cooling stream water temperatures over a 300 m stream length between stations A4 and A3. While small in magnitude, the change in EC suggests this section may receive increased groundwater contribution. A negligible change in EC values and aqueous concentrations between the downstream extent of Reach A and the outlet suggests either the groundwater contribution over this length is also negligible, or that stream chemistry is representative of average groundwater conditions and further contribution of groundwater has no significant influence on stream water quality (Figure 3.7 and Figure 3.8). As discussed previously, the measured change in streamflow along this lower 2 km stream length was insignificant.

Assuming EC acts conservatively, streamflow and EC can be employed in a mass balance calculation to determine the relative contribution of two source waters to streamflow. For a mass balance at station B2, the two end members assumed to contribute to streamflow are (Figure 3.7): groundwater from the GLF deposit with low EC (165 μS/cm) and the spring water with elevated EC (400 μS/cm). During August baseflow conditions, a mass balance calculation suggests that 70% of the streamflow at station B2 originates as groundwater with the same EC as water in the GLF deposit. The wide range of EC values encountered within upwelling B-depth mini-piezometers (71 to 470 μS/cm, SD: 84; n=20), which are generally considered representative of upwelling groundwater, precludes the opportunity to use an average groundwater EC to estimate groundwater contribution elsewhere along Bertrand Creek (Figure 3.7).

3.4.5 Fluid Flux Across the Streambed

3.4.5.1 Mini-piezometers

Flux across the streambed calculated using mini-piezometer measurements on August 15 and 16, 2007, is shown in Figure 3.9 and included on Table 3.1. The magnitude and direction of flux across the streambed has high spatial variability at the local scale. For example, the seepage direction differed among mini-piezometers installed within a 100 m downstream distance [MP-B6(1) and MP-B6(2); MP-A3(2), MP-A3(3), and MP-A3(4)], at opposing banks within the same transect [MP-A1(1) and MP-A2(2)], and within nested mini-piezometers at the same location [MP-B4(1)]. The spatial variability is attributed to the influence of hyporheic flow in addition to exchange with groundwater (e.g., Harvey and Bencala, 1993; Wroblicky et al., 1998; Storey et al., 2003). Hyporheic flow increases the spatial variability at the local scale by creating upwelling and downwelling patterns associated with riffle-pool sequences (Storey et al., 2003) and differences in streambed permeability (Hinton et al., 1993; Hill et al., 1998; Cardenas et al., 2004). This local-scale spatial variability creates noise among measurements along Reach A and much of Reach B (Figure 3.9).

In contrast with the aforementioned variability, a consistent direction of vertical hydraulic gradient was observed among all mini-piezometers within Reach C and surrounding station B2 (Figure 3.9). The consistent direction along Reach C is attributed to the low permeability streambed; Storey et al. (2003) suggest that a minimum permeability exists below which hyporheic flow will not develop for a given elevation difference in a riffle-pool sequence. Therefore, streambed fluxes along Reach C represent stream water infiltration to

the aquifer. The B2 site is located where the highest gains in streamflow were measured along Bertrand Creek. Hyporheic exchange can be limited by strongly upwelling groundwater (Cardenas and Wilson, 2006), and these fluxes are likely representative of discharging groundwater.

Comparison of EC values in stream water with values in mini-piezometers can help elucidate if streambed fluxes are representative of hyporheic flow or an interaction with groundwater. Where gaining conditions are present, a significant difference (±20 μS/cm) between surface water and B-depth mini-piezometer EC values can indicate locations where subsurface water predominantly consists of groundwater and streambed fluxes are likely representative of groundwater conditions. EC values in mini-piezometers differed from stream water values by more than 20 μS/cm at the B2 site, which was previously discussed to be representative of groundwater conditions, and at MP-B6(1) and MP-A3(4)w (Figure 3.7). Since water temperatures cooler than stream water were measured within mini-piezometers MP-B6(1) and MP-A3(4)w, these locations likely represent upwelling groundwater. As discussed below, the vertical hydraulic gradient at all mini-piezometers at the A4 site indicate downwelling conditions (Figure 3.9), but EC values were significantly different than stream water in these mini-piezometers (Figure 3.7).

Due to hyporheic flow and heterogeneities in streambed sediments, the interpretation of streambed flux is sensitive to the vertical resolution of nested mini-piezometer measurements. Specifically, the magnitude of the hydraulic gradient associated with B-depth mini-piezometers differs if calculated with respect to the stream stage or the A-depth

hydraulic head. While measurement error can contribute to the magnitude of discrepancy, the discrepancy between water levels was visible in the field at MP-A4(1): water levels within both A- and B-depth mini-piezometers were lower than the stream, indicating downwelling conditions. However, the A- water level was lower than the B-water level, which indicates that upwelling conditions were present between the screen depths of the A- and B-mini-piezometers. This discrepancy explains the significant difference between EC values within mini-piezometers and stream water mentioned above in the presence of a negative vertical hydraulic gradient. It further demonstrates the challenge of using point-based measurements to calculate area-averaged estimates of streambed flux and the effect of measurement resolution on calculated fluxes.

3.4.5.2 Streambed Temperature

The direction of flux interpreted using stream water and streambed temperature records at three locations along Reach B (Figure 3.2, inset b) agrees with the direction of flux determined using mini-piezometers. The direction of flux was estimated by comparing the diurnal variation of temperature measured in stream water with the temperature variation measured in streambed sediments (Silliman and Booth, 1993). At T-B1(2), the measured thermal variation was less than 10% at and below 0.2 m depth within the streambed (Figure 3.10). Silliman et al. (1995) demonstrate that conduction of heat can account for 15-20% of the streambed temperature variation at 25 cm depth, which suggests that upwelling conditions were present at T-B1(2). Similarly at T-B2(1), a low amplitude of temperature variation (20%) combined with a streambed temperature very close to the average groundwater temperature (10°C; Cox and Kahle, 1999) at 1.0 m depth suggests

groundwater was upwelling at T-B2(1). Mini-piezometer measurements also indicated upwelling conditions at these two sites.

At T-B4(1), the diurnal temperature variation in streambed sediments was 60% of the stream water variation at 20 cm and 20% at 50 cm depth (Figure 3.10). This larger temperature variation suggests stream water is infiltrating at this location (Silliman and Booth, 1993). Given the low magnitude and conflicting direction of vertical gradients measured using mini-piezometers and the highly permeable streambed sediments (MP-B4(1), Table 3.1), the streambed temperature variation is likely influenced by local-scale lateral and vertical hyporheic flow.

3.4.6 Groundwater Systems in Bertrand Creek Watershed

3.4.6.1 Hydraulic Head Fluctuations Beneath the Stream

Figure 3.11 shows the change in hydraulic head in mini-piezometers installed 1 m beneath the streambed between the middle of June and September, 2007. Only locations with measurements available over this period are included on Figure 3.11. The following summarizes the measured change in hydraulic head beneath the channel in 2007 with distance upstream:

- Hydraulic heads declined less than 15 cm along Reach A and the downstream portion of Reach B (to an upstream distance of 6.3 km). An exception was a hydraulic head decline of 20 cm (km.5.7) where the channel geomorphology transitioned from a well defined channel into a broad gravel floodplain. With time into the dry season, a greater decline in stream water height with respect to the sub-stream hydraulic head

caused an increasingly upward gradient at some mini-piezometer locations. Hydraulic heads did not decline below the elevation of the streambed.

- Hydraulic head at station B3 (km.6.3) declined below the elevation of the streambed. The decline in hydraulic head became less pronounced with distance upstream within the GLF deposit to km.7.5.
- The largest fluctuations in hydraulic head were measured along Reach C, where all hydraulic heads declined below the elevation of the streambed and caused the stream to become perched.

Substantial rainfall at the end of the dry season increased the hydraulic heads above the stream stage and gaining conditions were present at all measurement sites.

In 2006, a piezometer was installed in the streambed at station B4 (km.6.7). The hydraulic head within the piezometer dropped 0.7 m below the streambed and the stream went dry (Figure 3.12). Several rain events were subsequently necessary to raise the water level and resume streamflow. In 2007, water remained in the channel at this location and hydraulic heads within the piezometer were within millimetres of the stream water height.

3.4.6.2 Hydraulic Head in Private Wells

Water levels within private groundwater wells installed in the unconfined aquifer indicate that the water table follows topography (Figure 3.9). A potentiometric map at a scale useful to interpret surface water–groundwater interaction at the stream could not be constructed due to the undulating glacial terrain and the limited number of measurements. Figure 3.13 shows the decline in groundwater level between June and September, 2007, versus distance of the

well from Bertrand Creek. The plot reveals that seasonal water level fluctuation is greater in wells more distant from the creek. However, this relationship is muted for wells located within the GLF deposit.

3.4.6.3 Groundwater Flow

Average ratios of the lateral (valley) to longitudinal (channel) slope along sections of Bertrand Creek are presented in Table 3.2. The slope ratio is <1 upstream of km.6.8 (within the GLF deposit) and east of the channel 2 km prior to the watershed outlet. The ratio increases elsewhere within the watershed owing to an increase in lateral slope. Given the assumption that the water table in a phreatic aquifer is a replica of topography, the component of groundwater flow in the downstream direction is expected to increase as the topographic slope ratio in Table 3.2 decreases. Therefore, a greater component of underflow (Meinzer, 1923; Larkin and Sharp, 1992) is expected along Bertrand Creek within the upper portion of the GLF deposit and near the outlet while a baseflow-dominant groundwater flow direction is expected elsewhere within the unconfined aquifer (Table 3.2). Recognizing that the groundwater flow direction adjacent to a stream is sensitive to recharge (Meigs and Bahr, 1995; Wroblicky et al., 1998; Vidon and Hill, 2004), groundwater flow within the unconfined Abbotsford aquifer is expected to have a greater component of flow toward the stream following winter rains than late in the summer.

Several topographic features in the lower watershed indicate that groundwater contribution along the lower 2 km of the stream may be negligible or that the stream is losing water to groundwater within this reach. First, the slope ratio on the east side of the stream is <1

(Table 3.2) which suggests the predominant direction of groundwater flow is parallel the stream. Second, a stream valley situated just beyond the eastern watershed boundary is 5 m lower in elevation than Bertrand Creek (Figure 3.2). In the absence of a significant lateral gradient to maintain groundwater flow toward Bertrand Creek, groundwater flow paths that originate within the watershed may cross the topographic divide and flow toward the adjacent, lower-elevation valley during dry conditions (Winter, 1976, 1999). This topography-based interpretation is corroborated by negligible changes in measured streamflows (Figure 3.5) and stream water chemistry (Figure 3.8) along the lower 2 km of the stream.

3.4.7 Geomorphic Controls on Surface Water–Groundwater Interaction

3.4.7.1 Topographic Controls

The topographic slope adjacent to Bertrand Creek is an important control of the seasonal nature of stream–aquifer exchange. Topography influences the development of underflow- and baseflow-dominant groundwater flow systems, which in turn exhibit different hydrologic responses in stream–aquifer interaction as the dry season progresses. These differences in hydrologic response, and the role that upslope and downslope topographic characteristics play in influencing the responses along Bertrand Creek, are discussed below.

Baseflow-dominant stream reaches have smaller seasonal water table fluctuations adjacent the stream and maintain more persistent gaining conditions than underflow-dominant stream reaches. For example, along Reach C topographic conditions are conducive to the development of underflow-dominant groundwater flow, and the stream seasonally transitions

from gaining to losing as the water table adjacent the stream declines below the channel (Figure 3.11). The seasonal water table decline does not appear to significantly increase with distance from the stream (Figure 3.13). In contrast, where groundwater flow is baseflow-dominant along Reach A, stream sections remain gaining and seasonal hydraulic head fluctuations beneath the stream are small (Figure 3.11). Where the vertical hydraulic gradient within mini-piezometers suggests losing conditions are present along Reach A (Figure 3.9), the losing conditions appear to be the influence of local hyporheic flow as opposed to conditions representative of a losing stream reach. The greatest seasonal decline of the water table along this segment occurs within wells located farthest from Bertrand Creek (Figure 3.13).

The height of the adjacent ground surface above the stream, and by inference the water table, is an important attribute governing the persistence of groundwater discharge along the stream. Groundwater recharge within upland areas maintains baseflow-dominant stream segments as gaining reaches through the dry season (Figure 3.1a). Absent of an adjacent upland, underflow-dominant segments of Bertrand Creek recharge the aquifer as hydraulic heads decrease through the dry season (Figure 3.1b). These observations agree with studies by Devito et al. (1996) and Vidon and Hill (2004), who demonstrated that the likelihood of a surface water body to remain connected to the water table and remain fed by groundwater discharge is positively correlated with the thickness of the adjacent upland permeable sediments.

In addition to characteristics of the upslope aquifer, previous studies in hillslope environments have discussed the importance of the downslope topography in influencing the hydraulic potential at a subsurface point (Speight, 1974, 1980; Hjerdt et al., 2004). As discussed by Hjerdt et al. (2004), a shallow downstream slope impedes drainage of groundwater beneath a stream while a steeper slope enhances drainage and promotes water table decline. In this study, the drop in streambed elevation downstream of station B3 appears to facilitate drainage from the upgradient aquifer and promote seasonal decline of the upstream water table. Assuming that water table drawdown is not locally affected by pumping or vegetative water use, the maximum possible decline of the water table upstream of station B3 will be controlled by the water table elevation in the downgradient groundwater discharge zone.

The losing conditions upstream of station B3 develop in exception to the preceding discussion. The slope ratio in Table 3.2 indicates that baseflow-dominant groundwater flow could be expected along the channel immediately upstream of station B3; however, this section of the stream became losing during both years, and dry in 2006. When the slope ratio surrounding station B3 is assessed at a spatial resolution of only 10's of metres, the drop in streambed elevation at B3 has a greater influence on the slope ratio, and indicates a greater potential for underflow-dominant groundwater flow. This discrepancy suggests that changes in topographic slope at a resolution finer than the 300 m scale assessed in Table 3.2 may exert a significant control on stream–aquifer interaction.

The slope ratio in Table 3.2 indicates the relative balance between the upslope ability to supply groundwater flow toward the stream (lateral slope) and the downslope ability to convey groundwater downstream (longitudinal slope). Essentially, where upstream supply exceeds downstream conveyance groundwater flow lines converge, and groundwater discharge to the stream and gaining conditions are more likely. The slope ratio therefore indicates the influence of landscape on the seasonal nature of surface water–groundwater exchange (Ivkovic, 2009). Using the slope ratio to assess the potential development of convergent groundwater flow requires simplifying assumptions: (1) the aquifer is unconfined; (2) the thickness of the aquifer under the stream does not increase as topography decreases; and (3) the subsurface hydraulic conductivity within the aquifer is relatively homogeneous. In addition to lateral convergence, groundwater flow paths may converge vertically if a decreasing aquifer thickness accompanies a decrease in topography and (e.g., Konrad, 2006b).

3.4.7.2 Locations of Focused Groundwater Discharge to Bertrand Creek

Groundwater discharge is expected to be focused along Bertrand Creek at locations where groundwater flow lines converge. Subsurface flow lines are known to converge at: breaks in slope, decreases in thickness of a permeable unit, concave hillslopes, and locations where two flow lines meet such as beneath a stream (Kirkby and Chorley, 1967; Winter, 1976, 1999). The greatest contribution of groundwater discharge to Bertrand Creek occurs at the break in slope downstream of station B3. This location contributes approximately 40 percent of the baseflow measured at the outlet. Along Reach A, the change in stream water EC value along a 300 m stream section between stations A3 and A4 (Figure 3.7) suggests that this

stream length receives an increased contribution of groundwater. This stream length is located adjacent to a concave hillslope. Similar locations of focused groundwater discharge could be inferred from a study of watershed topography for any stream–aquifer system.

3.4.7.3 Permeability Controls

Permeability controls surface water–groundwater interaction at multiple scales within the Bertrand Creek Watershed. At the large-scale, Bertrand Creek is well connected to the unconfined Abbotsford aquifer in a manner similar to other streams with high permeability streambed sediments overlying alluvial aquifers (e.g., Christensen et al., 1998; Becker et al., 2004). The rate of streambed seepage varies along the stream length owing to differences in streambed permeability (Fleckstein et al., 2006; Frei et al., 2009). This influence of streambed permeability is apparent where the water table declines below the streambed along the GLF deposit: along Reach C, the low permeability streambed limits infiltration and the stream becomes perched as the water table declines. In contrast, a strong hydrologic connection between the stream and aquifer is established by the high permeability streambed farther downstream, and the channel goes dry when the water table declines.

At the local-scale, hyporheic flow dominates fluxes along the Bertrand Creek streambed where a high permeability streambed exists without strongly upwelling groundwater. Previous field and modeling work has shown that the depth of hyporheic influence can exceed 1 to 3 m in coarse-grained streambeds (Hill et al., 1998; Woessner, 2000; Puckett et al., 2008). Studies that compare Darcy-based streambed flux estimates with area-averaged measurements have found measurements differ by up to two orders of magnitude (Cey et al.,

1998; Becker et al., 2004). In this study, the seepage direction determined from point-based measurements at 1 m depth along the sandy streambed has high spatial variability and these values could not be extrapolated to areal estimates of streambed flux.

3.4.8 Conceptual Model of Bertrand Creek Watershed

A conceptual model of surface water–groundwater interaction along Bertrand Creek has been developed based on the findings of this study (Figure 3.14). Within the upper watershed, streamflow is sustained by rainfall, significant discharge from a groundwater well, and perched groundwater zones. Exchange across the streambed is small due to the low permeability of streambed sediments. Where the channel flows over the downstream GLF deposit of the unconfined aquifer, the direction of streambed exchange is seasonally dependent: baseflows are groundwater-fed following heavy winter rains, but during the summer the water table declines along stream segments conducive to underflow-dominant groundwater flow and the stream recharges the aquifers. Along this length, infiltration can exceed streamflow during summers with low rainfall, and the channel can become dry. The largest groundwater contributions to streamflow occur at the break in slope at the downstream end of the GLF deposit (km.6.2) prior to the southward bend in the channel. Within the lower watershed, the stream is groundwater-fed and variably gaining. Gaining conditions are sustained through the dry season along much of this lower stream length by baseflow-dominant groundwater flow. Negligible change in streamflow occurs along the 2 km of stream preceding the outlet where underflow-dominant groundwater flow exists. Hyporheic flow creates local-scale upwelling and downwelling systems along much of the sandy streambed unless strongly upwelling groundwater is present.

Development of streamflow along Bertrand Creek is similar to flow in streams originating in mountain valleys and flowing onto alluvial plains. These river systems can broadly be described as runoff-fed along upper reaches, groundwater-recharging along the upper alluvial plain, and groundwater fed along lower reaches (see discussion in Larned et al., 2008). Well documented examples of these larger river systems, which also become dry mid-watershed, include the Selwyn River in New Zealand (Larned et al., 2008) and Methow River in Washington, U.S. (Konrad, 2006a).

3.5 Conclusions

In this study, a conceptual model of stream–aquifer interaction along Bertrand Creek during the baseflow conditions has been developed using hydrologic measurements, stream water chemistry, and point-based measurements of streambed flux. These measurements are complemented by an assessment of the topographic slope over the alluvial aquifer to assess the groundwater flow direction and the primary controls of stream–aquifer interaction along the creek. The results improve our understanding of stream–aquifer interaction in a glaciated watershed:

1) Groundwater discharge to Bertrand Creek is spatially variable. The greatest groundwater contributions are focused at locations where groundwater flow lines are expected to converge. These locations can be predicted based on topography.
2) Small-scale hyporheic flow dominates fluxes within the Bertrand Creek where a high permeability streambed exists without strongly upwelling groundwater. Hyporheic flow creates significant local-scale variability amongst point-based measurements and the influences of which exceed 1 m depth at many locations. The spatial variability of these

measurements precludes the ability to extrapolate values into areal estimates of streambed flux.

3) The use of topographic slope to infer groundwater flow direction as underflow- or baseflow-dominant provides insight to stream–aquifer interaction. This relationship can be expressed in terms of the slope ratio. As shown by data collected in Bertrand Creek Watershed, where the groundwater flow direction is baseflow-dominant, groundwater flow toward the stream is maintained by recharge in nearby topographic highs, and hydraulic head fluctuations beneath the stream remain small. In contrast, where groundwater flow is underflow-dominant, losing conditions can develop on a seasonal basis driven by larger fluctuations in hydraulic head.
4) At any location beneath the stream, the connectivity of the stream–aquifer system develops as a balance between the supply of water from upslope deposits and the capacity of the downslope deposits to convey water beneath the channel. This balance is evident at station B3 where a drop in streambed elevation facilitates drainage from the upstream aquifer and establishes conditions that created a dry streambed exceeding 500 m in length in 2006.
5) This study demonstrates how a combination of hydrometric and tracer based methods combined with a study of topography can be used to characterize surface water–groundwater interaction along a stream. Results from streamflow measurements, geochemical sampling, electrical conductivity profiles, and mini-piezometers can be used to characterize the variability of the interaction along the stream length. An analysis of topography can provide insight into why the variability occurs.

6) A watershed-scale characterization must consider processes operating at many different spatial scales. These large- and small-scale processes influence streambed fluxes and both the chemistry of stream water and the water beneath the streambed.

This chapter presented an analysis of field data collected during dry season conditions that allowed the development of a watershed-scale conceptual model of surface water–groundwater interaction along Bertrand Creek. In the following chapter, a fully integrated surface-subsurface hydrologic model of Bertrand Creek Watershed is developed to further explore the nature of the stream–aquifer interactions and to investigate how to represent the mechanisms which controls these interactions within the model. The numerical model is based on the conceptual model developed in this chapter and is calibrated to the 2007 field data set.

Table 3.1 Hydraulic conductivity of streambed sediments and calculated vertical flux

		A-depth (0.3 m)				B-depth (1.0 m)			
Upstream distance (km)	Mini-piezometer Name	Hydraulic conductivity (m/s)	Head dif.[a] (cm)	Vertical hydraulic gradient (-)	Vertical flux (cm/d)	Hydraulic conductivity (m/s)	Head dif. (cm)	Vertical hydraulic gradient (-)	Vertical flux[b] (cm/d)
0.01	BC(1)E	8×10^{-9}	-0.1	-3.3×10^{-3}	<[c]	4×10^{-7}	-22	-2.0×10^{-1}	<
0.06	BC(2)N	--[d]	--	--	--	2×10^{-4}	1.1	1.3×10^{-2}	20
2.06	A1(1)E	8×10^{-4}	-3.5	-1.3×10^{-1}	-900	2×10^{-5}	-4.0	-3.9×10^{-2}	-10
2.06	A1(1)C	2×10^{-4}	0.3	1.0×10^{-2}	20	4×10^{-8}	0.1	9.5×10^{-4}	<
2.06	A1(1)W	6×10^{-5}	0.4	1.3×10^{-2}	7	6×10^{-7}	0.5	4.8×10^{-3}	<
2.10	A1(2)E	--	--	--	--	9×10^{-8}	0.6	1.1×10^{-2}	<
2.10	A1(2)W	3×10^{-4}	0.6	2.0×10^{-2}	50	1×10^{-7}	-0.1	-9.3×10^{-4}	<
2.34	A2(1)E	6×10^{-4}	-0.6	-2.0×10^{-2}	-100	2×10^{-4}	-7.0	-7.3×10^{-2}	-200
2.34	A2(1)W	5×10^{-4}	-8.2	-3.3×10^{-1}	-1500	--	--	--	--
2.40	A2(2)E	3×10^{-4}	-4.7	-1.6×10^{-1}	-440	low[e]	--	--	<
2.40	A2(2)W	7×10^{-5}	0.7	2.3×10^{-2}	20	low	--	--	<
2.59	A3(1)E	--	--	--	--	low	--	--	<
2.62	A3(2)E	--	--	--	--	4×10^{-5}	0.1	1.1×10^{-3}	0.4
2.62	A3(2)W	--	--	--	--	3×10^{-6}	0.6	5.6×10^{-3}	0.1
2.66	A3(3)W	--	--	--	--	2×10^{-4}	-5.0	-4.8×10^{-2}	-70
2.68	A3(4)E	2×10^{-4}	1.1	3.7×10^{-2}	70	4×10^{-5}	1.4	1.4×10^{-2}	8
2.68	A3(4)W	7×10^{-4}	0.6	2.0×10^{-2}	120	4×10^{-5}	1.2	1.2×10^{-2}	8
3.14	A4(1)E	3×10^{-4}	-0.9	-3.0×10^{-2}	-80	1×10^{-5}	-0.3	-3.4×10^{-3}	-1[f]
3.14	A4(1)W	2×10^{-4}	-1.7	-5.7×10^{-2}	-80	1×10^{-5}	-1.2	-1.1×10^{-2}	-2[f]
3.16	A4(2)E	2×10^{-4}	0.0	0	0	2×10^{-5}	-0.9	-9.9×10^{-3}	-3
3.16	A4(2)W	1×10^{-4}	-0.1	-3.3×10^{-3}	-3	8×10^{-6}	-2.6	-2.4×10^{-2}	-3
5.57	B1(1)C	2×10^{-4}	1.6	5.5×10^{-2}	90	low	--	--	<
5.63	B1(2)E	--	--	--	--	3×10^{-4}	0.6	9.4×10^{-3}	20
5.63	B1(2)W	9×10^{-4}	0.5	1.7×10^{-2}	120	4×10^{-4}	0.5	6.0×10^{-3}	30
5.70	B1(3)E	9×10^{-5}	-2.1	-7.0×10^{-2}	-50	3×10^{-4}	-2.8	-2.4×10^{-2}	-30
5.70	B1(3)W	1×10^{-4}	-2.6	-8.7×10^{-2}	-100	3×10^{-4}	-3.8	-4.2×10^{-2}	-70
6.08	B2(1)E	6×10^{-5}	0.4	1.3×10^{-2}	7	3×10^{-4}	2.4	2.6×10^{-2}	20
6.08	B2(1)W	4×10^{-4}	1.0	3.3×10^{-2}	120	3×10^{-4}	1.1	1.3×10^{-2}	40
6.23	B2(2)N	2×10^{-4}	0.9	2.8×10^{-2}	40	9×10^{-5}	3.2	3.2×10^{-2}	30
6.23	B2(2)S	3×10^{-4}	0.4	2.5×10^{-2}	60	3×10^{-4}	0.4	4.5×10^{-3}	10
6.29	B3(1)C	--	--	--	--	3×10^{-5}	-24	-3.0×10^{-1}	-80
6.74	B4(1)N	2×10^{-4}	0.2	9.1×10^{-3}	20	3×10^{-4}	0.0	0	0
6.74	B4(1)S	9×10^{-5}	0.3	1.4×10^{-2}	10	3×10^{-4}	-0.3	-3.1×10^{-3}	-4
7.19	B5(1)N	--	--	--	--	low	--	--	<
7.35	B6(1)N	7×10^{-5}	1.6	5.2×10^{-2}	30	4×10^{-4}	2.4	2.2×10^{-2}	20
7.35	B6(1)S	7×10^{-5}	1.5	4.8×10^{-2}	30	8×10^{-5}	2.7	2.8×10^{-2}	20
7.46	B6(2)N	3×10^{-4}	0.0	0	0	2×10^{-4}	-14	-1.3×10^{-1}	-220
7.46	B6(2)S	7×10^{-5}	-0.9	-2.7×10^{-2}	-20	8×10^{-5}	-11	-1.1×10^{-1}	-70
10.50	C(1)N	1×10^{-5}	-23	-1.4×10^{0}	-140	3×10^{-4}	-25	-4.9×10^{-1}	-90
10.50	C(1)S	3×10^{-5}	-34	-7.7×10^{-1}	-190	3×10^{-4}	-40	-2.9×10^{-1}	-130
10.55	C(2)N	4×10^{-5}	-1.5	-7.5×10^{-2}	-20	2×10^{-5}	-35	-3.8×10^{-1}	-90
10.66	C(3)C	9×10^{-7}	-7.5	-1.0×10^{-1}	-1	5×10^{-4}	-50	-4.9×10^{-1}	-7
10.72	C(4)C	6×10^{-7}	-15	-5.0×10^{-1}	-3	3×10^{-4}	-57	-6.3×10^{-1}	-7
10.77	C(5)N	2×10^{-7}	-12	-4.0×10^{-1}	-1	1×10^{-3} [g]	-65	-7.3×10^{-1}	-3
10.77	C(5)S	3×10^{-7}	-9.0	-3.0×10^{-1}	-1	5×10^{-4}	-65	-7.6×10^{-1}	-4
10.79	C(6)N	6×10^{-8}	1.0	3.3×10^{-2}	<	low	-18	--	<
10.79	C(6)S	4×10^{-7}	-6.5	-2.2×10^{-1}	-1	low	-16	--	<
12.35	D(1)N	low	--	--	<	low	--	--	<
12.35	D(1)S	low	--	--	<	6×10^{-5}	0.0	0	0
14.12	D(2)W	low	--	--	<	low	--	--	<
14.30	D(3)W	low	--	--	<	low	--	--	<
16.84	D(4)W	low	--	--	<	low	--	--	<
17.01	D(5)W	low	--	--	<	low	--	--	<

[a] Head difference measured between center of screen and top of screen bed

[b] Flux calculated using the harmonic average hydraulic conductivity at the A- and B-screen depths

[c] Calculated or interpretted streambed flux is less than +/- 0.1 cm/d

[d] No mini-piezometer installed at this depth and location

[e] Hydraulic conductivity surrounding screen is too low to determine by mini-piezometer slug-test

[f] Direction of seepage flux is positive if calculated using A- and B- depth hydraulic heads instead of stream height and B-depth hydraulic head

[g] Hydraulic conductivity of sediments is too high to test, this value is assumed

Table 3.2. Average lateral valley slope, longitudinal slope, and dominant groundwater flow direction adjacent to Bertrand Creek, averaged over lengths of 300 m

	Segment of stream (stations)	Upstream distance (km)	Longitudinal slope[a] (%)	Lateral slope[b] (%)	Lateral slope/ long. slope ratio	Interpreted groundwater flow direction
OP	Outlet (east) - A1	0.0 to 2.0	0.5	0.3 - 0.4	0.6 - 0.8	Underflow
OP	Outlet (west) - A1	0.0 to 2.0	0.5	0.9	1.8	Baseflow
OP	A1 - A4	2.0 to 3.2	0.4	0.7 - 3.6	2 - 9	Baseflow
OP	A4 - B1	3.2 to 5.5	0.7	2 - 9	3 -13	Baseflow
OP	B1 - B3	5.5 to 6.3	0.4	1.1 - 3.8	3 - 9	Baseflow
GLF	B3 - B4	6.3 to 6.8	0.4	1.5 - 1.8	4 - 5	Baseflow
GLF	B4 - Reach C	6.8 to 10.8	0.3	0.2 - 0.3	0.7 - 1	Underflow

[a] Topographic slope along axis parallel to the stream

[b] Topographic slope along axis perpendicular to the stream (valley slope)

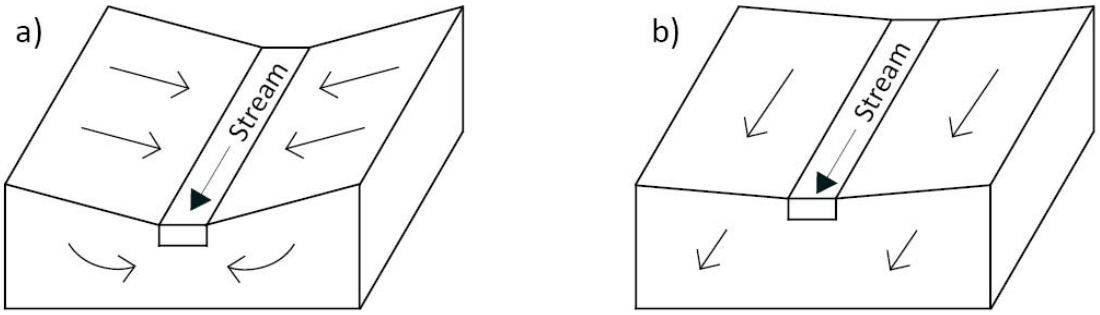

Figure 3.1 a) Baseflow-dominant groundwater flow system and b) underflow-dominant groundwater flow system. Open arrows indicate direction of groundwater flow.

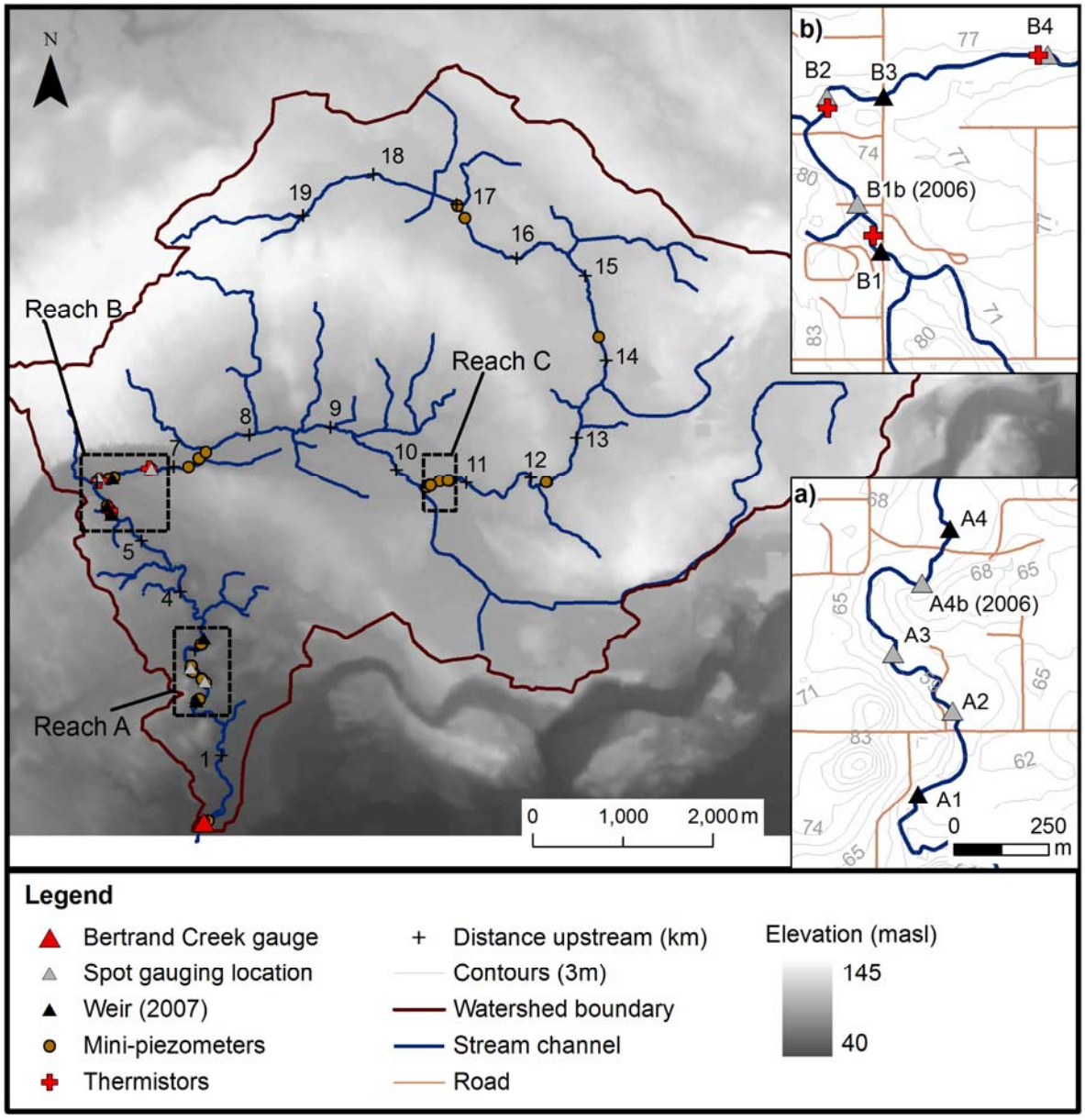

Figure 3.2 Bertrand Creek Watershed with topography and field instrumentation. Inset figures show gauging stations along a) Reach A and b) Reach B.

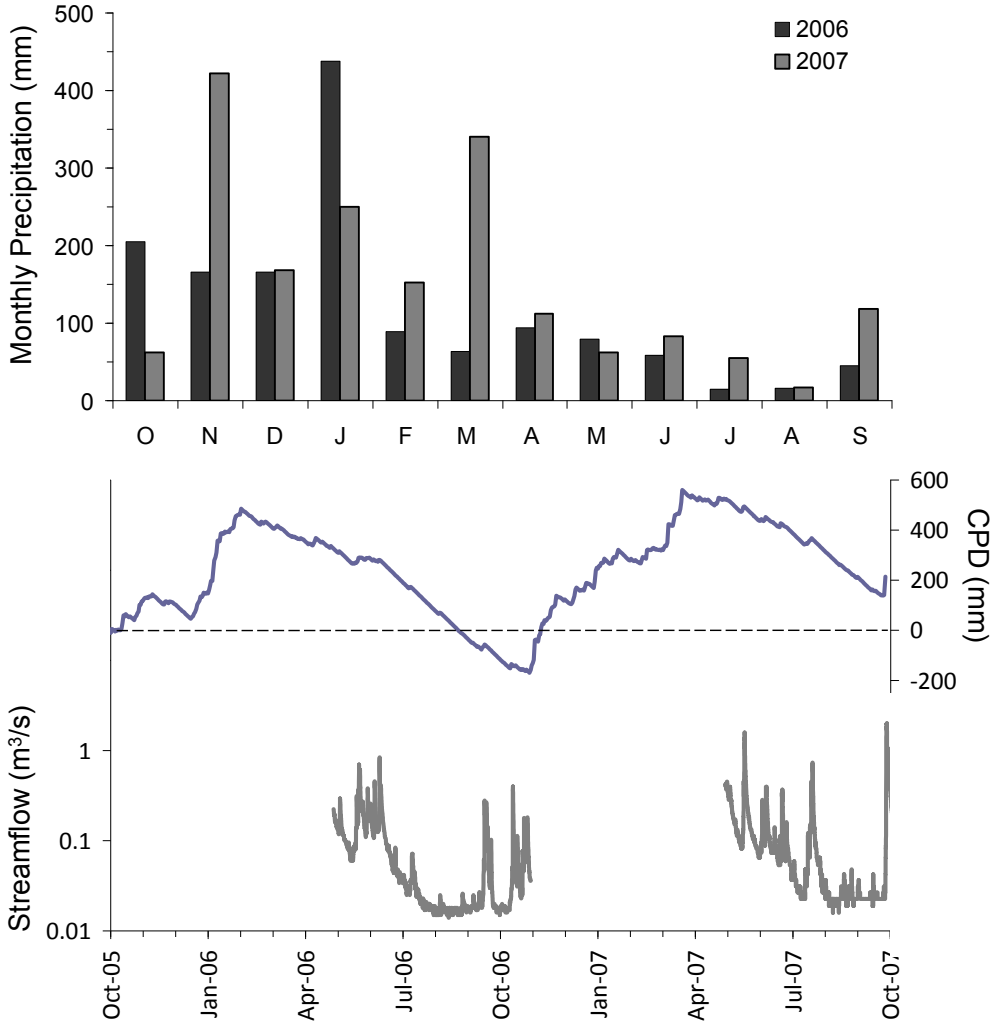

Figure 3.3 Precipitation, cumulative precipitation departure (CPD), and streamflow.

Top: monthly precipitation reported at Abbotsford Airport rain gauge during the 2006 and 2007 hydrologic years (Environment Canada, 2009); middle: cumulative precipitation departure (CPD) from average daily precipitation; and bottom: discharge recorded at the Bertrand Creek gauge (WSC, 2009; USGS, 2010) at the outlet of the watershed.

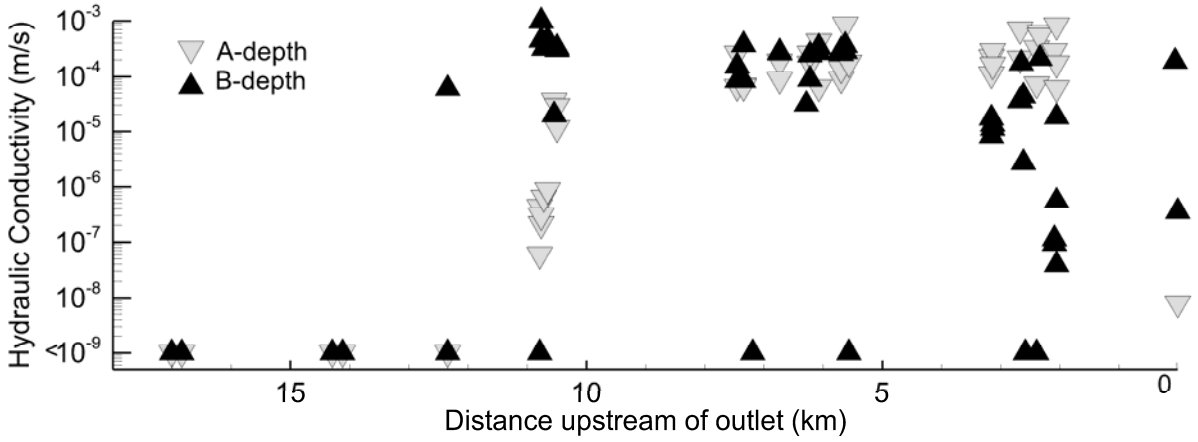

Figure 3.4 Plot of hydraulic conductivity calculated from slug tests in streambed mini-piezometers. A value of $<10^{-9}$ m/s has been assigned where the hydraulic response was too slow to determine by slug test.

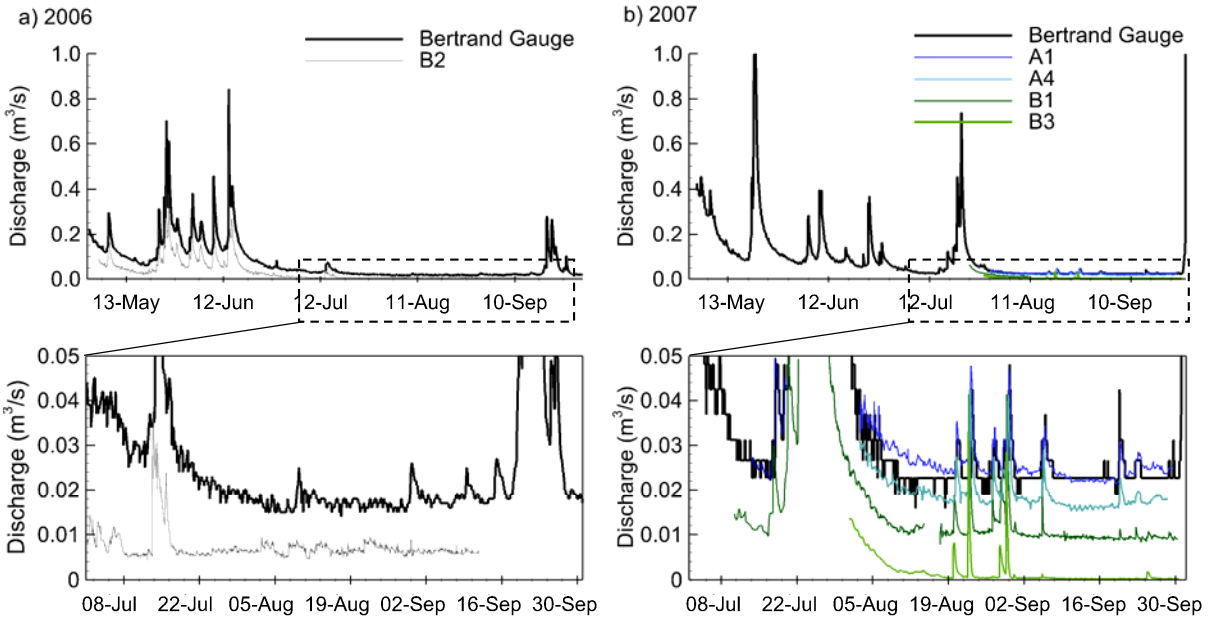

Figure 3.5 Discharge reported at the Bertrand Creek gauge at the watershed outlet along with flows measured at upstream gauging stations in a) 2006 and b) 2007. Inset plots show discharge during the baseflow conditions in greater detail.

Reach A:

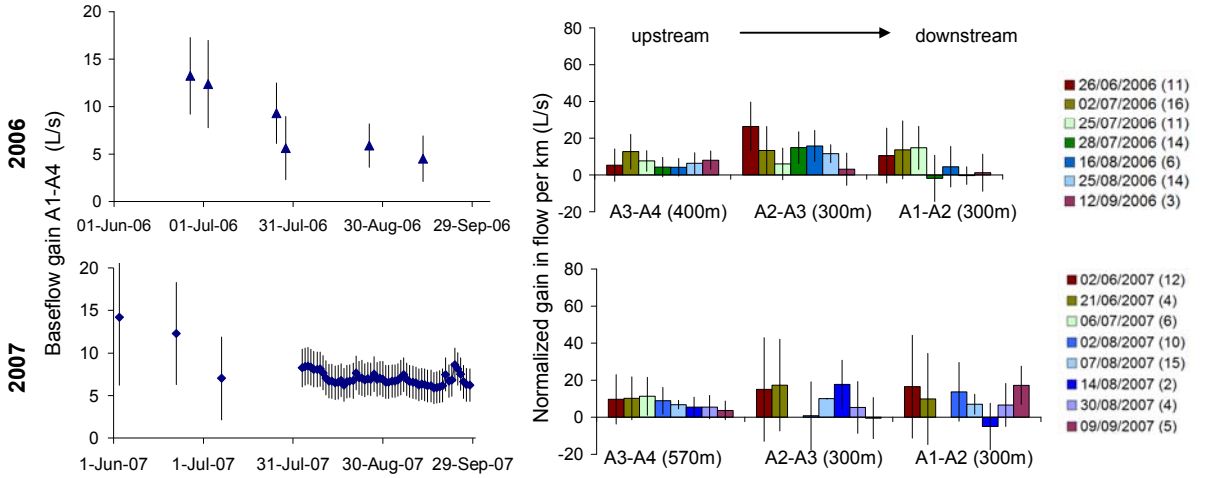

Reach B:

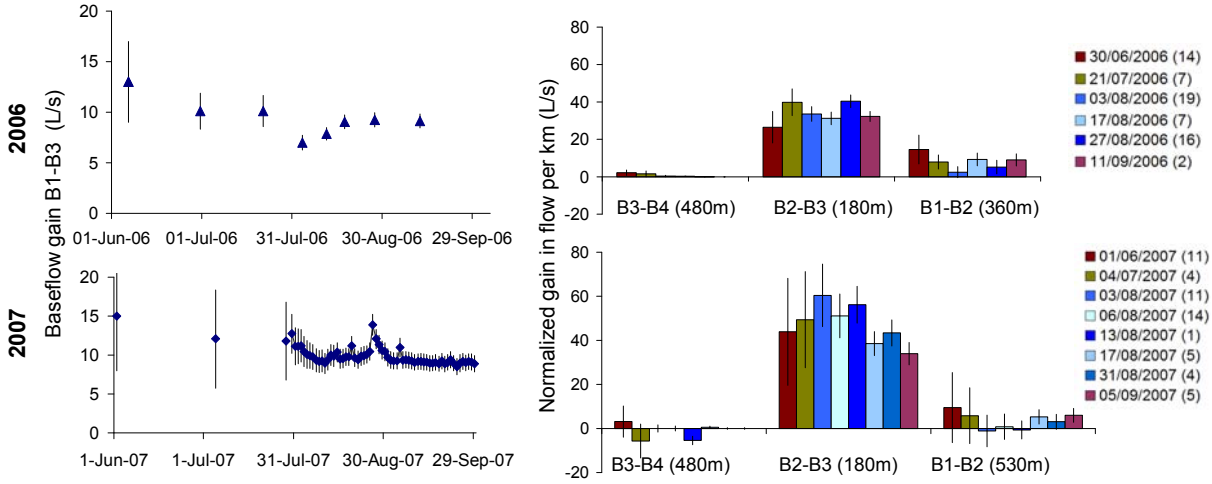

Figure 3.6 Baseflows gains across and within Reach A and Reach B in 2006 and 2007.

Left inset shows baseflow gains across the reaches, determined from spot measurements (triangles) and daily average streamflows where continuous records are available (circles). Right inset shows change in baseflow between successive stations within each reach based on spot measurements. The legend includes the date of measurement and the number of days since rain in brackets. All measurements are shown with estimates of measurement error.

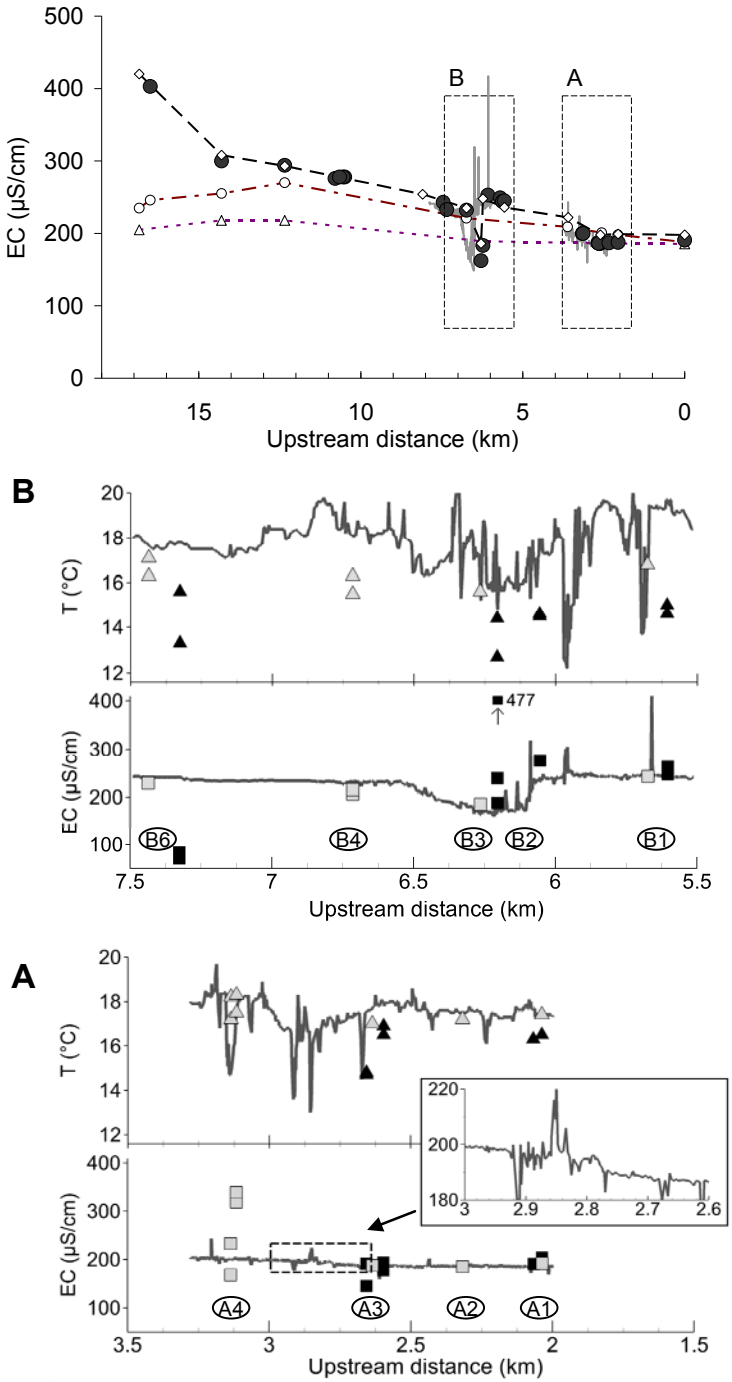

Figure 3.7 Top: EC values (at 25°C) at select locations along the stream in April 2007 (open triangles), May (open circles), July (open diamond), and August (black circles). Inset A and B show EC and temperature profiles along stream lengths encompassing Reach A (August 15, 2007) and Reach B (August 16, 2007) along with values in gaining (black) and losing (grey) mini-piezometers. Gauging station locations are shown on inset plots.

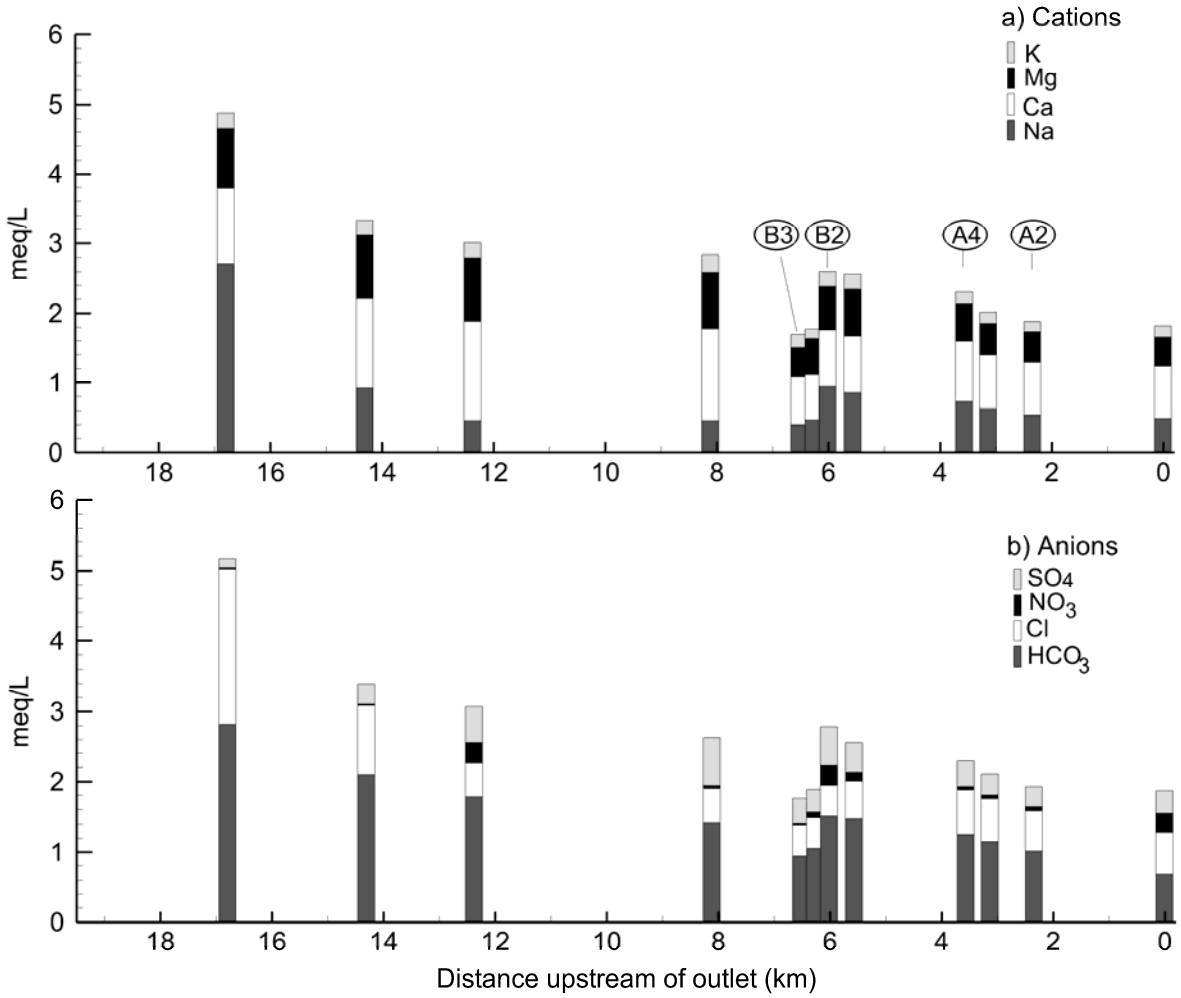

Figure 3.8 Concentrations of major ions at stream sampling locations on August 15, 2007.

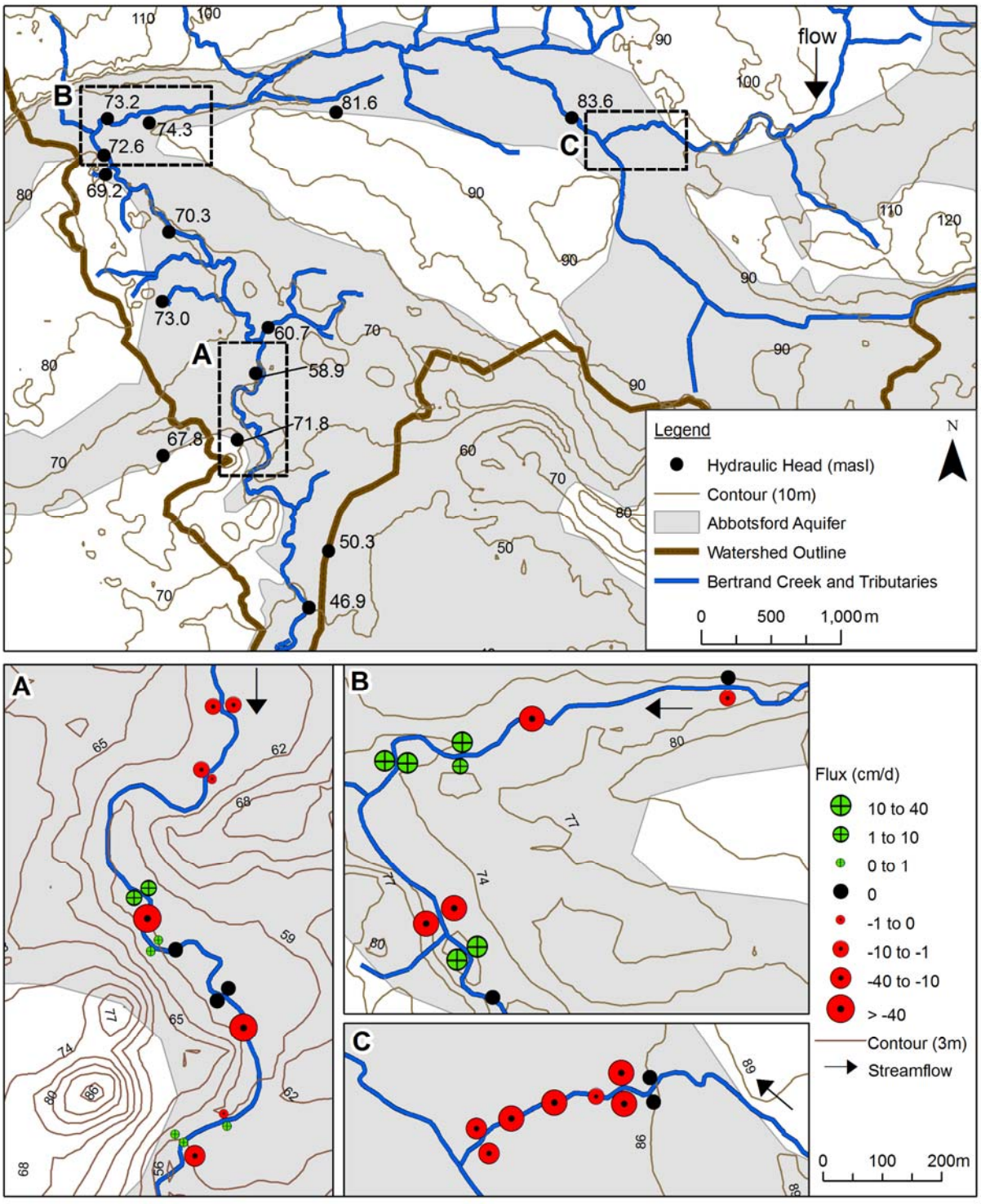

Figure 3.9 Top: Groundwater elevations within wells in the Abbotsford aquifer; Bottom: Darcy-based streambed flux calculated using mini-piezometer measurements on August 15 and 16, 2007, along Reaches A, B, and C. Mini-piezometers were located within the stream channel.

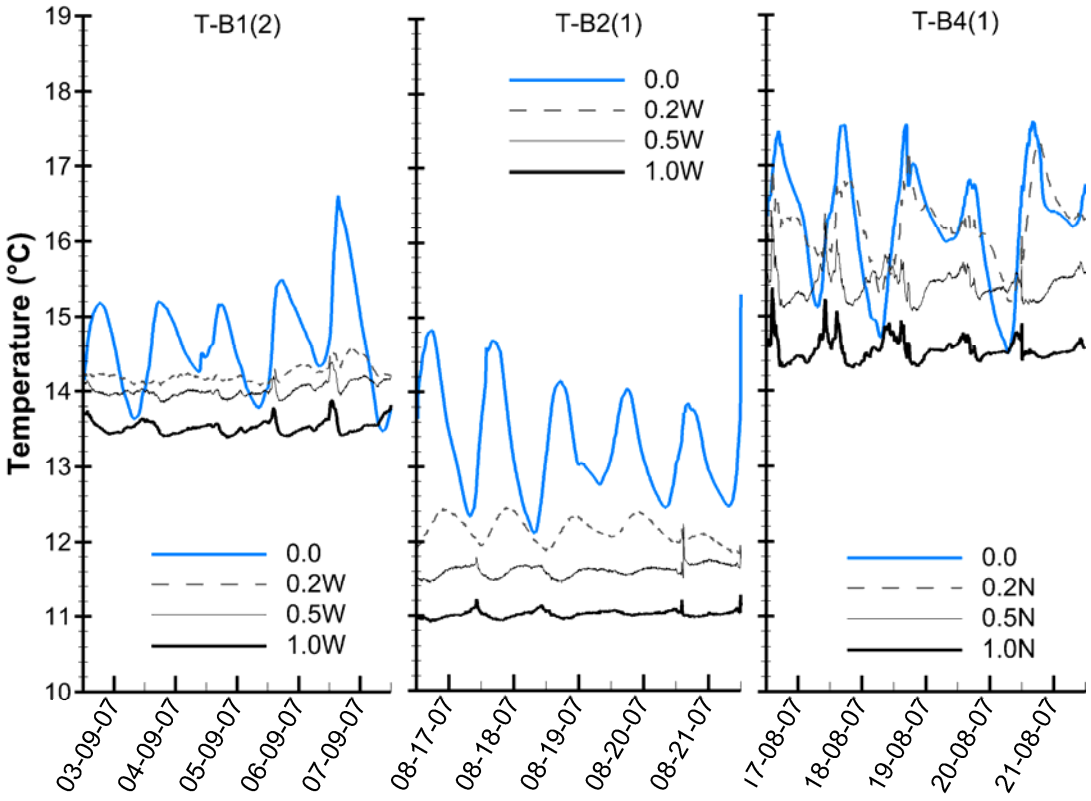

Figure 3.10 Stream water (0.0) and streambed temperature records. Location of temperature measurement is indicated by depth below the streambed (m) and cardinal direction of stream bank (i.e., N = north, W = west).

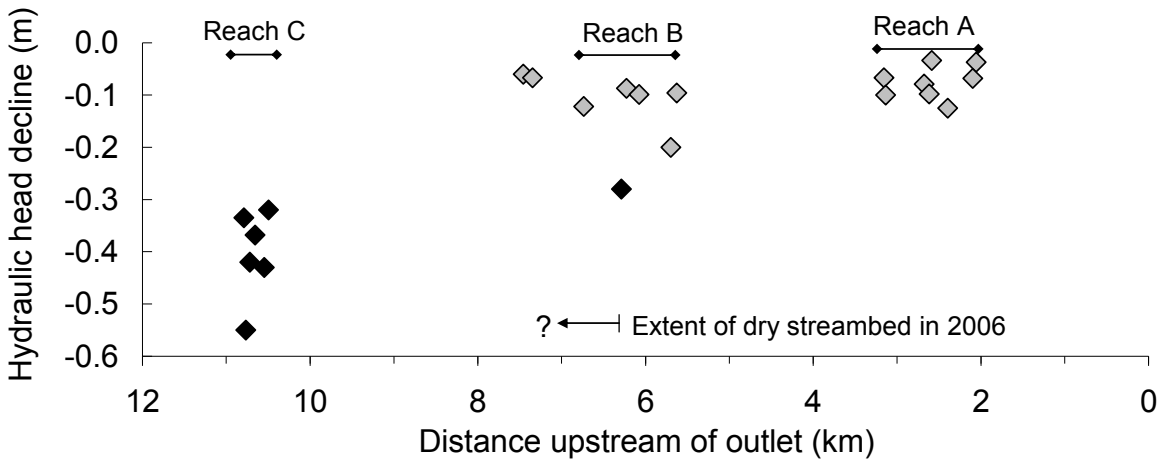

Figure 3.11 The measured decline in hydraulic head within mini-piezometers installed 1 m beneath the streambed between June and September, 2007. Dark symbols indicate locations where the hydraulic head declined below the elevation of the streambed, and grey symbols indicate where the hydraulic head remained above the streambed.

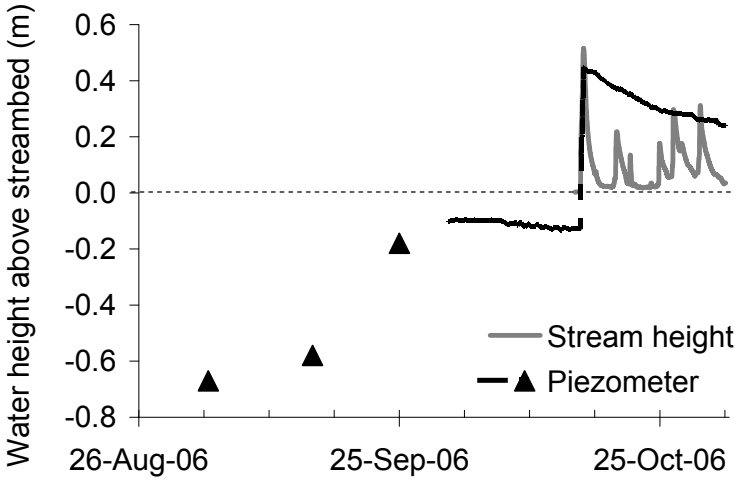

Figure 3.12 Surface water height and hydraulic head measured 1 m below the streambed at station B4 in 2006. The channel was dry at this location from early July to October 15, 2006. Triangles represent manual measurements while solid lines indicate continuous measurements obtained using a data logger.

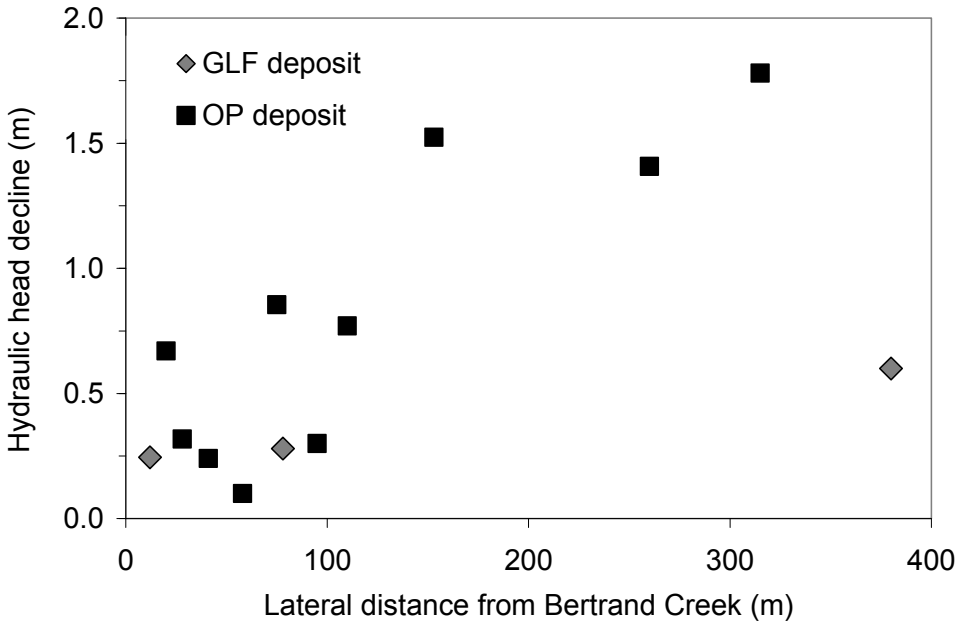

Figure 3.13 The measured decline in hydraulic head within groundwater wells between June and September, 2007, versus distance from Bertrand Creek. All wells were screened in the unconfined aquifer.

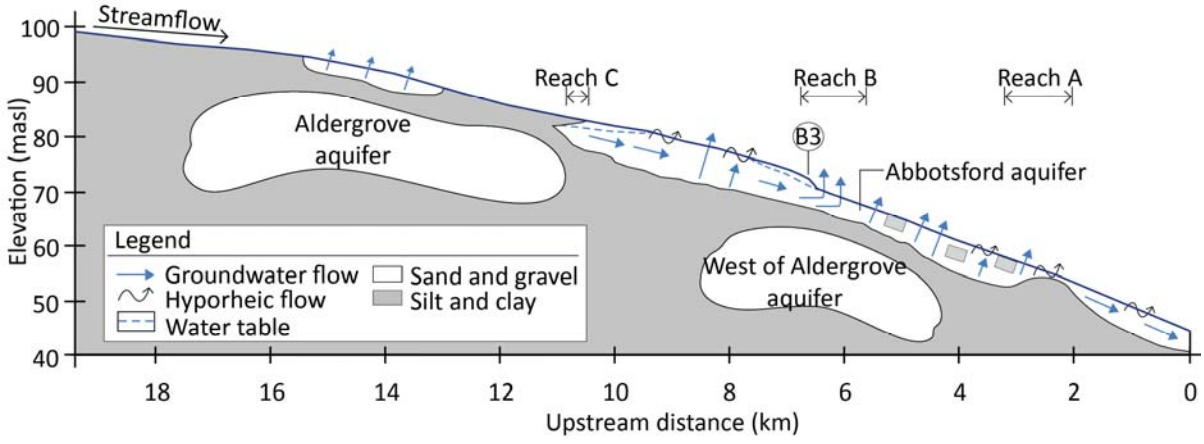

Figure 3.14 Conceptual model of surface water–groundwater interaction along Bertrand Creek. Boundaries of the confined aquifers are approximate.

Chapter 4: Simulating Fully Integrated Surface Water–Groundwater Interaction during Baseflow Conditions in the Bertrand Creek Watershed

4.1 Introduction

Groundwater-fed baseflow can comprise a large portion of streamflow necessary to support critical stream habitat during dry periods. There is growing concern, however, that future increases in urbanization and agricultural intensification will increase the demand on groundwater resources which will in turn jeopardize these baseflows (Council of Canadian Academies, 2009). Groundwater interaction with a stream is spatially variable owing to watershed-specific attributes such as topography and extent of aquifers, and temporally variable in response to regional climate and local anthropogenic activity (Tóth, 1963; Freeze 1972; Winter, 1999; Scibek and Allen, 2006). Hydrologic models designed to investigate the impact of increased groundwater withdrawals on streamflow, therefore, need to evaluate integrated surface water–groundwater flow under the influence of a heterogeneous landscape and variable climate.

A recent addition to the suite of tools available to assess aquifer and stream interaction is the fully integrated, physically based surface water–groundwater model (VanderKwaak, 1999; Panday and Huyakorn, 2004; Kollet and Maxwell, 2006; Therrien et al., 2010). A fully integrated (or fully coupled) model solves the governing equations for overland and subsurface flow simultaneously to obtain a solution of surface water depth and subsurface hydraulic head across the model domain. This coupling approach approximates the continuous movement of water between the saturated, unsaturated, and surface water zones

without the artificial definition of a water table or a-priori definition of flux between the surface and subsurface domains. Models investigating the effects of groundwater stress on baseflow have traditionally adopted a linked approach, for example by combining MODFLOW with one of its surface water packages (Prudic, 1989; Harbaugh et al., 2000) or an external surface water model (e.g., Ramireddygari et al., 2000; Sophocleous and Perkins, 2000; Said et al., 2005). These linked models solve surface and subsurface flow separately and the results of one hydrologic domain are applied as boundary conditions for the other. Since a fully coupled model conserves mass across the surface-subsurface boundary, it is considered a superior approach over a linked model in strongly connected hydrologic systems (Fairbanks et al., 2001; LaBolle and Fogg, 2001; Panday and Huyakorn, 2004).

Watershed and small catchment scale studies using integrated models have primarily focused on the analysis of rainfall-runoff mechanisms (VanderKwaak and Loague, 2001; Loague et al., 2005; Jones et al., 2008; Li et al., 2008; Sudicky et al., 2008; Mirus et al., 2011). Recent work has additionally investigated the impacts of climate change on groundwater reserves at the regional scale (Kollet and Maxwell, 2008; Goderniaux et al., 2009). These studies highlight key challenges associated with physics-based integrated modelling, including scale issues, establishing an initial condition, adequately representing heterogeneity, and identifying parameter values. Previous integrated modelling efforts have also shown that evaluating model performance against a distributed data set, which includes data from both the surface and subsurface domains, improves confidence in model results and reduces the problem of non-uniqueness (Christensen et al., 1998; Refsgaard, 2000; Mirus et al., 2011).

While application of integrated models to watershed and regional scale investigations is gaining attention, efforts that focus on baseflow generation using a fully integrated approach remain limited (e.g., Werner et al., 2006). Werner et al. (2006) present a modelling framework for applying an integrated stream–aquifer model to investigate regional scale groundwater contribution to streamflow. The model calculations indicated that groundwater discharge rates during low flow periods exceeded baseflow estimates determined using several different hydrograph separation methods. The authors attributed the excess groundwater discharge primarily to evapotranspiration from the riparian zone, which was not accounted for within the model. Evapotranspiration causes a seasonal non-linearity in the streamflow recession curve (Tallaksen, 1995; Wittenberg and Silvapalan, 1999); thus explicitly accounting for the evapotranspiration process may improve model results during low flows conditions. At present, there are no published studies that simulate all components of the water balance using a fully integrated model to focus on baseflow generation within a real-world watershed.

The objectives of this research are to: 1) examine the parameterization of a physically based integrated model for use at the watershed-scale, with a specific focus on simulating dry season baseflows, and 2) examine the nature of the surface water–groundwater exchange and how mechanisms which control this exchange influence construction of the hydrologic model. These objectives were met by modelling surface and subsurface flows within the 46 km^2 Bertrand Creek Watershed in southwestern British Columbia during the two consecutive dry seasons presented in Chapter 3. The model is calibrated to data collected during the 2007 dry season, a year that received above average rainfall and resulted in

sustained streamflows. The model is then verified using a less extensive data set collected during the 2006 dry season, during which time the streambed went dry mid-watershed following below average seasonal rainfall. The calibrated model is used to evaluate the nature of the stream–aquifer exchange and hydrologic dynamics within the watershed.

4.2 Study Site

Several watershed characteristics presented in Chapter 2 are highlighted here. The Bertrand Creek Watershed is situated within a glaciated, hummocky landscape with distinct uplands and lowlands. Low permeability silts and clays comprise surficial soils in the northern uplands, while sandy soils comprise the principal surficial deposits within the lowlands (Figure 2.4). Five principal aquifers underlie the footprint of the watershed (Figure 2.4): the unconfined Abbotsford aquifer; a semi-confined Aldergrove aquifer; and three confined aquifers, the West of Aldergrove (WALD), South of Hopington (SHOP), and Quadra Sands (Quadra) aquifers.

The Bertrand Creek overlies the Abbotsford aquifer from the watershed outlet to an upstream distance of 10.8 km (Figure 4.1). Upstream of this, the stream overlies low permeability sediments that form the confining unit above the Aldergrove aquifer. A perched groundwater bearing zone is present adjacent to Bertrand Creek in the vicinity of the urban area of Aldergrove (km.14).

Bertrand Creek originates within a wetland in the northern portion of the watershed where flows appear to be augmented by significant discharge from a deep groundwater well

(Envirowest, 2000; Chapter 3). Distances along the stream are given upstream of the watershed outlet, which is coincident with the Canada–USA border, as shown on Figure 2.1.

4.3 Numerical Simulations

4.3.1 Numerical Model

The Bertrand Creek Watershed model was developed using HydroGeoSphere, a fully-integrated, physics-based numerical model capable of simulating surface-subsurface flow in a three-dimensional framework (Therrien et al., 2010). The finite element model accounts for the complete hydrologic cycle by partitioning rainfall into components of interception, evapotranspiration, surface flow, and unsaturated and saturated subsurface flow. Subsurface flow through variably-saturated porous medium is solved using Richards equation and surface flow is solved using a two-dimensional depth-averaged, diffusion-wave approximation to the Saint Venant equation. The surface and subsurface flow equations are implicitly coupled; flow equations are solved for hydraulic head simultaneously at each time step within one matrix of equations. Further description of the equations governing flow is given within Appendix E and Therrien et al. (2010).

Water exchange between coincident surface and subsurface nodes in the Bertrand Creek Watershed model employs the dual-node coupling approach. Using this approach, water exchange is represented as a leakance (Darcy) flux across a thin layer of porous material. The length of the layer is specified as a model parameter, the coupling length (L_c, [L]), where an increase in coupling length decreases the connection between the surface and subsurface domains.

Precipitation and evapotranspiration (ET) are applied within HydroGeoSphere as boundary conditions to surface and near surface nodes. HydroGeoSphere explicitly accounts for interception, transpiration, surface evaporation, and evaporation from porous media for each time step following the ET model by Kristensen and Jensen (1975). Given the empirical nature of the Kristensen and Jensen (1975) model yet importance in the water balance, further description of the methodology used to calculate actual evapotranspiration (ET_{act}) is provided below.

HydroGeoSphere calculates ET_{act} based on relationships between potential evapotranspiration (ET_p), and functions that represent moisture availability and plant development. Potential evapotranspiration is determined a-priori (e.g., Penman, 1948; Monteith, 1965) and specified as a model input. The capacity for ET_p is first apportioned to canopy evaporation (E_{can}) to evaporate water held in interception storage (S_{int}). Interception storage is simulated as a bucket model that fills by precipitation and empties by evaporation and is a time variable function of leaf area index (LAI) and a canopy storage parameter (c_{int}; Equation 1). The remaining ET_p is partitioned between transpiration from the root zone (T_p) and surface and subsurface evaporation (E_s) according to the LAI dependent function, f_1 (Equations 2 and 3). In addition to LAI, T_p further depends on soil moisture content (f_2, Equation 4): T_p is limited by moisture availability below the field capacity (θ_{fc}) and becomes zero below the wilting point (θ_{wp}). At high moisture contents, T_p is limited at moisture contents above the oxic moisture content (θ_o, Equation 4) owing to root stress from a lack of aeration (Feddes et al., 1988), and becomes zero above the anoxic moisture content (θ_{an}).

$$S_{\text{int}} = c_{\text{int}}\, LAI \qquad [1]$$

$$T_p = f_1(LAI)\, f_2(\theta)\, RDF\, [ET_p - E_{can}] \qquad [2]$$

$$f_1(LAI) = \max\{0, \min[1, (C_2 + C_1 \text{ LAI})]\} \qquad [3]$$

$$f_2(\theta) = \begin{cases} 0 & \text{for} \quad 0 \le \theta \le \theta_{wp} \\ 1 - \left[\dfrac{\theta_{fc} - \theta}{\theta_{fc} - \theta_{wp}}\right]^{C_3} & \text{for} \quad \theta_{wp} \le \theta \le \theta_{fc} \\ 1 & \text{for} \quad \theta_{fc} \le \theta \le \theta_o \\ 1 - \left[\dfrac{\theta_{an} - \theta}{\theta_{an} - \theta_o}\right]^{C_3} & \text{for} \quad \theta_{\text{o}} \le \theta \le \theta_{an} \\ 0 & \text{for} \quad \theta_{an} \le \theta \end{cases} \qquad [4]$$

$$E_s = \alpha^* (ET_p - E_{can})\, [1 - f_1(LAI)]\, EDF \qquad [5]$$

$$\alpha^* = \begin{cases} \dfrac{\theta - \theta_{e2}}{\theta_{e1} - \theta_{e2}} & \text{for} \quad \theta_{\text{e2}} \le \theta \le \theta_{\text{e1}} \\ 1 & \text{for} \quad \theta > \theta_{e1} \\ 0 & \text{for} \quad \theta < \theta_{\text{e2}} \end{cases} \qquad [6]$$

HydroGeoSphere incorporates dimensionless empirical parameters into the calculation of T_p to account for canopy dependence (C_1), a base evaporation value (C_2), and dependence on soil and vegetation type (C_3; Kristensen and Jensen, 1975). A higher value of C_3 reduces the influence of soil dryness and is generally associated with light soils and shallow roots (Kristensen and Jensen, 1975). Large values of LAI cause the value of f_1 to equal one (Equation 3), which in turn causes all ET_p in excess of E_{can} to be apportioned to transpiration (Equation 2). Conversely, lower values of LAI result in a greater percent of ET_p to be partitioned to surface and subsurface evaporation (Equation 5).

Water availability limits E_s according to a wetness factor (α^*, Equation 6), where full evaporation becomes limited below the energy-limiting moisture content (θ_{e1}) and reduces to

zero below the moisture content θ_{e2}. The presence of C_2 in Equation 3 determines the amount of evaporation that occurs from the subsurface regardless of the dominance of transpiration or the presence of water ponded on the surface. Capacity for transpiration and evaporation within subsurface nodal layers decreases with depth below the surface to their respective extinction depth (z_{rt} and z_{evap}) according to specified decay functions (RDF and EDF, respectively). If the potential for evapotranspiration is not met within an assigned nodal layer, it is not compensated for uptake within another layer.

4.3.2 Bertrand Creek Watershed Integrated Model

4.3.2.1 Conceptual Model

The conceptual model of the Bertrand Creek Watershed is based on distributed information characterizing the surface topography, surficial soils, subsurface stratigraphy, and land use (see Chapter 2). Boundary conditions additionally include pumping rates for municipal supply wells, discharge to the headwater wetland from a deep groundwater well, and time-variable climatic fluxes (i.e., precipitation and ET). The topographic outline of the Bertrand Creek watershed forms the lateral extent of the modelled area as well as the upper surface. The base of the model is set at 18 m above sea level (masl), which creates a model thickness that varies from 27 to 122 m and encompasses the four uppermost aquifers underlying the watershed footprint.

The surface topography was determined by kriging elevation points from adjacent 20 and 25 m horizontal resolution digital elevation models (DEM) obtained from the City of Abbotsford and Township of Langley (TOL). Land use information was also obtained from

municipal databases and was used to assign evaporation and surface flow routing parameters. Initial values for the Manning roughness coefficient for flow routing in overland and urban areas were obtained from literature (Chow, 1964). As discussed in Chapter 3, hydrographs at the weirs and the outlet exhibit a double peak characteristic late in the summer. The second peak is attributed to delayed runoff generated within the urban area which arrives at sequential weirs as a delayed pulse. The Manning roughness coefficient for channel flow was calibrated using a streamflow pulse that travelled through the watershed on August 29, 2007 (Chapter 3.4.3).

Subsurface stratigraphy was interpreted from borehole lithologies on water well logs available from the BC Ministry of Environment WELLS database (BC MoE, 2008). Boreholes extended up to 240 m below ground surface in the 1,463 available well logs within and surrounding the watershed. Borehole locations were considered approximate; boreholes were relocated up to 580 m within the model database where location discrepancies were identified. Soil units recorded on borehole logs were classified into lithofacies using textural descriptors (i.e., gravel, sand, silt, and clay) and colour. Elevations of the borehole surface and top and bottom of each lithologic unit were then determined with reference to the DEM. The ArcHydro Groundwater toolbar in GIS (CRWR, 2006) was used to visualize the borehole lithologies in a three-dimensional context.

Lithofacies were placed into one of six hydrostratigraphic units consisting of confining material, a near-surface permeable zone, and four aquifers (Figure 4.2). The aquifers, from youngest to oldest, consist of the: (1) Abbotsford aquifer, (2) Aldergrove aquifer, (3) West of

Aldergrove aquifer, and (4) South of Hopington aquifer. Borehole log information such as depth of well screen and descriptors indicating water bearing units were used in conjunction with previously mapped two-dimensional aquifer outlines to delineate the three-dimensional aquifer extents (Halstead, 1986; Kreye and Wei, 1994; Cox and Kahle, 1999; Golder, 2005). Aquifer surfaces were created by kriging the aquifer top and bottom elevations determined from borehole logs. Prior to kriging, descriptive statistics for the elevation points of each hydrostratigraphic unit were evaluated using the statistical software R (R Development Core Team, 2008) and geostatistical analysis was conducted using the geoR package within R (Ribeiro and Diggle, 2001). The high degree of geologic heterogeneity in the glacial sediments made assigning deposits to local hydrologic units challenging, similar to experiences reported by other modelling studies in the region (Golder, 2005; Scibek and Allen, 2005; Allen et al., 2008).

Spatially-variable surficial soils were assigned within the upper 1.5 m of the model (Figure 4.2), based on mapped soils by Luttmerding (1980). Description of spot samples within Luttmerding (1980) indicated that soils extend between 1 to 2 m below ground surface. The spatial distribution of streambed soils was additionally correlated with the streambed soil type encountered during the field investigation (Chapter 3.4.2). Soils were classified into one of six textural classes (Table 4.1), which were then used to assign saturated hydraulic conductivity and soil water retention curve parameters using pedotransfer functions in the Rosetta software (Schaap et al., 2001). Parameters describing the soil water characteristic function were assigned using the van Genuchten (1980) model.

4.3.2.2 Model Discretization

The two-dimensional surface mesh was created using Grid Builder (McLaren, 2009) and consisted of 9,827 triangular elements (5,062 nodes) draped over the surface topography (Figure 4.2). Nodal spacing of the finite-element mesh increased from 20 m along the creek to 300 m at nodes farther from the creek. Due to the coarse resolution of the DEM with respect to stream bank widths, it was necessary to explicitly specify stream node elevations. This was accomplished by first removing depressions from the creek length so creek nodal elevations decreased linearly with distance downstream, then incising stream nodes 1 m below the adjacent surface topography to create a 'V-shaped' creek geometry (Figure 4.2, inset). The nodal spacing of the final grid was chosen as a balance between grid complexity and computational efficiency.

The three-dimensional subsurface consisted of 196,540 prisms and had an equivalent nodal geometry as the two-dimensional surface mesh (i.e, subsurface nodes coincided with nodes on the surface mesh). As a result of the heterogeneous subsurface geology, grid layers within the model did not correspond with aquifer surfaces. Twenty-one vertical layers were used to represent the spatial distribution of the hydrostratigraphic units and capture the surface water –groundwater interaction near the surface. The vertical spacing of these layers increased with depth: 0.5 m for the upper 2 m, then 1 m layers to a depth of 6 m, and 3 m layers to a depth of 18 m. The remaining non-uniform thickness of the lower model was divided into 8 uniform layers that varied in thickness spatially between 8 and 15 m (Figure 4.2). A model grid with finer vertical discretization for the top layer (0.25 m) yielded a significant (> 200%)

increase in model run time with no appreciable difference in simulated streamflows or stream–aquifer exchange.

4.3.2.3 Boundary Conditions

The lower boundary of the model is a silt and clay deposit assumed to be impermeable and specified as a no-flow Neumann boundary (Figure 4.2). Subsurface boundary conditions along the horizontal limits of the model were also specified as impermeable except along the southeast boundary and at the outlet of the watershed. Dirichlet boundaries were imposed at these two locations to allow groundwater flow across the watershed boundary as predicted by regional groundwater models (Golder, 2005; Scibek and Allen, 2005). A steady state model of the Abbotsford aquifer yields an estimation that 13,000 m^3/d of groundwater crosses the southeast watershed boundary in the Abbotsford and Aldergrove aquifers (Scibek and Allen, 2005[2]). This southeastern boundary was assigned spatially variable head values ranging from 68 to 75 masl. A second Dirichlet boundary was assigned at the outlet of the watershed to allow groundwater to exit the model domain within the unconfined aquifer coincident the stream outlet. The head value along this boundary was specified as 0.5 m below the streambed elevation (44.5 masl). A reduced hydraulic conductivity was assigned to the streambed 100 m preceding the outlet to limit artificial stream water infiltration imposed by this specified head boundary. Values of both specified head boundary conditions were constant in time.

---

[2] The model is periodically updated. The reported groundwater flux is based on a model simulation conducted in November, 2010.

On the surface of the model, a no-flow Neumann boundary condition was assigned to all perimeter nodes except those corresponding to the Bertrand Creek outlet. The stream outlet nodes were assigned a critical-depth boundary condition which forces the surface flow depth to be equal the critical flow depth, the depth at which the specific energy is a minimum for a given rate of flow (Potter and Wiggert, 1997). The critical-depth boundary condition allows discharge to vary according to the calculated depth of water in the creek.

Groundwater discharge from a deep well augments streamflows within the upper portion of the watershed (Chapter 3). The well is screened within an aquifer located lower than, and not included within, the model domain. Discharge from the well was represented by applying a constant flux over the headwater wetland and adds 0.008 m^3/s water to the model domain.

Precipitation and evapotranspiration were applied as boundary conditions to the model surface. Precipitation rates were input to the model as event-based rain rates calculated based on the rain record from a tipping bucket rain gauge (TR-525M, Texas Electronics) installed within the watershed and referred to herein as the study rain gauge (Figure 4.1). To calculate rates as event-based, the start and end times and the average rainfall rates were determined for each rain event. A period of no rain for two hours signaled the end of a discrete rainfall event. Comparison of the study rain gauge record with the rainfall records of three other permanent rain gauges located within and surrounding the watershed indicates that the study rain gauge record represents all rain events of significance (i.e., >0.5 mm) reported by the surrounding gauges. Data gaps in the study gauge record due to data logger malfunction were supplemented with data from the nearest rain gauge.

Daily reference evapotranspiration (ET_o) was calculated according to the FAO-56 Penman-Monteith method for a grass reference crop (Allen et al., 1998). The required climatic data was obtained from the nearest Environment Canada climate station located 4 km east of the watershed (Figure 2.1) and solar radiation was estimated using station latitude. Potential evapotranspiration (ET_p) rates were calculated by applying crop coefficients (k_c) to ET_o based on values presented by the Food and Agriculture Organization (Allen et al., 1998) and the British Columbia Ministry of Agriculture, Food, and Fisheries (van der Gulik and Nyvall, 2001). As discussed later, final k_c values were calibrated. The ET_p rate was input to the model on a daily basis and was considered an average representation for the entire watershed.

Pumping rates were specified at seven municipal wells within the watershed that supply potable water to the town of Aldergrove. A constant average extraction rate was calculated for each well based on long-term pumping records (Table 4.2) and assigned to the nodes spanning each well screen. The seven wells extract a combined volume of 6,720 m^3/d from the Aldergrove aquifer. Groundwater withdrawals from private water wells are estimated at 1,000 to 2,000 m^3/d (Golder, 2005). Based on an assessment of the number of properties not serviced by municipal water supply, this volume of water is extracted by approximately 400 wells located throughout the watershed. The effect of extraction from these wells on discharge at the watershed outlet is expected to be less than 2 L/s, and within the error of estimation of evapotranspiration, and as a result the private wells were not included in the model.

4.3.3 Model Calibration Data

The Bertrand Creek watershed model was calibrated using publicly available hydraulic head and streamflow data, as well as data collected in the field during the 2007 dry season (Chapter 3). Hydraulic head values were obtained from water well driller's records and include wells installed between 1950 and 2007. Discharge at the watershed outlet, the Bertrand Creek gauge, was available from the Water Survey of Canada (WSC) preceding 2007 and from the United States Geological Survey (USGS) since spring 2007. The streamflow record at the Bertrand Creek gauge for the two years of study did not include winter streamflow measurements and only May through October streamflows were available.

During calibration, the model performance was evaluated against field data presented in Chapter 3 (Figure 4.1):

1) Streamflow measured at four sequential weirs (stations A1, A4, B1, and B3).
2) Baseflow contribution calculated between the pairs of weirs within Reach A (stations A1 and A4) and Reach B (stations B1 and B3).
3) Change in hydraulic head measured within 10 private groundwater wells screened within the unconfined and confined aquifers between June and September, 2007.
4) Soil moisture content measured at two locations within the watershed (SM1 and SM2) using capacitance soil moisture probes (5TE probe by Decagon Devices, Inc.). The probes were installed between 0.10 and 0.75 m below the soil surface.
5) Change in surface water height in a pond between April and October, 2007 (Figure 4.1; Figure A16). Precipitation and evaporation appear to control the pond's water height during the dry season: there is no surface discharge from the pond during periods of no

rain and seepage through the pond bottom appears negligible based on the hydraulic conductivity value (0.6 mm/d) determined by slug testing a piezometer installed 0.5 m beneath the pond. The pond water height decreased an average rate of 4.5 mm/d in the months of July and August. The pond was explicitly defined in the surface mesh of the model using a refined nodal spacing.

Given that the 2007 field data record was more extensive than 2006, the model was calibrated to the 2007 dry season and performance was evaluated against the smaller data record collected in 2006. Data collected in 2006 consisted of spot measurements of streamflow and calculated baseflow contributions at the same gauging station locations as 2007, as well as hydraulic head measurements within a streambed piezometer located 400 m upstream of station B3.

4.4 Results

4.4.1 Steady State Condition

To calibrate subsurface hydraulic conductivities, a steady state model representing average annual hydrologic conditions was first established. A rainfall rate equivalent to 35% of the average annual precipitation (550 mm/yr) was applied to the model surface based on a previous estimate of average regional recharge (Golder, 2005). The steady state model was calibrated using observed hydraulic heads available within 202 records from the water well database (BC MoE, 2008), in addition to water levels measured in June 2007 within 18 private water wells. Water well database records span a 50-year period and have an associated uncertainty in location; therefore, they can be considered accurate only to +/-5 m.

The time and location of water level measurements within private wells are well constrained, and they are considered accurate to +/-2 m owing to uncertainty in DEM elevations. Results of the calibration process are shown in Figure 4.3. Simulated hydraulic heads that plot below the lower 5 m line on Figure 4.3 are at wells located near the southeastern perimeter of the watershed, and are influenced by the specified heads along this boundary. Quality of fit of the steady state model was assessed by examining the root mean squared error (RMSE) and the goodness-of-fit, R^2. The model RMSE and R^2 values describing the fit to observed hydraulic head in all wells are 3.4 and 0.93, respectively. These values improve to 2.0 and 0.98, respectively when the model response is assessed using hydraulic head measurements from only the private wells. The model RMSE values are within the range of water table fluctuation and resolution of measurement uncertainty, and indicate a good match to observed data.

Initial estimates of saturated hydraulic conductivity values for aquifers and confining units were based on values from a regional groundwater model (Golder, 2005) and literature (Domenico and Schwartz, 1998). Final estimates of saturated hydraulic conductivity values and specific storage coefficients for each unit are provided in Table 4.3. Three aquitard zones with different hydraulic conductivities were necessary to represent the hydraulic head distribution. Porosity was set to 0.3 within all aquifers and to 0.45 within all aquitards.

A steady state initial condition was then established for the integrated hydrologic model on which to base subsequent transient simulations, commonly referred to as 'spinning-up' the model. The initial condition for an integrated model can be achieved by setting the water

table at the ground surface and allowing the model to drain (e.g., VanderKwaak and Loague, 2001) or by bringing the model to a steady state using a constant uniform rainfall rate applied to the topographic surface (e.g., Jones et al., 2008). This study employed the latter approach with a constant rainfall rate of 410 mm/yr. This rate represents the long-term average spring-season (March through May) effective precipitation determined using the Abbotsford Airport rain gauge (Environment Canada, 2009). The simulated baseflow contribution along the stream was sensitive to the choice of initial condition. For example, an initial condition established with a rainfall rate of 550 mm/yr increased discharge at the watershed outlet late in August by 0.004 m^3/s compared with the chosen steady state model. The initial condition is frequently one of the most sensitive parameters in a physically based model (Stephenson and Freeze, 1974; Grayson et al., 1992; Jones et al., 2008; Li et al., 2008).

4.4.2 Transient Model Calibration: 2007 Dry Season

Calibration of the steady state and transient models was an iterative process, i.e., the steady-state model was altered and improved to address deficiencies identified in earlier transient simulations. During calibration of the 2007 transient model, surficial soil parameters, surface routing parameters, and evapotranspiration parameters were varied to obtain a good match to the observed hydrologic response. The final calibrated parameter values and the fit to data (Figures 4.4 through 4.10) are discussed below.

Time steps for the transient model were adaptive; HydroGeoSphere determined the time steps necessary to limit the change in groundwater head and surface water depths during each time step to less than 0.5 m and 0.03 m, respectively. For the 2007 transient simulation,

these time steps ranged from several seconds to 27 hours. Simulation of April to October, 2007, conditions for the Bertrand Creek Watershed model took approximately 26 hours to complete using a 2.67 GHz Intel Core i7-920 desktop processor equipped with 12 GB RAM.

4.4.2.1 Subsurface Domain

Calibration revealed that assigning soil properties to the model based on the mapped distribution of soils (Luttmerding, 1980) and the values in Table 4.1 results in an unreasonably high amount of localized recharge along lowland soils located between km.6.3 and km.10 (Figure 4.1). The localized recharge originates primarily as subsurface runoff from the silty upland soils north of the stream. To reduce this localized recharge and continue conveyance of overland flow to the stream, the sandy soil adjacent to the stream at the base of the northern uplands was assigned the same soil properties as the silty upland soils.

Streamflows and hydraulic heads within the unconfined aquifer were sensitive to the streambed hydraulic conductivity. Reducing the hydraulic conductivity values within the streambed by a factor of 10 from the surficial soil values in Table 4.1 provided the most representative results to streamflows and hydraulic heads in adjacent permeable units. A uniform hydraulic conductivity of $1x10^{-7}$ m/s, which is lower than values of surficial soils, was assigned to the surface of the model within the urban area. This lower hydraulic conductivity provided the best match to hydrograph peaks and is attributed to the presence of the storm drain system in the urban area.

4.4.2.2 Surface Domain

Flow routing parameters are provided in Table 4.4 for overland and channel flow, and flow within the urban area. A watershed-specific Manning value was determined for the channel by fitting the travel time of an observed pulse of streamflow that travelled through the watershed on August 29, 2007 (Figure 4.4). A modelled pulse of streamflow similar in magnitude to the observed pulse was generated by simulating an 8-minute rain event at 40 cm/hr intensity on the headwater wetland. A Manning roughness coefficient of 0.012 s $m^{-1/3}$, which is a reasonable value for channel flow (Chow, 1964), provided a good fit between the observed and simulated travel of the water pulse through the lower watershed.

The rill storage (h_s), a depression storage that must be filled before lateral surface flow can occur, was assigned a higher value to the channel upstream of km.8.2 (Table 4.4). Assigning an increased rill storage value, and therefore stream water depth, to the upper watershed is justified by depths observed in the field and benefited model calibration by reducing runoff peaks late in the summer. Similar to previous studies (Ebel et al., 2009; Goderniaux et al., 2009), the exchange coupling length was not a sensitive parameter for streamflow simulation (between values of 10^{-1} and 10^{-5} m), and was set to 10^{-3} m for all areas of the surface domain.

4.4.2.3 Evapotranspiration

Calibrated evapotranspiration parameters assigned as uniform values across the model surface are included in Table 4.5. Incorporating the upper limit to transpiration in the model, specified by θ_o and θ_{an} (Equation 4), limited the decrease in soil moisture content through the dry season and consequently was not assigned within the calibrated model. Without this

upper limit to transpiration, the primary role of LAI is to control the partitioning of ET_p between transpiration and evaporation (Equations 2 and 5). While many integrated hydrologic models further distinguish land use types into forest, crop, or grass areas using spatially and temporally distributed values of LAI and root depth (e.g., Li et al., 2008; Goderniaux et al., 2009), distributing these parameter values across the rural area of the watershed had negligible effect on baseflows as will be discussed later (Section 4.5.2.2). Rural and urban areas were assigned an LAI value of 1.2 (Table 4.6), which causes ET_p to be drawn equally from evaporation and transpiration. An LAI value of 2.5 was assigned along the stream. Based on the values of C_1 and C_2 (Table 4.5), this assignment of LAI specifies that 95 percent of the ET_p along the stream is drawn from transpiration and only 5 percent from surface and subsurface evaporation (Equations 2 and 3).

As mentioned previously, parameterization within the urban area of the model is influenced by the storm drain system, which is expected to have negligible evaporation from stored water and a rapid mobilization of water in response to a rain event. An adequate match to hydrograph peaks at the watershed outlet was only possible when subsurface evapotranspiration was restricted within the urban area, and was simulated by assigning the extinction depths for evaporation and transpiration to zero. This parameterization prevented evapotranspiration from the subsurface but still allowed evaporation from surface water and water stored in interception. Within all other areas of the model, a quadratic function described the decrease in evaporation and transpiration with depth to maximum depths of 0.5 m and 2 m, respectively.

In addition to the parameters discussed above, simulated streamflows were sensitive to the input ET_p rate. Simulated streamflows were sensitive to changes in k_c as small as 0.1, and therefore, the timing and slope of the k_c curve were calibrated (Figure 4.5). Calibrated k_c values are similar to those found in literature (Allen et al., 1998).

4.4.2.4 Comparison to 2007 Field Data

Calibration of the Bertrand Creek Watershed model was evaluated using five measures:

1) Discharge at the watershed outlet between April and October, 2007 (Figure 4.6): Simulated discharge at the outlet is in close agreement with observed discharge at the Bertrand Creek gauge during baseflow and peak runoff conditions.

1) Streamflow at weirs and baseflow contribution between weirs from August to September, 2007 (Figure 4.7): Simulated streamflows at the four weir locations A1, A4, B1, and B3 provide a good match with observed streamflows during baseflow conditions. The streamflow record measured at the weirs during baseflow conditions is considered accurate to 1 L/s within the upstream weirs B1 and B3, and to 2 L/s at the downstream weirs A1 and A4. Predicted baseflow contributions are similar to calculated rates, including a greater groundwater contribution between weirs along Reach B than along Reach A. The model predicts the stream segment upstream of station B3, between B3 and a gauging station 480 m upstream ('station B4' in Chapter 3), transitions from gaining to losing on July 1, 2007 (not shown). Field measurements of streamflow indicate that stream conditions along this segment transitioned from gaining to losing sometime in June (Chapter 3.4.3). The model accurately predicts that streamflow at station B3 became negligible in late July. The absence of streamflow at station B3

indicates that discharge from the groundwater well at the headwater wetland, which was specified as a boundary condition within the model (Section 4.3.2.3), infiltrated the streambed upstream of this segment. Simulated discharge at the four weirs and outlet increased with distance downstream until August 16 when discharge at station A1 became greater than discharge at the outlet.

2) Surface water height in a pond (Figure 4.8): The simulated change in surface water height within the pond agrees well with observed data and deviates approximately 1 cm from the available record during dry conditions between July 28 and September 28, 2007.
3) Change in hydraulic head (Figure 4.9): The simulated change in hydraulic head within the majority of private groundwater wells between June and September was within 0.25 m of the measured change in hydraulic head. The greatest discrepancy between simulated and observed change in hydraulic head is within wells situated one or two nodes from the modelled stream (<75 m), which suggests the model is unable to resolve the water table dynamics measured adjacent to the stream. Simulated hydraulic heads did not consistently over- or underestimate hydraulic head measurements in private wells.
4) Soil moisture content (Figure 4.10): The modelled soil moisture content for a sandy loam provides a good match to measured data at sensor location SM1. The poorer match between the simulated response and observed data at sensor SM2 is attributed to the presence of sandier soils surrounding the sensor than indicated on the soils map and specified in the model (Luttmerding, 1980).

Based on the foregoing discussion, the model is considered to adequately represent the surface and subsurface hydrologic response during the dry season. The greatest

discrepancies between the simulated and observed response on Figures 4.6 through 4.10 are: (1) an underestimation of streamflow recession, (2) an overestimation of discharge following rain in late September, and (3) inconsistent reproduction of the hydrograph double peak late in August and September (see Figure 4.7). The calibrated model sufficiently predicts the late hydrograph peak in response to rainfall on August 26, but either does not generate or erroneously generates the late peak associated with rainfall on August 19 and September 4, 2007. Runoff generated within the urban area and the pre-event surface water height in the stream between km.6.3 and km.10 control the magnitude of these late hydrograph peaks, and demonstrate the sensitivity of streamflow peaks to baseflow conditions. Reducing the runoff generated in the urban area provided a better match to the second and third conditions listed above, but resulted in a poorer fit to spring rainfall events. Final parameter values were chosen to balance the match during wet and dry conditions while providing an adequate representation of volumetric runoff in the water balance. Simulation results are expected to improve if the urban area storm drain system is explicitly represented within the model using a network of pipes in addition to porous medium. The discrepancy during streamflow recession indicates that the slow release of water from either surface or subsurface storage zones within the model is inadequate and would benefit from further development of the watershed model.

4.4.2.5 Water Balance

Table 4.7 presents the main components of the water balance over the period of the 2007 transient simulation. Results indicate a moisture deficit developed across the watershed during the period of study, due largely to the predominance of evapotranspiration.

Comparison of the simulated and observed cumulative discharge at the watershed outlet indicates a good match to the runoff component of the water balance (Figure 4.11). At the onset of heavy rain in October, there is a 3 percent error between the simulated and observed cumulative volume of discharge at the watershed outlet.

Daily values of ET_{act}, including evapotranspiration from surface and subsurface domains as well as evaporation from interception storage, are shown on Figure 4.5. Simulated daily values of ET_{act} varied from 0.3 to 5.4 mm/d with a corresponding ratio of ET_{act}/ET_p between 0.7 and 1.0 (Figure 4.5). Daily ET_{act} values begin to decline below ET_p in early June, indicating watershed soils become moisture limited.

4.4.3 Surface Water–Groundwater Interaction

4.4.3.1 Flux across the Streambed

Figure 4.12a is a plot of predicted exchange flux [LT^{-1}] across the Bertrand Creek streambed on select dates when baseflow dominated the hydrograph. A positive value indicates upward seepage across the streambed while a negative value indicates downward seepage and the stream is losing water to the subsurface. The exchange flux exhibits significant spatial variability, even at the 100 m scale. The low permeability streambed limits the exchange flux along the upper 10 km stream length, except near km.14 where the stream overlies the perched groundwater unit (Figure 4.1). The magnitude of upwelling decreases and losing conditions develop along the channel as the 2007 dry season progresses.

To further illustrate the spatial variation in the exchange flux, a plot of cumulative flux [L^2T^{-1}] calculated along the stream center nodes is presented in Figure 4.12b. A negative value of cumulative flux indicates that streamflow originating as overland flow is additionally infiltrating the streambed. During calibration, changes to subsurface hydraulic conductivity values (within reason) caused the magnitude of the cumulative flux plot to vary, but the general shape of the plot and locations of greatest upwelling remained consistent. Changes to the model structure, however, such as thickness of the unconfined aquifer or presence of permeable surficial units, changed the shape of the cumulative flux plot.

The model predicts that significant upwelling occurs at locations (Figure 4.12) that were identified as strongly gaining during the field investigation (Chapter 3.4.5). The strong upwelling immediately downstream of station B3 (km.6.2), is where the largest gain in streamflow was measured along Bertrand Creek. Similarly, the significant upwelling predicted by the model at km.2.8 is coincident with the location identified to have the greatest baseflow contribution along Reach A. The simulated direction of flux at other locations compares favourably with the direction of flux observed during the 2007 field investigation using mini-piezometers (Chapter 3.4.5.1). The model predicts stream conditions transition from gaining to losing along the upstream extent of the unconfined aquifer within two weeks of the observed transition. The model also correctly predicts the development of perched stream conditions at km.10.8 where the unconfined aquifer is overlain by a thin confining layer. However, the model over-predicts the magnitude of streambed hydraulic heads adjacent to the low permeability streambed surrounding km.10.8 during spring conditions by approximately 1 m.

4.4.3.2 Water Table Configuration

Figure 4.13 shows the simulated water table configuration on June 1 and September 1, 2007, and highlights the direction of the surface-subsurface flux across the model surface. Groundwater flow generally follows topography, and groundwater exits the watershed along the southern boundary. The simulated water table contours support the hypothesis presented in Chapter 3 that underflow-dominant (parallel to the stream; Larkin and Sharp, 1992) and baseflow-dominant (perpendicular to the stream) groundwater flow directions develop based on the topographic slope surrounding the stream channel. Water table contours indicate that groundwater flow parallels the channel within the upstream extent of the unconfined aquifer, becomes predominantly perpendicular to the stream downstream, and parallels the stream again immediately upstream of station B3 (Figure 4.13, inset). Groundwater flow downstream of station B3 is predominantly perpendicular to the stream except near the watershed outlet (Figure 4.13). As discussed in Chapter 3, a drop in streambed elevation at station B3 appears to influence the development of underflow-dominant groundwater flow immediately upstream of this location.

Stream locations that sustain gaining conditions through the dry season are locations where groundwater maintains a component of flow perpendicular to the stream (Figure 4.13). Beyond the stream channel, an upward direction of flux is also predicted at the base of hills within the lower portion of the watershed. Seeps and springs were observed during the field investigation and are reported to sustain tributaries within the lower watershed (Johanson, 1988).

4.4.4 Transient Model Evaluation: 2006 Dry Season

The simulated hydrograph at the watershed outlet using precipitation and evaporation rates in 2006 is shown with the observed 2006 hydrograph in Figure 4.14. Simulated streamflows versus spot gauging measurements and calculated baseflow contributions across Reaches A and B are presented in Figure 4.15. Simulated results compare favourably with measured data, especially considering that all parameter values and the initial condition remained unchanged from the 2007 transient model. Consistent with the drier rainfall record, the 2006 model predicts minimum streamflow and baseflow contributions are lower than in 2007. Similar to results of the 2007 model, streamflow recession is underestimated and discharge is overestimated following September rains (Figure 4.14).

The 2006 transient simulation predicts that the streambed goes dry in 2006, although the observed timing and extent of the dry streambed differ somewhat in the model simulation (Figure 4.16). The observed streambed was dry along a distance of at least 500 m immediately upstream of station B3 (the maximum upstream extent of the dry streambed was not observed). The model correctly predicts the channel became dry at the observed location, but development of dry streambed was delayed three weeks and only extended 260 m upstream. The model predicts that several other stream segments overlying the narrow constrained portion of the unconfined aquifer also became dry, which is inconsistent with field observations.

The model predicts that streamflows resumed within the channel following a rain event mid-September, but observed streamflows did not resume until mid-October. The water level

within a streambed piezometer located within the dry streambed at km.6.7 was 0.1 m below the streambed on October 1, 2007 (Figure 3.12). The difference between this measured water table at km.6.7 and the height of the simulated water table and flowing stream was only 0.25 m. As a result of the early resumption of streamflow, simulated discharge exceeds observed discharge at the watershed outlet during September and October (Figure 4.14).

4.4.5 Impact of Evapotranspiration Parameters on Model Response

4.4.5.1 Evapotranspiration within the Riparian Zone

The purpose of this section is to assess the magnitude of evapotranspiration within the riparian zone, as well as the sensitivity of model predictions to partitioning of evaporation and transpiration. To consider the impact of evapotranspiration within the riparian zone, leaf area index (LAI) and ET_p values were varied only along the stream. Results of these test simulations are compared against the 2007 transient model.

A simulation was conducted with LAI set to zero along the stream channel. Specifying LAI as zero shuts-off transpiration along the stream and forces the capacity for ET_p to be met by evaporation only. As a reminder, the potential for evapotranspiration along modelled stream elements in the calibrated model is met primarily by transpiration (by setting LAI = 2.5). In the test simulation, flux across the streambed increased (Figure 4.17) and a shorter length of stream developed losing conditions in comparison with the calibrated model. The increase in flux was equal to the ET_p rate where the stream was strongly connected to the unconfined aquifer, and was less than the ET_p rate where the unconfined aquifer was absent or the

streambed hydraulic conductivity was low. Streamflow and baseflow contributions along Reaches A and B were insensitive to the LAI value assigned along the stream.

A simulation was conducted with ET_p set to zero along the stream channel. With evapotranspiration excluded, the cumulative flux across the streambed increased significantly relative to the calibrated model (Figure 4.17). As a result, discharge at the watershed outlet increased between 0.01 and 0.02 m^3/s over the study period, which amounts to an 8 mm (10%) increase in the runoff component of the water balance (Table 4.7). Since evaporation was limited along the stream in the calibrated model, the increase in streamflow is considered equivalent to the rate of transpiration within the Bertrand Creek riparian zone.

4.4.5.2 Water Balance Sensitivity to Evapotranspiration

To evaluate the effect of excluding the upper limit to transpiration on the 2007 calibrated model response, the upper limit to transpiration was included in a test simulation with values of 0.85 and 0.90 assigned to θ_o and θ_{an} (Equation 4), respectively. All other values from the calibrated model remained unchanged during the test simulation. With the upper limit to transpiration included in the model, total ET_{act} was reduced by 11% (44 mm) from the base case. The decrease in ET_{act} was balanced primarily by a smaller decrease in subsurface storage (35 mm) and to a lesser extent an increase in runoff (8 mm) and decrease in surface storage (1 mm). Discharge at the outlet for the test case and calibrated model differed by only 0.001 m^3/s during baseflow conditions; therefore, both models provide an equally good match to observed streamflows but have considerable differences in water balance

components. Evaluating model results with soil moisture content and change in hydraulic head clearly identified the test case as the poorer model.

4.4.6 Influence of Streambed and Aquifer Properties on Extent of Losing Conditions

Several model scenarios were completed to assess how characterization of the unconfined aquifer and streambed affects the development of losing conditions along Bertrand Creek. The assessment focused on the narrow portion of the unconfined aquifer between km.6.3 and km.11, along which stream segments were predicted to go dry in 2006. The scenarios consider the influence of (1) saturated hydraulic conductivity (K_{sat}) of the unconfined aquifer, (2) K_{sat} of the streambed, and (3) thickness of the unconfined aquifer. Results are compared with results from the 2006 transient model (Section 4.4.4), which is considered the base case, for September 1, 2006.

To explore the impact of hydraulic conductivity of the unconfined aquifer, K_{sat} was varied by a factor of 2 from the base case value of 0.0001 m/s. Increasing K_{sat} increased the extent of water table decline upstream of station B3 which created losing conditions over a greater stream length (Figure 4.18). The change in K_{sat} had the opposite effect on the water table decline farther upstream. Only the base case and reduced conductivity scenarios sustained gaining conditions along this stream segment. Gaining conditions within both cases were limited to a stream section several hundred metres in length downstream of km.7.1.

To examine the influence of streambed hydraulic conductivity on stream–aquifer interaction, the streambed K_{sat} was varied by an order of magnitude from base case values indicated on

Figure 4.19. Changing the streambed K_{sat} had a negligible effect on the water table decline immediately upstream of station B3. Further upstream, a reduced streambed K_{sat} limited the water table decline and resulted in a shorter length of streambed going dry. In contrast, a higher value of streambed K_{sat} increased the water table decline, likely due in part to a greater length of streambed going dry.

Given the heterogeneous subsurface geology, there is uncertainty in the thickness of the unconfined aquifer. To address this uncertainty, the unconfined aquifer was assigned a constant thickness (7 m), which increased the aquifer depth along the study segment by 1 to 3 m. Assigning a uniform aquifer thickness to the model effectively increased the transmissivity and, therefore, had the same effect on the water table decline upstream of station B3 as increasing the hydraulic conductivity (not shown). The increased aquifer thickness also caused an additional 100 m length of channel to go dry downstream of station B3. The change in aquifer thickness had no effect on the water table within the upstream portion of the stream segment.

4.5 Discussion

Simulating baseflow in Bertrand Creek is sensitive to how land surface processes, such as recharge and evapotranspiration, are represented in the model. The following discussion presents how representing these processes within the model affects baseflows and model performance.

4.5.1 Recharge within the Watershed

Simulating the spatial distribution of baseflow to Bertrand Creek relied on a satisfactory representation of the rates and spatial distribution of recharge. Baseflow contributions demonstrated sensitivity to parameter values dependent on the origin of recharge, differentiated here as either direct recharge to the aquifer (de Vries and Simmers, 2002) or indirect recharge, such as infiltration through the streambed. Specifically, where the stream was fed by groundwater originating as recharge to the aquifer (i.e, Reach A), the volume of baseflow contribution was positively correlated with parameters that controlled upland recharge and groundwater flow toward the stream. These included the hydraulic conductivity values of surficial soils and the unconfined aquifer. Where baseflow originated as upgradient infiltration through the streambed (i.e., Reach B), the baseflow contribution was also influenced by characteristics of the upstream channel, such as the rill storage and streambed K_{sat}. The sensitivity of baseflow contribution along Reach B to streambed infiltration along the upstream reach illustrates the ability of the integrated model to account for dynamic feedback between the surface and subsurface domains.

Previous studies have demonstrated that specifying recharge to groundwater models as spatially variable can improve model performance evaluated against hydraulic heads (Jyrkama et al., 2002) and influence the spatial distribution of baseflows (Juckem et al., 2006). By partitioning precipitation into runoff and infiltration, a physics-based model offers a desirable alternative to specifying recharge a-priori in a traditional groundwater model. However, simulations of the Bertrand Creek Watershed demonstrate that adopting this integrated approach requires that controlling features, such as topography and surficial soils,

be adequately characterized and represented within the model. The influence of these controls on direct and indirect recharge to the Bertrand Creek Watershed model is discussed below.

4.5.1.1 Direct Recharge

A comparison of simulated and observed streamflow and baseflows indicates the Bertrand Creek Watershed model adequately simulates recharge during spring to mid-summer conditions, but overestimates recharge following significant rain events at the end of summer (Figure 4.6 and Figure 4.14). Two possible explanations are offered for the overestimation of streamflow late summer: (1) optimum parameter values representing saturated hydraulic conductivities (K_{sat}) of surficial soils are lower than the effective parameter values assigned based on pedotransfer functions, and (2) the model grid does not represent runoff and infiltration effectively. Despite the important role rainfall resolution can have on the simulated hydrologic response (e.g., Grayson et al., 1992), the overestimation of streamflow at the end of both dry seasons suggests the discrepancy is not primarily related to rainfall resolution.

Of the possible explanations offered above, the surface mesh is considered the likely cause for the baseflow discrepancy. Previous work has shown that topography in a finite element mesh can influence the dynamic saturation pattern along a channel, which in turn affects the surface–subsurface response (Vivoni et al., 2005). Topography in the Bertrand Creek Watershed model was assigned to the surface mesh using a DEM with a resolution coarser than the width of the stream channel (i.e., 20 m). As a result, the mesh may not effectively

represent the tributary network feeding the main channel. Since the distribution of surficial soils is dependent on position within the watershed (i.e., low permeability soils are located within the uplands and high permeability soils in the lowlands), runoff generated over upland soils likely infiltrates the sandy lowland soils. Therefore, explicitly defining tributary nodes and assigning a low K_{sat} value to these surface nodes is expected to improve the model response during baseflow conditions late summer by conveying upland runoff to the stream. The adjustment to soils properties at the base of the upland during calibration (Section 4.4.2.1) effectively conveys runoff to the stream in a manner similar to tributaries.

The level of detail represented in the model is a tradeoff between computational efficiency and necessary complexity. An earlier model design included increased resolution of the channel network and explicitly defined tributary nodes, however, this finer resolution model resulted in excessive simulation run times. The coarser mesh of the calibrated model increased the computational efficiency of simulations which was fundamental for calibration and for investigating the mechanisms that control stream–aquifer interaction along the stream.

4.5.1.2 Indirect Recharge: Streambed Infiltration

The stream–aquifer interaction was replicated in the calibrated model by reducing the surficial soils K_{sat} by a factor of 10 along the stream. Where stream lengths become losing or ephemeral, however, the modelled surface water height and hydraulic head beneath the streambed suggest the streambed K_{sat} value that provides the best fit to losing conditions differs from the value for gaining conditions. Decreased streambed K_{sat} values reduced

streambed transmission losses and prevented stream reaches from becoming dry during losing conditions (Figure 4.19), but contributed to hydraulic heads beneath the stream that were above realistic values during gaining conditions. The sensitivity suggests that either increased resolution of streambed heterogeneity is required or mechanisms controlling streambed seepage are dependent on the direction of the hydraulic gradient. Elaborating on these controls, three possible explanations are offered, which are not considered exclusive: (1) Gaining conditions are fed by stream bank seepage and governed by properties of the banks (Langhoff et al., 2006), while losing conditions are governed by streambed properties which control vertical infiltration; (2) Streambed hydraulic conductivity decreases through a dry season as an increased deposition of fines accompanies lower flows (Hatch et al., 2010); and (3) Increased resolution of aquifer or streambed heterogeneity is needed to represent spatial seepage patterns (Fleckstein et al., 2006; Frei et al., 2009; Engdahl et al., 2010). Resolving the discrepancy will require further field investigation within the upper watershed to complement model evaluation.

4.5.2 Evapotranspiration

4.5.2.1 Evapotranspiration in the Riparian Zone

Evapotranspiration within the riparian corridor is an important control of streamflow in Bertrand Creek. Due to the low magnitude of streamflows, the predicted rate of riparian zone evapotranspiration is equivalent to approximately half the discharge at the watershed outlet during baseflow conditions. Evapotranspiration is known to cause seasonal differences in the recession curve, with steeper recession in summer months when evapotranspiration rates are higher (Tallaksen, 1995; Wittenberg and Sivapalan, 1999). As a result, when

evaporation is not accounted for in baseflow estimation techniques, groundwater discharge can be overestimated (Halford and Mayer, 2000; Peters and van Lanen, 2005; Werner et al., 2006). In an investigation of baseflow along the Sandy Creek in Australia, where low flows can drop below 0.01 m^3/s (1 ML/d), Werner et al., (2006) note that estimates of riparian vegetation water use may account for 0.5 ML/d (0.006 m^3/s averaged over a 24-hour period). Other studies estimate that evaporation reduces streamflow by up to 0.04 m^3/s in the 170 km^2 Pang catchment in the UK (Peters and van Lanen, 2005), and reduces annual discharge by 20 percent (10 mm) in a semi-arid catchment in Australia (Wittenberg and Sivapalan, 1999). The estimate of riparian zone evapotranspiration in this study (8 mm, Section 4.4.5.1), which is the first to be based on a three-dimensional, integrated surface-subsurface model, supports the findings of previous investigations and indicates evapotranspiration has an important influence on low flows.

The rate of streambed seepage and the length of Bertrand Creek over which losing conditions develop are sensitive to the partitioning of evaporation and transpiration along stream elements. Assigning only evaporation along the stream effectively causes the creek to act as an "evaporation window" (e.g., Smerdon et al., 2007), which promotes groundwater upwelling to the stream (Figure 4.17). Assigning an increased percentage of transpiration along the stream (i.e., 95% in the calibrated model) reduces groundwater upwelling and can induce streambed infiltration as vegetation increasingly competes for water. These findings are supported by studies examining vegetative water use, which have shown transpiration can induce losing conditions along a stream (Culler et al., 1982; Chen, 2007), and under high vegetation water demand, may create an unsaturated zone beneath the stream by drawing

down the water table (Banks et al., 2011a). Partitioning modelled ET into its two components will have important consequence for studies examining fluxes across the streambed, especially nutrient or contaminant fluxes in areas where ET_p rates are high. Within the Bertrand Creek Watershed model, it is considered appropriate to assign transpiration as the dominant ET process along the stream. This assignment takes into consideration the comparatively small area the stream represents within each model element, and that direct evaporation can be negligible from streamflow where a riparian zone is present (e.g., Brown, 1969; Webb and Zhang, 1997).

4.5.2.2 Influence of Evapotranspiration Parameters on Simulated Hydrologic Response

Since evapotranspiration comprises a significant component of the Bertrand Creek Watershed water balance, ET parameter values have a greater potential to influence model results. The experience of this study suggests that evapotranspiration parameters assigned within a model employing the Kristensen and Jensen (1975) methodology require thorough testing even when based on representative literature values. For example, increasing the root depth across the Bertrand Creek Watershed model from 2 m to 5 m resulted in a slight increase in baseflow (2 percent), a response that is counter-intuitive to increased forestation. Where a shallow water table is present, such as adjacent the stream, the increase in root depth effectively causes less water to be drawn from each nodal depth and groundwater flow through saturated grid cells increases. Plant rooting strategies are influenced by moisture availability and climate (Laio et al., 2006; Collins and Bras, 2007), and the assignment of root depth should therefore take local hydrologic conditions, such as water table depth, into

consideration. A similar experience resulted when LAI values were varied, and following the principle of parsimony both parameters were assigned constant values (McLeod, 1993; Jakeman and Hornberger, 1993). This suggests that utility of integrated models employing the Kristensen and Jensen (1975) evapotranspiration methodology to evaluate effects of deforestation or land management practices on low flow conditions requires careful consideration of the influence of evapotranspiration parameter values and methodology on modelled response.

A further departure in this study from typical literature values for ET parameters is the exclusion of the upper limit to transpiration (e.g., Feddes et al., 1978). When included, the upper limit to transpiration restricts transpiration from wet soils and the water table, and has a considerable effect on the calculated Bertrand Creek Watershed water balance. Sciuto and Diekkrüger (2010) demonstrated that during wet conditions the upper limit to transpiration creates a nonlinear relationship between soil moisture and evapotranspiration which causes the water balance to be sensitive to grid resolution. Excluding the upper limit to transpiration provides not only a better match against evaluated criteria, but given the dominance of phreatophytic vegetation in the watershed (such as alder trees), also accommodates transpiration from a shallow water table (Meyboom, 1966; Bond et al., 2002; Gribovszki et al., 2008).

4.5.3 Surface Water–Groundwater Interaction

4.5.3.1 Nature of the Surface Water–Groundwater Interaction

Previous work has shown the flux across a streambed is spatially variable (Cey et al., 1998; Sudicky et al., 2008). The simulations here show significant variability at the local scale, even when hyporheic flow driven by differences in streambed topography is not accounted for (Figure 4.12). These findings are significant for field studies attempting to quantify the magnitude of flux across the streambed by point-based measurements, and indicate a high degree of variability amongst measurements should be expected.

4.5.3.2 Seasonal Hydrologic Response along the Stream

The direction of flux across the streambed suggests that gaining and losing conditions along Bertrand Creek are influenced by topography. Specifically, the model predicts losing conditions dominate where: (1) the topographic slope of the valley (perpendicular to the stream) is insignificant, or (2) the downstream slope along the direction of the channel increases. In contrast, the model predicts gaining conditions are sustained along Bertrand Creek where a significant valley (lateral) slope sustains a predominant component of groundwater flow perpendicular to the stream (baseflow-dominant; Larkin and Sharp, 1992). The relation between topography and simulated direction of flux across the Bertrand Creek streambed suggest that topography, specifically the ratio between the valley and channel slope (Chapter 3.4.6.3), are promising metrics for anticipating losing conditions along other streams connected to an unconfined aquifer.

The integrated model contributes a better understanding of water table dynamics adjacent to a stream, which has important implications for the function of riparian zones on water quality (Burt et al., 2002; Vidon and Hill, 2004). For example, where losing conditions are generated upstream of an increase in channel slope, model results indicate the water table decline originates at the increase in slope and propagates upstream with time, enhanced by increased aquifer transmissivity (Figure 4.18). Where losing conditions are generated along stream reaches with a negligible topographic slope perpendicular to the channel, the water table decline is spatially variable and the extent of decline varies with hydraulic conductivity of the streambed and aquifer (Figure 4.18 and Figure 4.19). Where gaining conditions are sustained by groundwater flow perpendicular to the stream, the water table fluctuation through the dry season can be negligible (Figure 4.16).

The spatially variable nature of the water table decline beneath the streambed is influenced by a variety of factors, some of which are incorporated within the model: (1) topography, as discussed above; and (2) position of the channel relative to the groundwater flow systems (e.g., Winter, 1999). Other factors, which are not incorporated within the model, are expected to contribute further to the variability in water table decline: (3) spatially variable evapotranspiration (Meyboom, 1966; Section 4.5.2); and (4) heterogeneity of the subsurface deposits (Fleckenstein et al., 2006; Frei et al., 2009).

4.6 Assessing the Impact of a Large Capacity Groundwater Well

To illustrate the application of the Bertrand Creek Watershed model as a predictive tool, a scenario is evaluated where a large capacity groundwater well is installed in the West of

Aldergrove (WALD) aquifer (Figure 4.20). The numerical model is used to assess potential changes in spatial extent of the dry streambed for placement of the well at distances varying from 150 m (P1) to 1000 m (P4) from the stream. Groundwater is withdrawn from the well at a rate of 1,600 m^3/d, which is equivalent to the highest extraction rate drawn from the municipal wells supplying the town of Aldergrove (Table 4.2). The predictive demonstration uses climate data from the 2006 hydrologic year, and results are compared against results from the 2006 model presented in Section 4.4.4. Groundwater withdrawals begin coincident with the start of the transient simulation on April 1, 2006.

The distance of each well from the stream, the net decrease in flow at the watershed outlet, and the increase in dry streambed length are presented in Table 4.8. Results indicate that placement of the well 150 m from the stream (P1) reduces streamflows by 3.3 L/s, which contributes to a 23% reduction in minimum streamflow at the watershed outlet. This well placement results in the streambed going dry an estimated 11 days earlier than the base case, delays the return of streamflows by 7 days, and increases the length of the dry streambed by 160 m (Figure 4.20). Impacts on streamflows diminish with increased distance of the well from the stream (Table 4.8). Used in this way, the integrated model provides water managers with a tool for assessing optimal groundwater withdrawal strategies.

4.7 Recommendations for Integrated Modelling and Field Studies

The development and calibration of an integrated numerical model can benefit from a well designed field data collection program. Based on the findings of this study,

recommendations for field programs collecting data to calibrate a surface water–groundwater model include the collection of:

- Measurements quantifying the change in baseflow along the stream. These measurements are considered fundamental for constraining estimates of subsurface parameter values. Incremental baseflow measurements provide a local measure against which parameters controlling groundwater flow between the recharge and discharge zone can be assessed. Simulated baseflows along Bertrand Creek demonstrated less sensitivity to ET parameterization during calibration than individual measurements of streamflow.
- Measurement of surface water height influenced primarily by climatic conditions (i.e., have limited hydrologic connection with the subsurface). If the specified ET_p rate is treated as a calibrated model parameter, such as in this study (Section 4.4.2.3), a non-unique solution is created between the ET_p rate and hydraulic conductivity values controlling the magnitude of groundwater discharge to the stream. As a result, the measurement of surface water height in the pond was useful in confirming that the magnitude of evapotranspiration in the Bertrand Creek Watershed model was realistic.
- Water table fluctuations adjacent to the channel where stream conditions transition from gaining to losing. These measurements are useful for constraining the timing of the transition between gaining and losing conditions, which has an important influence on the hydrologic response during baseflow conditions as well as on runoff generation in the dry season.

Numerical model results can additionally be used to identify key locations to focus field efforts. These locations can be identified, for example, by the plot of cumulative flux (Figure 4.12b). This plot presents an integrated representation of a watershed's geomorphic characteristics which control baseflow generation, including topography, streambed permeability, and extent of permeable units adjacent the stream. The resulting plot is unique to each watershed and can be considered a 'flux signature'. Changes to the flux signature's downstream slope reveal changes in the regional and local architecture of a watershed, which govern groundwater flow systems feeding the stream. Transient changes to the flux signature reveal stream reaches that are susceptible to losing conditions under climatic or anthropogenic stress. Because the shape of the flux signature is reproduced during the model calibration process, it can be used as a tool to identify key locations to focus efforts during a field investigation where larger and more easily quantified groundwater contributions are expected.

4.8 Conclusions

An integrated surface-subsurface model of the Bertrand Creek Watershed has been developed to study stream–aquifer interaction during baseflow conditions. The model allows simultaneous simulation of exchange fluxes between the surface and subsurface, without any a-priori assumptions regarding these fluxes. The watershed model was calibrated using distributed field data collected in 2007, including streamflows, groundwater contributions to streamflow, soil moisture content, change in hydraulic heads, and change in surface water height in a pond. The calibrated model was then used to simulate the 2006 dry season by changing only the climate boundary conditions. The magnitude of streamflows and baseflow

contributions simulated by the 2006 transient model compare favourably with field observations and provides further corroboration that the model adequately represents the dry season hydrology of the watershed.

Using diverse data types from the surface and subsurface domain to evaluate model performance was fundamental for increasing confidence both in calibrated parameter values and the conceptual hydrologic model of the watershed. Of the evaluated criteria, measurements of baseflow contribution were the most beneficial targets for constraining parameter values during calibration, while the change in ponded surface water height was valuable for confirming that the simulated evapotranspiration rates were reasonable.

The simulated development of gaining and losing stream conditions supports the hypothesis presented in Chapter 3 that losing conditions develop seasonally along stream reaches with a negligible topographic slope perpendicular the stream or upstream of an increase in channel slope. The extent of water table decline is controlled by characteristics of both the upgradient and downstream aquifer and streambed. The implication of these results extends to a wide range of watershed environments beyond the lowland watershed in this study, and can be used to identify stream locations that have potential to become losing reaches.

Evapotranspiration within the Bertrand Creek riparian zone has a significant influence on baseflows, and confirms observations made by others that evapotranspiration effects should be considered during low flow conditions. Streambed seepage rates predicted by the model indicate that transpiration by riparian vegetation can induce streambed infiltration, which in

turn increases the longitudinal extent of losing conditions along a stream. Parameterization of evapotranspiration into components of transpiration and evaporation along the stream has implications for studies assessing contaminant and nutrient fluxes across the streambed. Even though the evapotranspiration methodology within HydroGeoSphere has limitations, the ability to explicitly represent the evapotranspiration as a modelled process allows an improved and more realistic representation of real-world hydrologic processes.

In addition to evapotranspiration, simulating baseflows relied on an adequate representation of topography and surficial soils across the model surface. These factors control the partitioning of rainfall into runoff and infiltration, and therefore also control the occurrence, magnitude, and spatial distribution of recharge to the unconfined aquifer.

Adopting an integrated modelling approach is beneficial in comparison to a traditional groundwater modelling approach within watershed-scale baseflow studies where stream conditions transition from gaining to losing and streambed infiltration contributes to downstream flows. Under these conditions, the feedback between domains makes calibration of the physically based model considerably more challenging, but allows a greater understanding of the hydrologic dynamics that influence baseflow generation. An integrated modelling approach also provides a sound framework for water managers to evaluate the impacts of different water allocation strategies on baseflows and make more informed water management decisions.

Table 4.1 Surficial soil saturated hydraulic conductivity values and van Genuchten parameters

Textural class	Residual water saturation	Total porosity	Saturated hydraulic conductivity	van Genuchten parameters	
	S_{wr} [–]	n [–]	K_s [m/s]	α [m^{-1}]	β [–]
Silty clay loam	0.09	0.48	1.3×10^{-6}	0.84	1.52
Loam	0.06	0.40	1.4×10^{-6}	1.11	1.47
Silt loam	0.06	0.44	2.1×10^{-6}	0.51	1.66
Sandy loam	0.04	0.39	4.4×10^{-6}	2.67	1.45
Loamy sand	0.05	0.39	6.4×10^{-6}	3.47	1.70
Sand	0.03	0.37	8.0×10^{-5}	4.50	3.20

Table 4.2 Average pumping rates of municipal supply wells

Well	Pumping rate [m^3/d]
Aldergrove #3	450
Aldergrove #4	460
Aldergrove #6	1,610
Aldergrove #7	1,060
Aldergrove #8	1,610
Aldergrove #9	960
Aldergrove #10	570

Table 4.3 Saturated hydraulic conductivity and specific storage values of hydrostratigraphic units

Hydrostratigraphic unit	Hydraulic conductivity K [m/s]	Specific storage S [m^{-1}]
Unconfined aquifers		
Abbotsford	1×10^{-4}	1×10^{-7}
Perched water zone	1×10^{-4}	1×10^{-7}
Confined aquifers		
Aldergrove	1×10^{-4}	1×10^{-5}
West of Aldergrove	2×10^{-4}	1×10^{-5}
South of Hopington	1×10^{-4}	1×10^{-5}
Confining units		
Aquitard 1	1×10^{-8}	1×10^{-4}
Aquitard 2	1×10^{-9}	1×10^{-4}
Aquitard 3	1×10^{-10}	1×10^{-4}

Table 4.4 Values for the Manning roughness coefficient and rill storage

	Manning $n_{x,y}$ [s $m^{-1/3}$]	Rill storage h_s [m]
Rural (overland)	0.1	0.01
Urban	0.015	0.005
Upper stream	0.012	0.2
Lower stream	0.012	0.1

Table 4.5 Evaporation parameters assigned uniform values across the watershed

Model parameter	Value	Units
Transpiration fitting parameter (C_1)	0.3	
Transpiration fitting parameter (C_2)	0.2	
Transpiration fitting parameter (C_3)	1	
Evaporation limiting saturation (min)	0.5 x WP	
Evaporation limiting saturation (max)	FC-REW[a]	
Field capacity (FC)	-1	m[b]
Wilting point (WP)	-150	m[b]
Canopy interception (c_{int})	5 x 10^{-4}	m

[a] Readily evaporable water (Table 19, Allen et al., 1998)

[b] metres pressure head of water

Table 4.6 LAI values assigned in the calibrated model

	Leaf area index LAI [–]
Rural	1.2
Urban	1.2
Stream	2.5
Ponded water	0

Table 4.7 Water balance terms for the 2007 transient model (April 1 to October 10)

	Rain[a]	Water addition	ET_{act} [a]	Runoff	Subsurface flow	Water abstraction	Net change storage	Water balance error
mm	379	3	-414	-73	-51	-28	-190	-5
% of rainfall	100%	1%	-109%	-19%	-13%	-7%	-50%	-1%

[a] values account for intercepted volumes

Table 4.8 Results of predictive demonstration

Well	Distance from stream [m]	Reduced discharge at outlet [L/s]	Maximum increase in length of dry streambed [m]	Increase in time streambed is dry [days]
P1	150	3.3	160	18
P2	400	1.5	100	12
P3	700	1.0	40	8
P4	1000	0.8	30	7

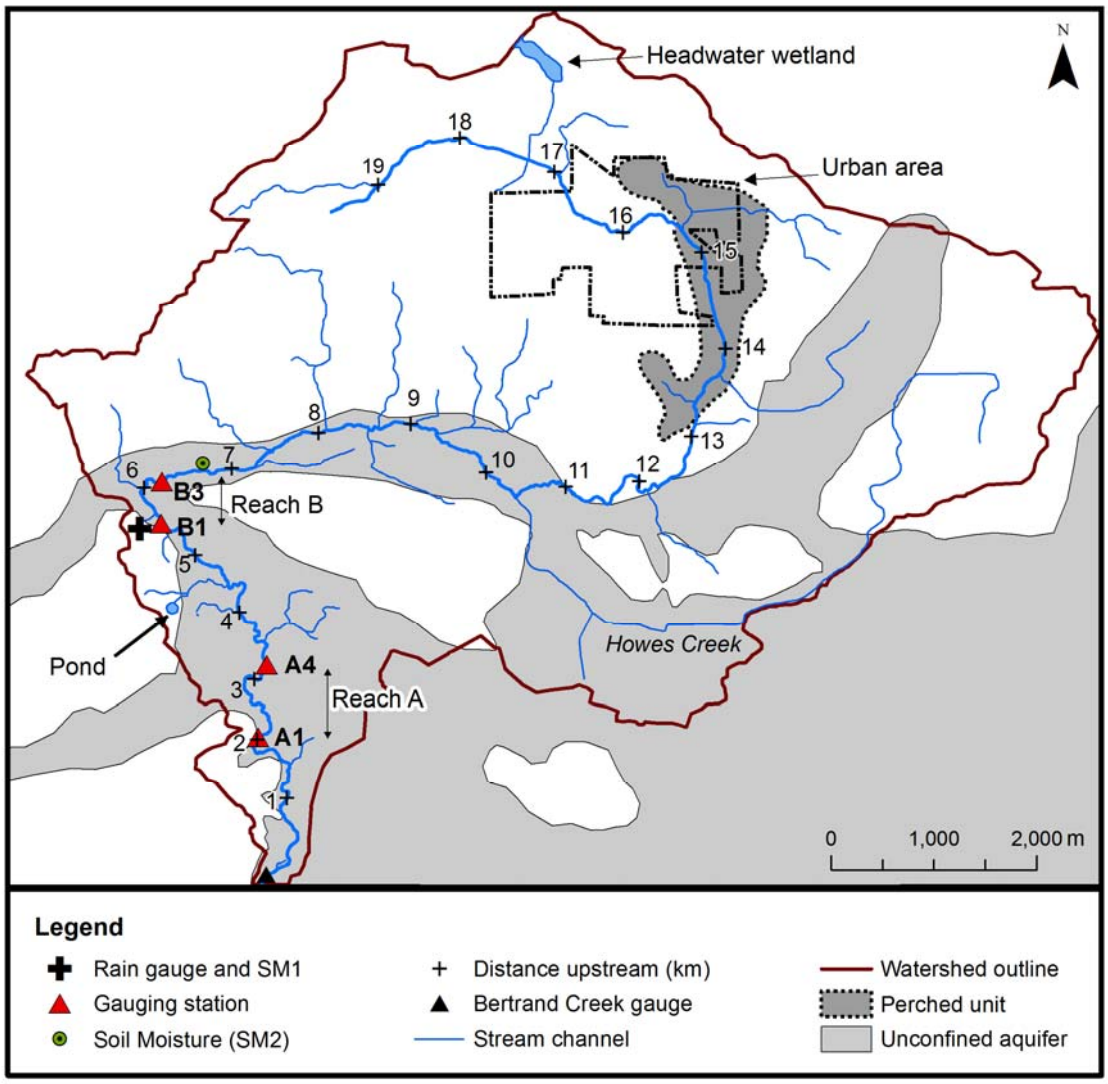

Figure 4.1 Bertrand Creek Watershed study area shown with locations of field instrumentation and unconfined water bearing units.

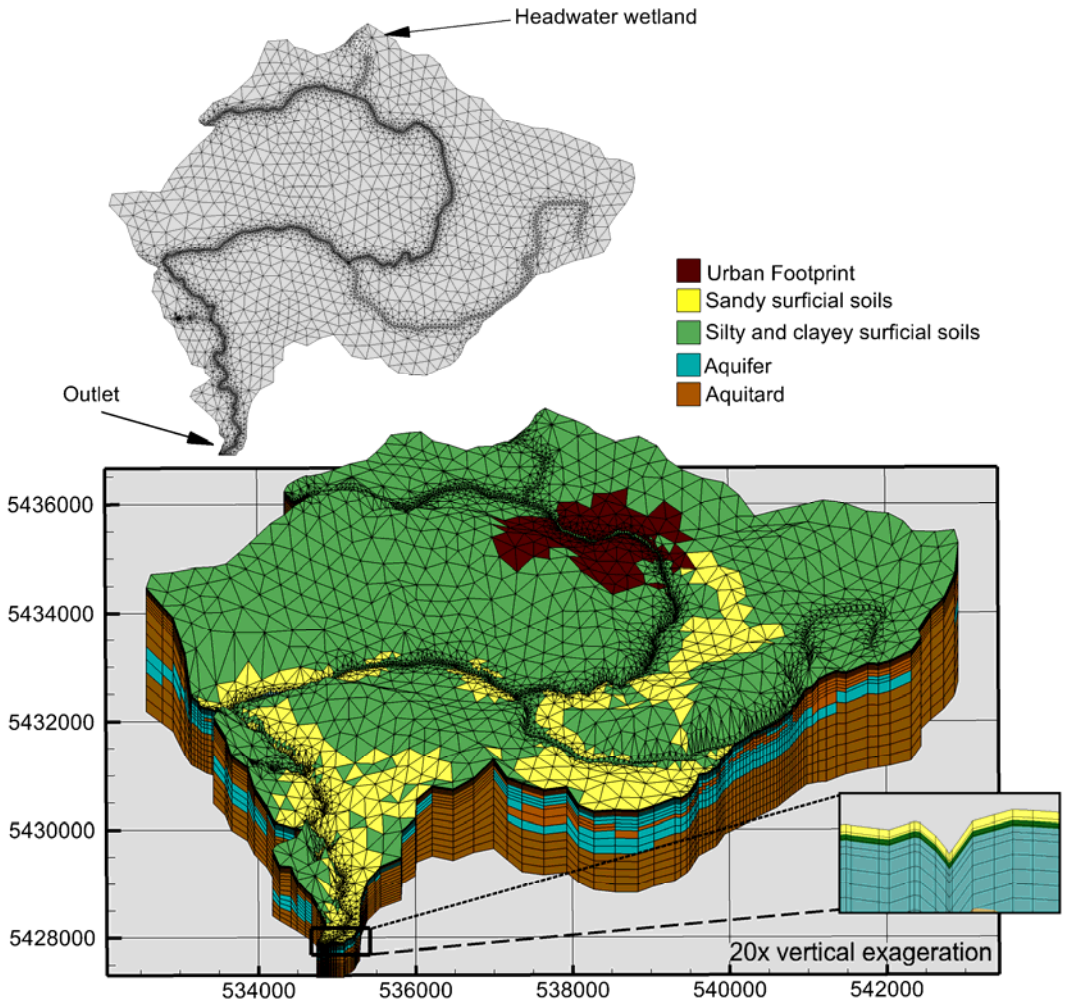

Figure 4.2 Spatial discretization of the Bertrand Creek Watershed model with the distribution of surficial soils, hydrostratigraphy, and location of the urban area.

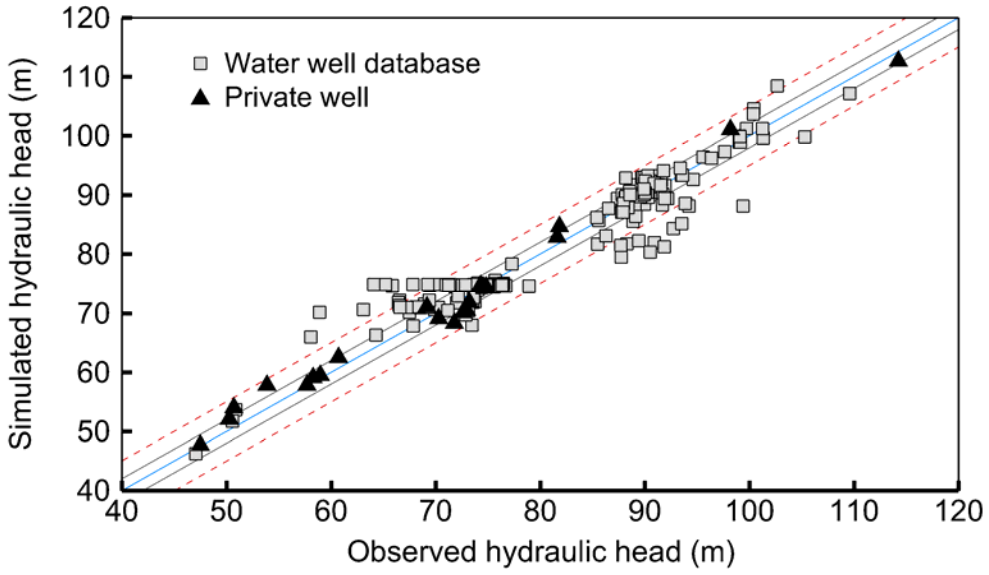

Figure 4.3 Simulated and observed hydraulic heads within the Bertrand Creek steady state model. Solid gray lines indicate ±2 m from a 1:1 fit and dashed red lines indicate ±5 m.

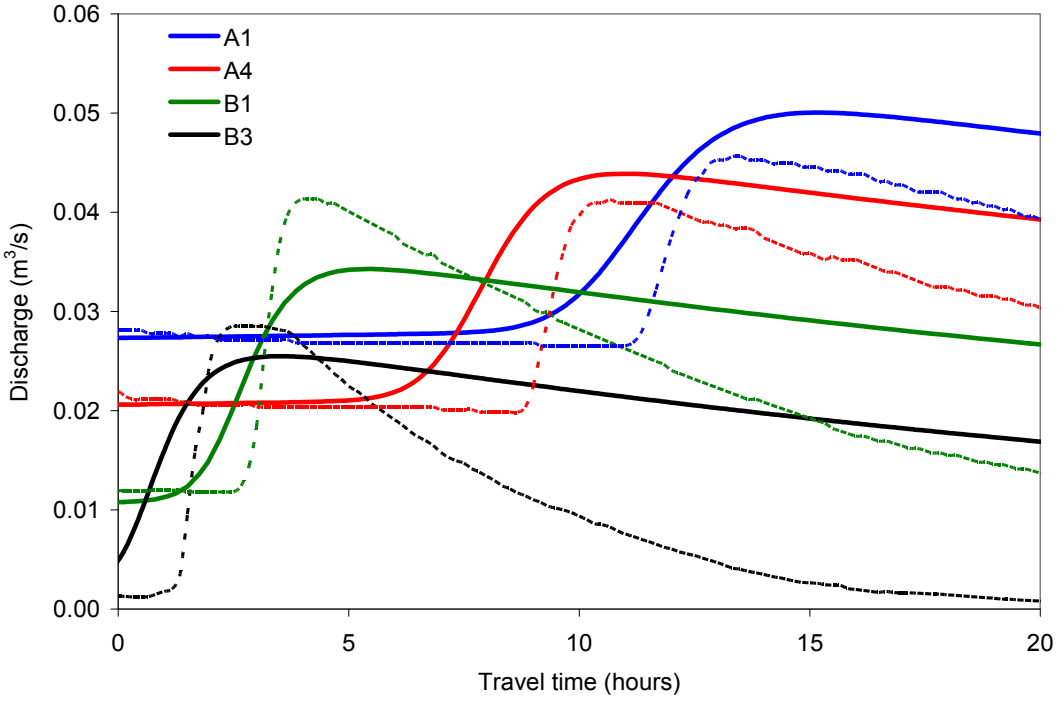

Figure 4.4 Simulated (solid) and observed (dashed) travel times for a pulse of water that travelled along Bertrand Creek on August 29, 2007. Results are shown for a Manning coefficient of 0.012 s m $^{-1/3}$.

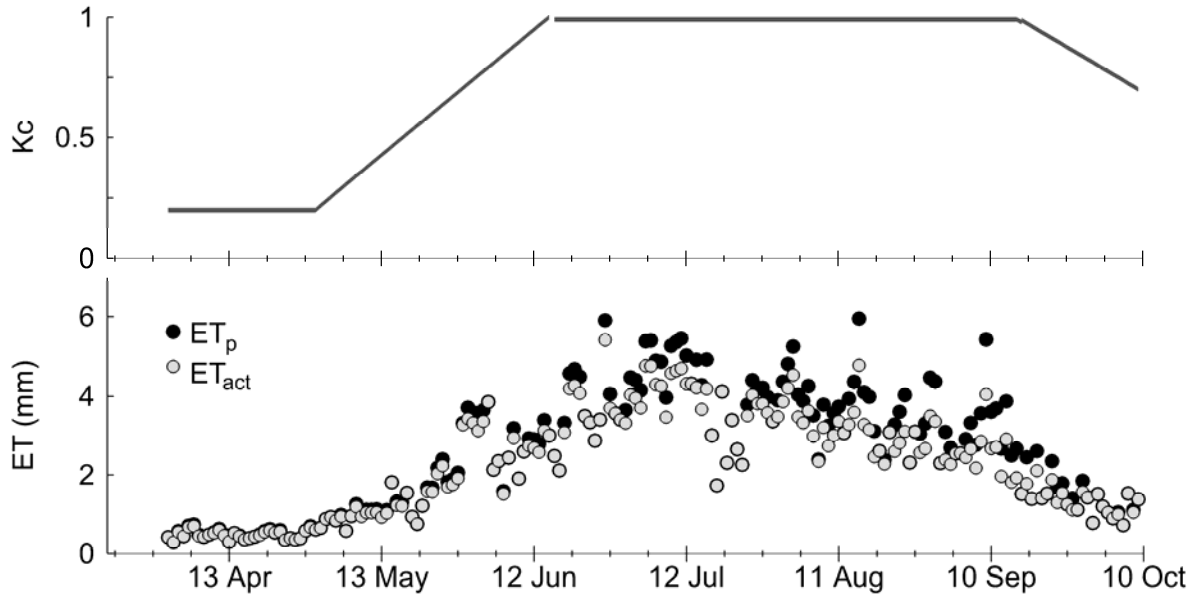

Figure 4.5 Calibrated crop coefficients applied to ET_o (top); ET_p and simulated ET_{act} for the 2007 transient model (bottom). ET_{act} values include water evaporated from interception storage.

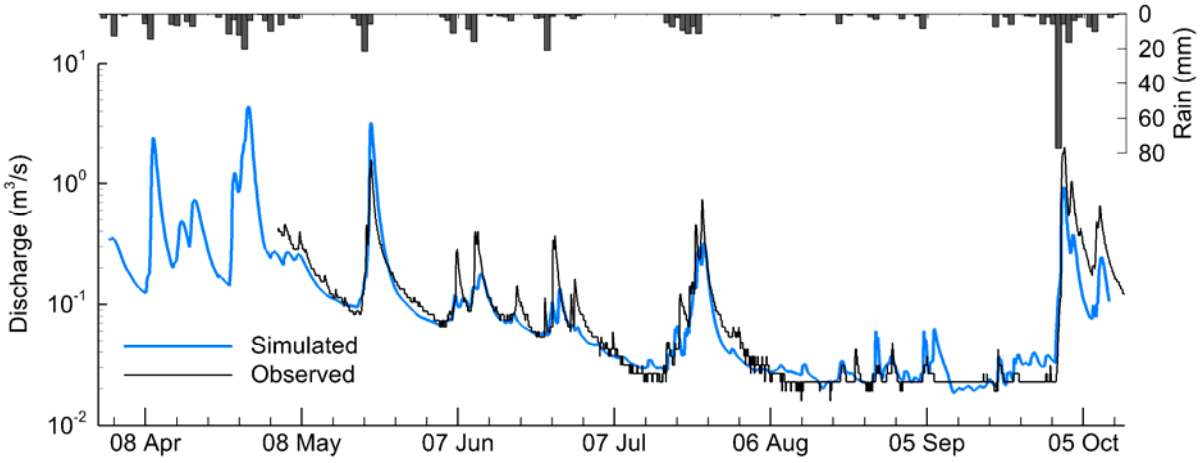

Figure 4.6 Simulated and observed discharge at the watershed outlet in 2007 shown with daily precipitation.

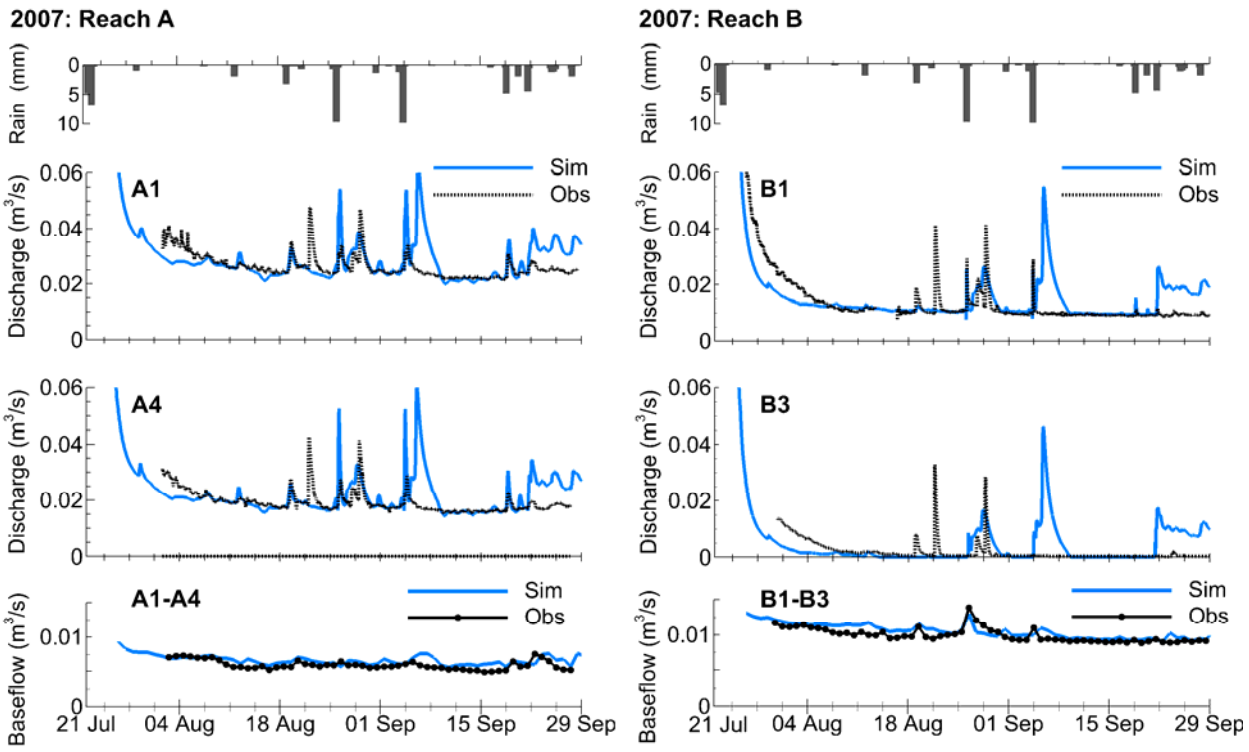

Figure 4.7 Simulated and observed streamflow and daily average baseflow at gauging stations within Reaches A and B. Rain values shown are the event-based values input into the model.

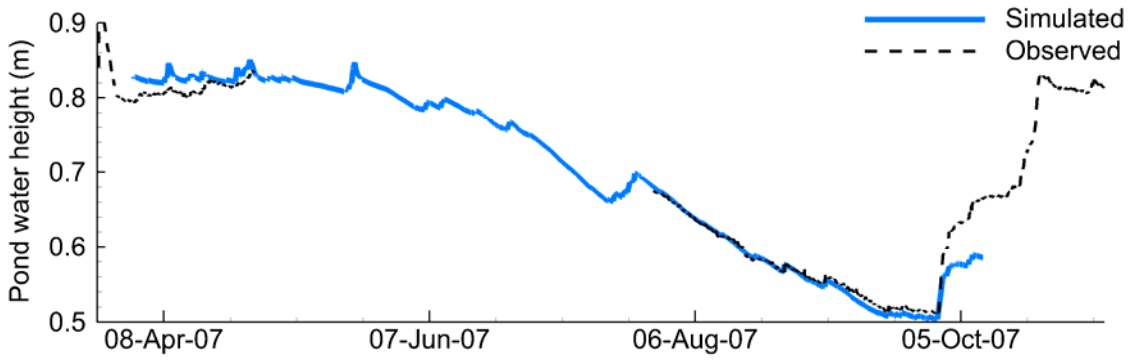

Figure 4.8 Simulated and observed surface water height within a pond situated in the watershed.

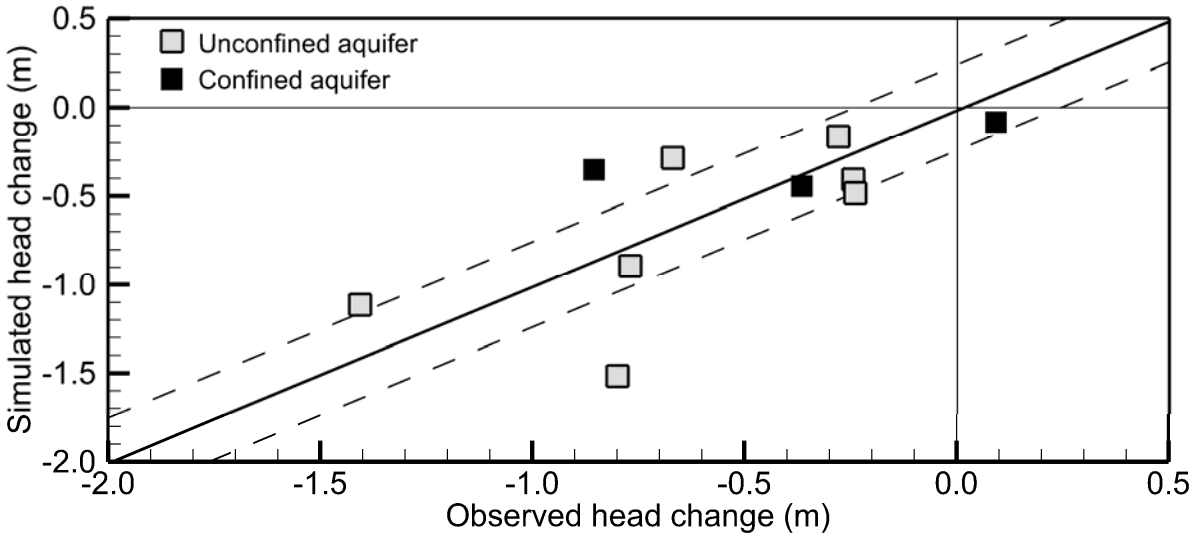

Figure 4.9 Simulated and measured drop in hydraulic head within private groundwater wells between June and September, 2007, shown with 0.25 m bounds.

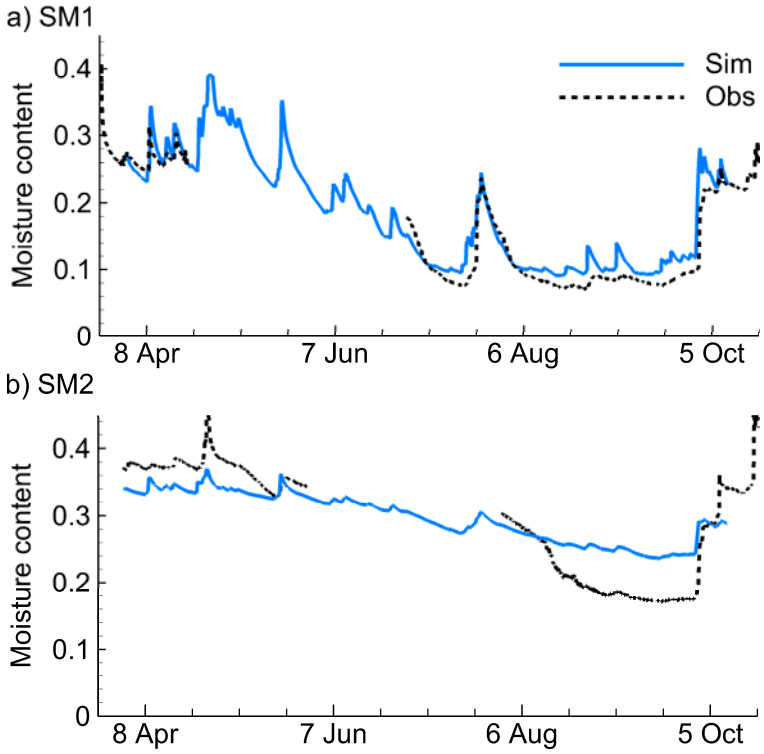

Figure 4.10 Simulated (0.5 m) and observed (0.35 m) soil moisture contents at sensor locations a) SM1 and b) SM2.

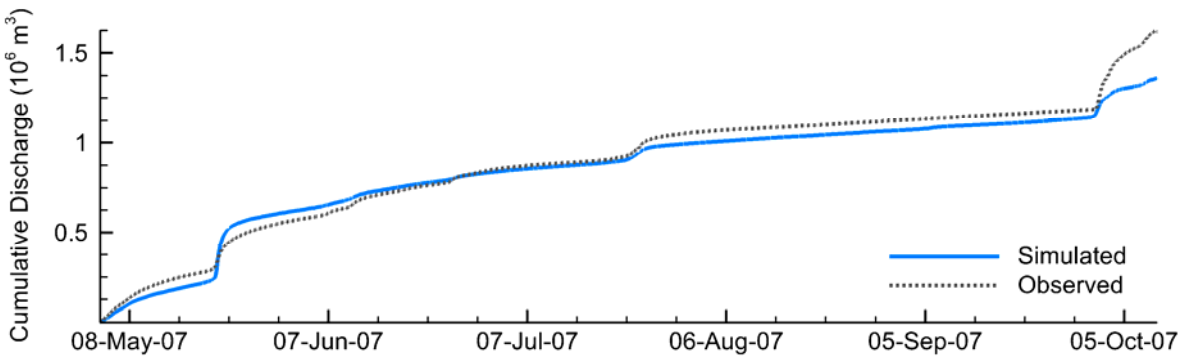

Figure 4.11 Simulated and observed cumulative discharge at the watershed outlet in 2007.

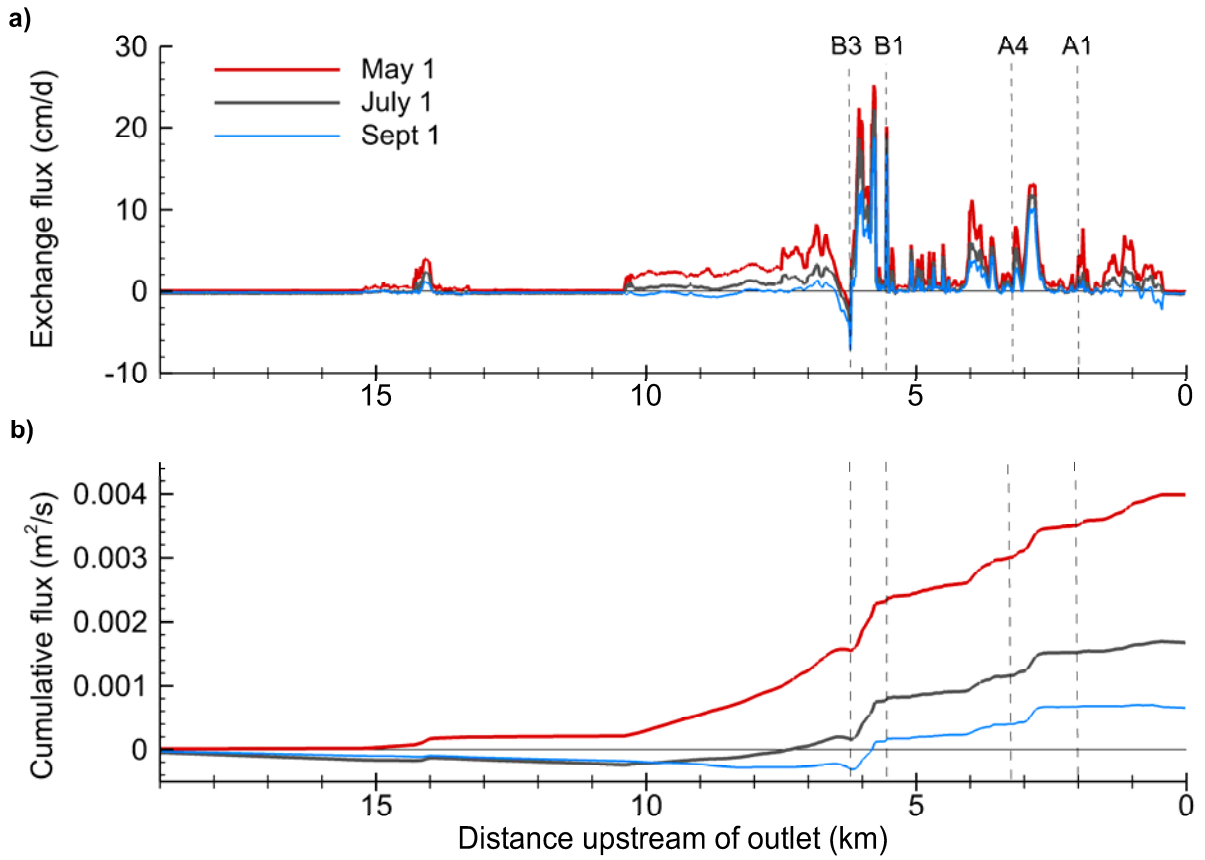

Figure 4.12 a) The exchange flux across the Bertrand Creek streambed with distance upstream of the watershed outlet shown on select days with baseflow conditions, and b) the cumulative exchange flux along the stream center, calculated from the upstream-most extent of the stream.

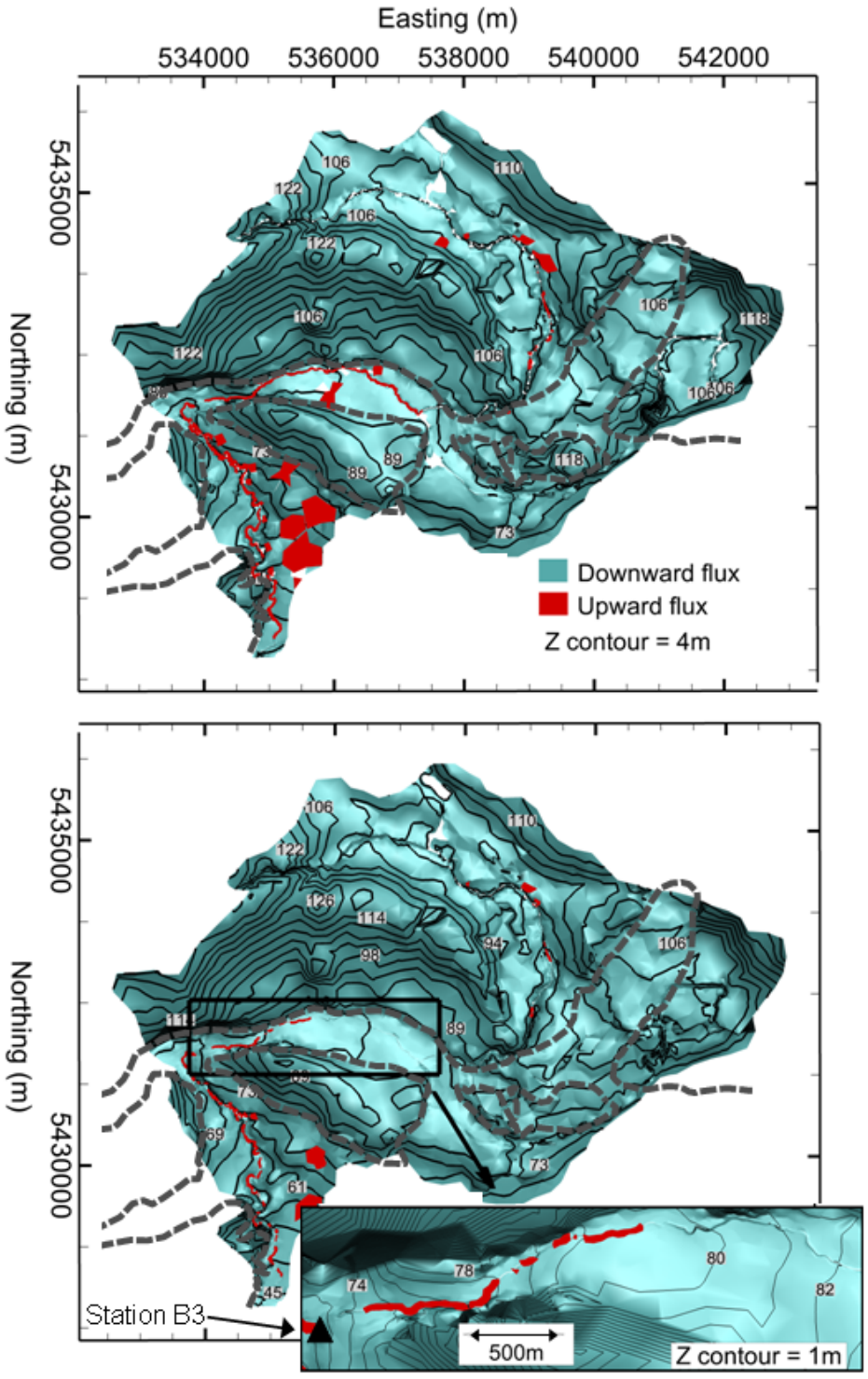

Figure 4.13 Hydraulic heads and direction of surface-subsurface exchange simulated by the transient model for June 1 (top) and September 1, 2007 (bottom). The dashed grey line indicates the extent of the unconfined aquifer.

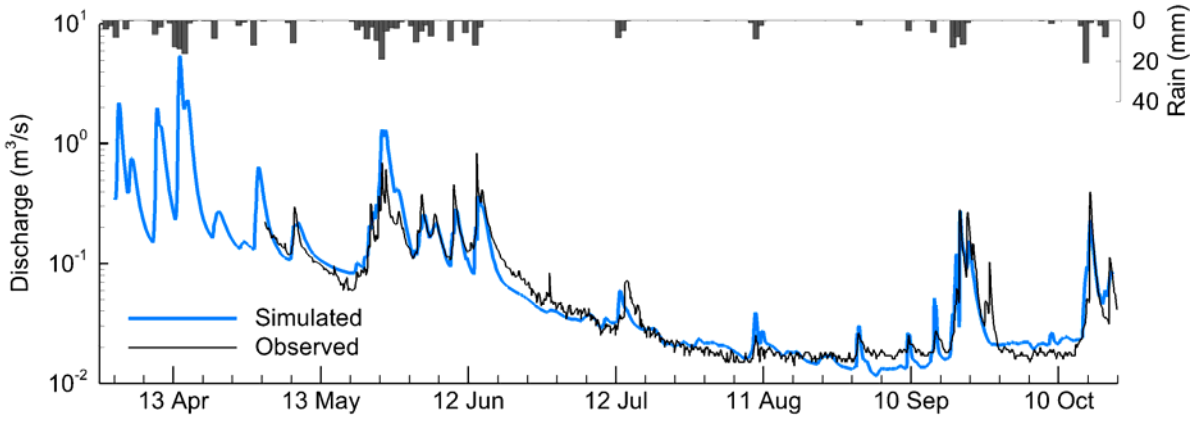

Figure 4.14 Simulated and observed discharge at the watershed outlet in 2006 shown with daily precipitation.

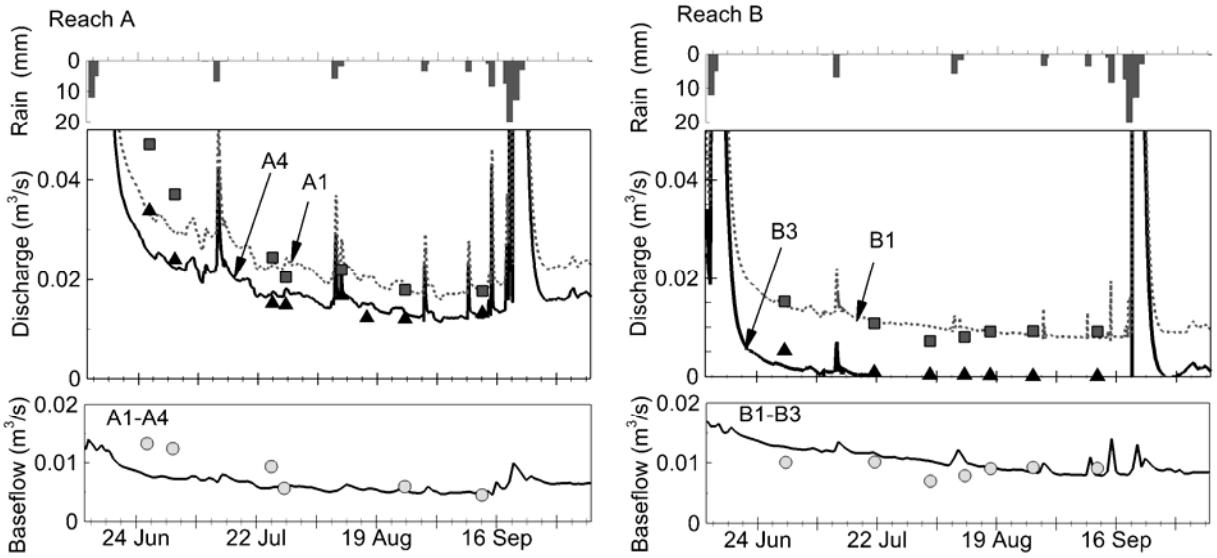

Figure 4.15 2006 simulated (lines) and measured (points) streamflows and baseflow contributions at gauging stations within Reaches A and B. Simulated baseflow values are daily averages and rain values shown are event-based.

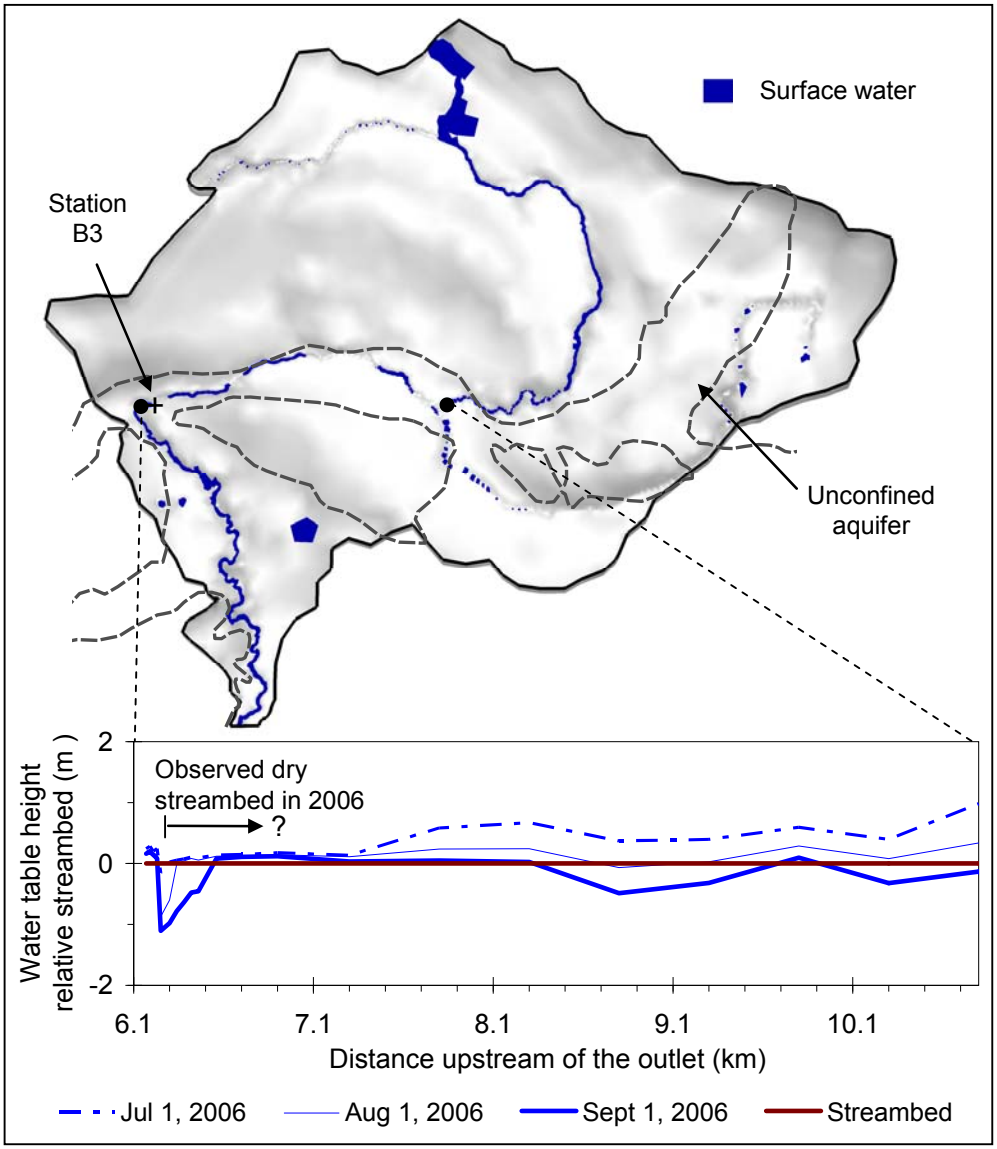

Figure 4.16 Top: 2006 transient model results showing the presence of surface water across the model surface on September 1, 2006. Bottom: Height of the water table beneath the streambed shown relative to the height of the streambed for a stream segment on select dates. The longitudinal extent of the dry streambed observed in 2006 is also shown; however, the maximum upstream extent beyond 500 m is unknown. Note that the distance upstream of the watershed outlet increases along the horizontal scale.

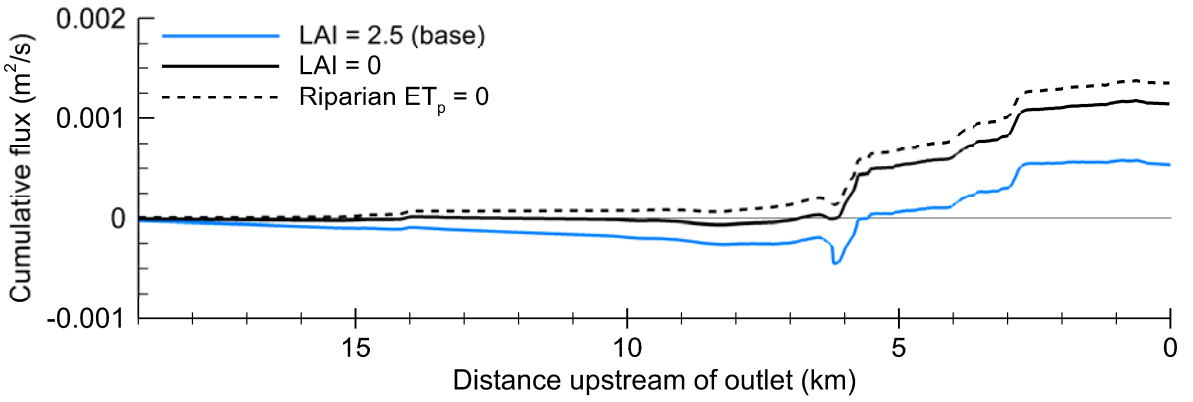

Figure 4.17 Comparison of cumulative flux across the streambed for the 2007 base case simulation with transpiration as the dominant ET process along the stream (LAI = 2.5), evaporation only specified along the stream (LAI = 0), and no evapotranspiration along the stream (ET_p = 0).

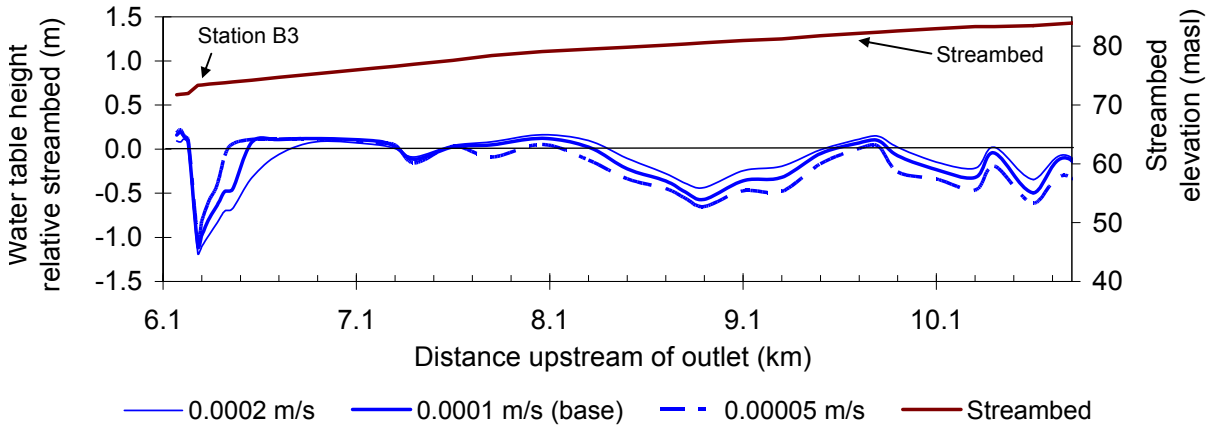

Figure 4.18 Sensitivity of the water table beneath the streambed to hydraulic conductivity in the unconfined aquifer. The elevation of the streambed is also shown. Note that the distance upstream of the watershed outlet increases along the horizontal scale.

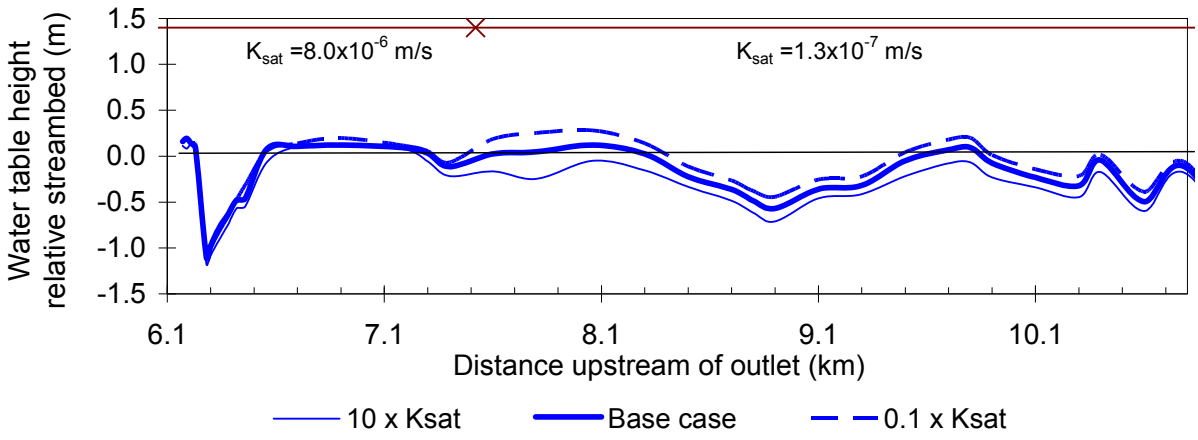

Figure 4.19 Sensitivity of the water table beneath the streambed to streambed hydraulic conductivity. Distribution and value of K_{sat} along the stream is shown at top. Note that the distance upstream of the watershed outlet increases along the horizontal scale.

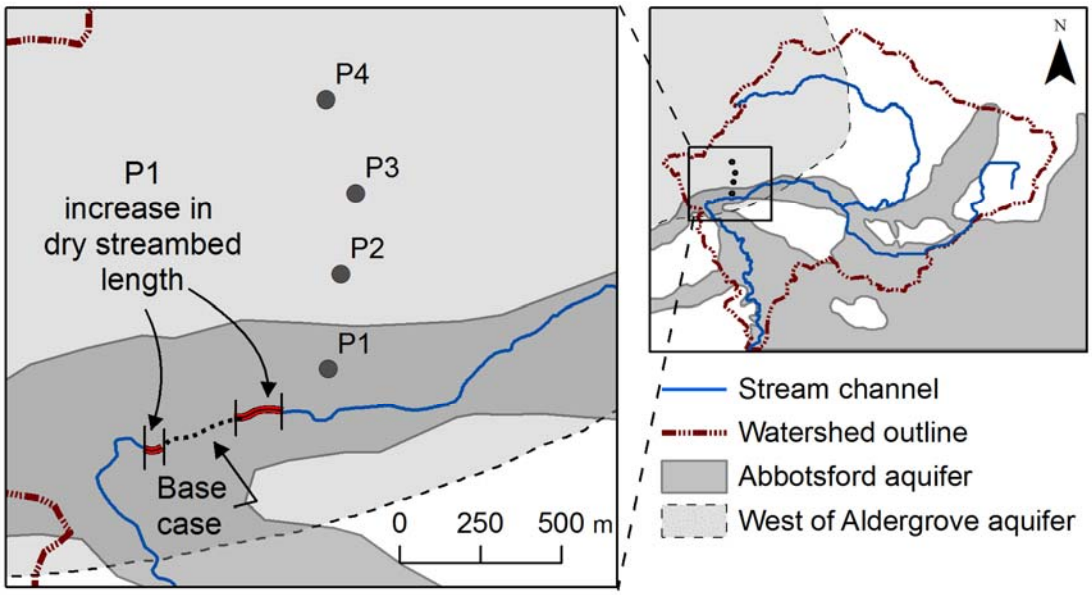

Figure 4.20 Location of pumping wells for the predictive demonstration and extent of dry streambed for the base case and pumping well placed at P1.

Chapter 5: Conclusions

Understanding the nature and controls of stream–aquifer interaction is key for effective water resource management, particularly in the face of increasing stress on groundwater resources (Council of Canadian Academies, 2009). As highlighted in Chapter 1, the interaction between a stream and underlying aquifer is dynamic (Winter, 1999; Sophocleous, 2002) and characterizing this interaction at the scale of a watershed is a comprehensive endeavour. In the past decade, there has been continued improvement in physics-based numerical models that simulate coupled surface and subsurface hydrologic flow (e.g., VanderKwaak, 1999; Panday and Huyakorn, 2004; Kollet and Maxwell, 2006; Therrien et al., 2010). These sophisticated models may provide an improved representation of the hydrologic exchange between a stream and underlying aquifer than traditional groundwater models. Due to their recent development, however, their application in watershed-scale studies is limited.

In this thesis I investigated the nature and controls of stream–aquifer interaction within the 46 km^2 Bertrand Creek watershed, and investigated how mechanisms which control this interaction are represented within an integrated surface-subsurface numerical model. The Bertrand Creek Watershed is situated in a glaciated landscape and includes an unconfined aquifer in hydrologic connection with the stream, which provides an ideal setting for studying stream–aquifer interaction (Chapter 2). The research was conducted by developing a conceptual model of Bertrand Creek Watershed based on field data collection throughout the watershed (Chapter 3). The conceptual model was then used to develop a three-dimensional, integrated surface-subsurface numerical model of the watershed (Chapter 4)

using HydroGeoSphere (Therrien et al., 2010). This thesis provides the first comprehensive study of baseflows along Bertrand Creek. More importantly, it is the first study to evaluate the response of a watershed-scale integrated model against a data set that includes baseflow contributions, soil moisture content, and surface water height, in addition to streamflow and hydraulic head criteria. It is also the first study that demonstrates that an integrated hydrologic model can serve as a tool for assessing the impact of groundwater management strategies on surface water resources.

In combination, the conceptual and numerical models developed here highlight the complex and three-dimensional nature of stream-aquifer interaction in real-world watersheds. This thesis helps in reshaping the conceptualization of stream–aquifer interaction from the classic two-dimensional cross-sectional view of groundwater flow to a stream, into a three-dimensional holistic perspective dependent on both upstream and downstream characteristics. This three-dimensional perspective builds upon the concepts presented by Speight (1980), Larkin and Sharp (1992), and Hjerdt et al., (2004).

The field and modelling methodology can be applied to other watersheds – especially those with a similar climate to the Pacific Northwest. In other words, settings where winter rains provide groundwater recharge to shallow aquifers that sustain streamflows during dry summer months.

5.1 Characterizing the Nature and Controls of Stream–Aquifer Interaction

In Chapter 3, I present a framework for assessing watershed-scale stream–aquifer interaction using a field data collection program complemented with an assessment of topography adjacent to the stream. The primary objective of the fieldwork was to characterize the nature and controls of surface water–groundwater interaction in a glaciated watershed. The second goal of the field program was to create a conceptual hydrologic model suitable for the development of a numerical model of the Bertrand Creek Watershed, and to collect a data set for evaluating model performance. Data collected included hydrologic measurements, stream water chemistry, and point-based measurements of streambed flux. Field data were collected within the stream and across the watershed during the dry seasons of 2006 and 2007.

Results show that topography is a primary control of surface water–groundwater interaction along Bertrand Creek. The novelty of this approach is in demonstrating that the topographic slope adjacent to the stream is useful for anticipating locations where losing conditions seasonally develop along Bertrand Creek. By attributing topographic features with seasonal hydrologic response, this study provides a top-down method for associating landscape features with characteristics of stream–aquifer interaction (see Ivkovic, 2009). The assessment is based upon the geomorphic classification of groundwater flow direction by Larkin and Sharp (1992), which identifies groundwater flow as either underflow-dominant (parallel to the stream) or baseflow-dominant (perpendicular to the stream). Since the characterization of stream–aquifer interaction presented is founded on a desk-based

assessment, the methodology may be useful for designing data collection programs elsewhere prior to comprehensive field efforts.

The conceptual model of Bertrand Creek Watershed indicates that baseflows are sustained by groundwater discharge from a deep groundwater well, perched groundwater zones, and groundwater from an unconfined aquifer (Figure 4.12). In the lower watershed, the stream exchanges water with the unconfined Abbotsford aquifer across multiple scales controlled by topography and permeability:

(1) At the large-scale, groundwater contributions are focused at stream locations where groundwater flow lines are expected to converge (i.e., Kirkby and Chorley, 1967; Winter, 1999), and these locations can be predicted based on topography. As an example, almost half of the streamflow measured at the watershed outlet is contributed from a mid-watershed stream segment only 180 m in length located downstream of a break in streambed slope.

(2) At the small-scale, hyporheic flow dominates fluxes across the Bertrand Creek streambed where high permeability streambed deposits exist without strongly upwelling groundwater. The influence of hyporheic flow exceeds 1 m depth at many locations and creates significant local-scale variability within point-based measurements. The spatial variability of these measurements precludes the ability to extrapolate values into areal estimates of streambed flux.

A watershed-scale characterization must consider processes operating at many different spatial scales and is therefore best evaluated using a suite of field techniques. In this study,

streamflow measurements provided the only direct measure of gains or losses to flow, but were limited by measurement error. Stream water chemistry and electrical conductivity measurements identified locations along the stream where gains in baseflow occur along shorter stream lengths than could be assessed using incremental streamflow measurements. Finally, point-based measurements using mini-piezometers were fundamental as a window into the subsurface, to characterize the distribution of streambed deposits and to quantify hydraulic head fluctuations beneath the stream.

5.2 Simulating Surface Water–Groundwater Interaction

Investigating the exchange of water between a stream and underlying aquifer requires a numerical model that can simulate surface water–groundwater interaction under the influences of heterogeneous topography, geology, and climate. In Chapter 4, the integrated numerical model HydroGeoSphere was used to simulate the hydrologic processes within the Bertrand Creek Watershed, with a specific focus on simulating dry season streamflows. The watershed model was developed based on the conceptual work detailed in Chapter 3, and the model calibrated using 2007 field data. These data consisted of streamflows, groundwater contributions to streamflow, soil moisture content, and the change in height of hydraulic heads and surface water in a pond. The calibrated model was then evaluated against the less extensive 2006 field data set. Finally, the utility of the model as a management tool was demonstrated by exploring groundwater withdrawal options.

The findings of this study highlight the spatially variable nature of surface water–groundwater interaction. The study shows that the connectivity between a stream and water

table depends on topography and properties of the unconfined aquifer and streambed. Recharge and evapotranspiration further control the rates and spatial distribution of baseflow generation:

(1) Recharge to the unconfined aquifer requires that the controlling features of topography and surficial soils be adequately represented in the model. By partitioning rainfall into runoff and infiltration, these features govern the magnitude and spatial distribution of subsurface infiltration, which directly influence baseflows.

(2) Evapotranspiration is a significant control of baseflows within Bertrand Creek. The magnitude of evapotranspiration within the Bertrand Creek riparian zone is approximately half of the quantity of streamflow discharging from the watershed outlet. The magnitude and direction of water flux across the streambed is sensitive to the parameterization and partitioning of evapotranspiration into components of evaporation and transpiration. This parameterization affects the longitudinal extent of losing conditions along a stream.

Development of the Bertrand Creek Watershed model benefited from a data collection program specifically designed for model construction and evaluation, which included diverse data types from both the surface and subsurface domains. This data set was fundamental in reducing the uncertainty of parameter values and augmenting the predictive power of model simulations. For example, the calibration process demonstrated that evaluating the model only against streamflows at the watershed outlet presented a non-unique solution of parameter values that was insensitive to stream conditions mid-watershed. Of the criteria evaluated in the Bertrand Creek Watershed model, measurements of baseflow contribution

and the change in ponded surface water height were the most important for constraining parameter values during calibration.

This thesis demonstrates how a field and modelling study can be used together to develop and test a conceptual model. Results of the modelling work supports the hypothesis presented in Chapter 3, that topographic slope can be useful for anticipating the seasonal development of losing conditions along Bertrand Creek. Conversely, modelling results can identify locations to focus field efforts, such as where the exchange of water between a stream and aquifer is expected to be greater, and therefore more easily quantified. Ideally, model development and data collection should progress iteratively, so that uncertainties in the numerical model can be the focus of upcoming field programs.

Finally, the utility of the Bertrand Creek Watershed model to serve as a predictive tool was demonstrated. The model was used to evaluate the placement of a large capacity groundwater well within the West of Aldergrove (WALD) aquifer. Results show that increasing the proximity of the well to the stream has implications on streamflows, as well as the development of a dry streambed. Specifically, placing the well 150 m from the stream reduced baseflows at the watershed outlet by 23% and increased the period of time the streambed was dry by 2.5 weeks. The model provides a sound framework for water managers to evaluate the impacts of different water allocation strategies on baseflows and make more informed water management decisions.

5.3 Future Research

Several directions for future research can be identified based on the studies reported here. Future improvements to the conceptual and numerical models of Bertrand Creek Watershed will contribute to an improved understanding of surface water–groundwater interaction, as well as identify how to represent controlling processes of this interaction in integrated models. Specifically, future simulations of Bertrand Creek Watershed should include:

(1) Evaluating the effect of spatial resolution of the surface mesh on model performance. Specifically, this should assess the impact of adding tributaries on model performance.

(2) Investigating the controls of streambed seepage along stream segments that transition from gaining to losing, and how these controls influence parameterization of an integrated model. For example, is model performance improved by assigning a temporally variable streambed hydraulic conductivity (i.e., Hatch et al., 2010) or by increasing the resolution of heterogeneity represented within subsurface deposits?

(3) Quantifying baseflow contributions along the upper portion of the watershed and the nature of the contribution (i.e., streambed versus stream bank seepage). Then, investigating how to represent this contribution given the low permeability streambed, within an integrated model.

(4) Evaluating the influence of spatially distributing evapotranspiration rates (ET_p) across the watershed. Modelled baseflows were sensitive to the evapotranspiration rate, but were largely insensitive to parameters that indicate vegetation type and stages of growth, such as leaf area index (LAI) and root depth. A better understanding of how to represent evapotranspiration across watershed-scales using the Kristensen and Jenson (1975)

methodology in models such as HydroGeoSphere is needed before these models can assist managers in evaluating land-use changes.

(5) Delineating the source of significant groundwater contribution to streamflow surrounding station B2. Given that the groundwater contribution in this area amounts to almost half of the total baseflow measured at the study site outlet, further investigation to delineate this source is warranted. Since a significant change in stream water chemistry occurs at this location, isotopic analysis of surface water and groundwater surrounding station B2 appears promising for delineating source waters. Kriging aquifer surfaces based on borehole data suggests there is potential for hydrologic connection between the unconfined Abbotsford aquifer and the underlying West of Aldergrove (WALD) aquifer at this location. The potential for hydrologic connection could alternatively be assessed using a geophysics investigation.

Water management strategies typically focus on impacts to streamflow from pumping scenarios. However, evaluating scenarios that have the potential to increase baseflows provide equally interesting areas for research. An example application within Bertrand Creek Watershed could be to evaluate the installation of subsurface infiltration wells or infiltration beds: Would the construction of these wells/beds upstream of the Abbotsford aquifer contribute to increased baseflow within the Bertrand Creek?

With future increases in computational power, watershed-scale simulations spanning multiple years will become increasingly plausible. Such studies are needed to improve our understanding of hydrologic response to a range of conditions, such as consecutive years of

drought, whose impacts may have emergent properties. However, considering that infiltration is sensitive to hydraulic conductivity of the surficial soils as well as the temporal resolution of the input rainfall, studies conducted across different (and larger) time scales will likely be affected by issues of scale in parameterization. Conjunctive field and modelling studies are needed that resolve issues of scale on subsurface infiltration and identify field methods most useful for assigning parameter values across a range of temporal scales.

Applying the topographic analysis in Chapter 3 to other watersheds with hummocky topography is an important future research direction that may be useful for anticipating the seasonal changes in stream–aquifer interaction. The importance of associating identifiable features of landscape with traits or seasonal changes in stream–aquifer interaction has been highlighted by Ivkovic (2009). Given the mounting pressures on water resources, similar studies are needed across a wide range of landscapes and climates.

References

Allen, D.M., Schuurman, N., Deshpande, A. and Scibek, J., 2008. Data integration and standardization in cross-border hydrogeological studies: a novel approach to hydrostratigraphic model development. Environmental Geology, 53(7): 1441-1453.

Allen, R.G., Pereira, L.S., Raes, D. and Smith, M., 1998. Crop evapotranspiration, guidelines for computing crop water requirements, FAO Irrigation and Drainage Paper 56, Food and Agriculture Organization of the United Nations, Rome, Italy. 300 pp.

Andersen, M. and Acworth, R., 2009. Stream-aquifer interactions in the Maules Creek catchment, Namoi Valley, New South Wales, Australia. Hydrogeology Journal, 17(8): 2005-2021.

Armstrong, J.E., 1960. Surficial geology of the Sumas map-area, British Columbia. Map 92G/1. Geological Survey of Canada Paper 59-9, 27 pp. Scale 1: 63,360.

Armstrong, J.E., 1977. Quaternary Stratigraphy of the Fraser Lowland, Field Excursion No. 10, Guidebook, Geological Association of Canada Cordilleran Section, 204-226.

Armstrong, J.E., 1981. Post-Vashon Wisconsin Glaciation, Fraser Lowland British Columbia. Geological Survey of Canada Bulletin 322, 34 pp.

Armstrong, J.E., 1984. Environmental and engineering applications of the surficial geology of the Fraser Lowland, British Columbia. Geological Survey of Canada Paper 83–23, 54 pp.

Armstrong, J.E., Crandell, D.R., Easterbrook, D.J. and Noble, J.B., 1965. Late Pleistocene Stratigraphy and Chronology in Southwestern British Columbia and Northwestern Washington. Geological Society of America Bulletin, 76(3): 321-330.

Banks, E.W., Brunner, P. and Simmons, C.T., 2011a. Vegetation controls on variably saturated processes between surface water and groundwater and their impact on the state of connection. Water Resources Research, 47(11): W11517.

Banks, E.W., Simmons, C.T., Love, A.J. and Shand, P., 2011b. Assessing spatial and temporal connectivity between surface water and groundwater in a regional catchment: Implications for regional scale water quantity and quality. Journal of Hydrology, 404(1-2): 30-49.

Baxter, C., Hauer, F.R. and Woessner, W.W., 2003. Measuring groundwater-stream water exchange: New techniques for installing minipiezometers and estimating hydraulic conductivity. Transactions of the American Fisheries Society, 132(3): 493-502.

BC Ministry of Environment (BC MoE), 2008. WELLS online database. https://a100.gov.bc.ca/pub/wells/public/indexreports.jsp. Website accessed March 15, 2008.

Becker, M.W., Georgian, T., Ambrose, H., Siniscalchi, J. and Fredrick, K., 2004. Estimating flow and flux of ground water discharge using water temperature and velocity. Journal of Hydrology, 296(1-4): 221-233.

Bencala, K.E., Gooseff, M.N. and Kimball, B.A., 2011. Rethinking hyporheic flow and transient storage to advance understanding of stream-catchment connections. Water Resources Research, 47: W00H03.

Berg, M.A. and Allen, D.M., 2007. Low flow variability in groundwater-fed streams. Canadian Water Resources Journal, 32(3): 227-246.

Bond, B.J., Jones, J.A., Moore, G., Phillips, N., Post, D. and McDonnell, J.J., 2002. The zone of vegetation influence on baseflow revealed by diel patterns of streamflow and vegetation water use in a headwater basin. Hydrological Processes, 16(8): 1671-1677.

Bren, L.J., 1997. Effects of slope vegetation removal on the diurnal variation of a small mountain stream. Water Resources Research, 33(2): 321–331.

Brown, G.W., 1969; Predicting temperatures of small streams. Water Resources Research, 5(1): 68-75.

Brunke, M. and Gonser, T.O.M., 1997. The ecological significance of exchange processes between rivers and groundwater. Freshwater Biology, 37(1): 1-33.

Burt, T.P., Pinay, G., Matheson, F.E., Haycock, N.E., Butturini, A., Clement, J.C., Danielescu, S., Dowrick, D.J., Hefting, M.M., Hillbricht-Ilkowska, A. and Maitre, V., 2002. Water table fluctuations in the riparian zone: comparative results from a pan-European experiment. Journal of Hydrology, 265(1-4): 129-148.

Canadian Network for Isotopes in Precipitation, 2009. Monthly isotopes in precipitation. Retrieved from: http://www.science.uwaterloo.ca/~twdedwar/cnip/cniphome.html, on March 1, 2009.

Cardenas, M.B., Wilson, J.L. and Zlotnik, V.A., 2004. Impact of heterogeneity, bed forms, and stream curvature on subchannel hyporheic exchange. Water Resources Research, 40(8): W08307.

Cardenas, M.B. and Wilson, J.L., 2006. The influence of ambient groundwater discharge on exchange zones induced by current-bedform interactions. Journal of Hydrology, 331(1-2): 103-109.

Carmichael, V., Wei, M. and Ringham, L., 1995. Fraser Valley Groundwater Monitoring Program: Final Report, BC Ministry of Health, BC Ministry of Environment, Lands and Parks, BC Ministry of Agriculture, Fisheries and Food, Victoria, BC.

Cey, E.E., Rudolph, D.L., Parkin, G.W. and Aravena, R., 1998. Quantifying groundwater discharge to a small perennial stream in southern Ontario, Canada. Journal of Hydrology, 210(1-4): 21-37.

Chan, D., 2006. Assessing the water balance and future consumption scenarios for demand management of the Aldergrove aquifer in B.C., M.Sc. thesis, University of British Columbia, Vancouver.

Chen, X., 2007. Hydrologic connections of a stream-aquifer-vegetation zone in south-central Platte River valley, Nebraska. Journal of Hydrology, 333(2-4): 554-568.

Chow, V.T., 1964. Handbook of Applied Hydrology: a Compendium of Water-resources Technology. McGraw-Hill Book Co. New York.

Christensen, S., Rasmussen, K.R. and Moller, K., 1998. Prediction of regional ground water flow to streams. Ground Water, 36(2): 351-360.

Clague, J.J., 1977. Quadra Sand: A Study of the Late Pleistocene Geology and Geomorphic History of Coastal Southwest British Columbia. Geological Survey of Canada, Paper 77-17, 24 pp.

Clague, J.J., 1981. Late Quaternary Geology and Geochronology of British Columbia. Part 2: summary and discussion of radiocarbon-dated Quaternary history. Geological Survey of Canada Paper 8035, 41 pp.

Clague, J.J., 1994. Quaternary stratigraphy and history of south-coastal British Columbia. In: J.W.H. Monger (editor), Geology and Geological Hazards of the Vancouver Region, Southern British Columbia, Geological Survey of Canada, Bulletin 481, p 181-192.

Clague, J.J. and Luternauer, J.L., 1983. Late Quaternary Geology of Southwestern British Columbia, Geological Association of Canada - Victoria Section. Field Trip Guidebook, Trip 6, 112 pp.

Clague, J.J., Mathewes, R.W., Guilbault, J.P., Hutchinson, I. and Ricketts, B.D., 1997. Pre-Younger Dryas resurgence of the southwestern margin of the Cordilleran ice sheet, British Columbia, Canada. Boreas, 26(3): 261-278.

Collins, D.B.G. and Bras, R.L., 2007. Plant rooting strategies in water-limited ecosystems. Water Resources Research, 43(6): W06407.

Conant, B., Jr., 2004. Delineating and quantifying ground water discharge zones using streambed temperatures. Ground Water, 42(2): 243-257.

Constantz, J., 1998. Interaction between stream temperature, streamflow and groundwater exchanges in alpine streams. Water Resources Research, 34(7): 1609-1615.

Constantz, J., Thomas, C.L. and Zellweger, G., 1994. Influence of diurnal variations in stream temperature on streamflow loss and groundwater recharge. Water Resources Research, 30(12): 3253-3264.

Council of Canadian Academies, 2009. The sustainable management of groundwater in Canada. Report of the Expert Panel on Groundwater, Ottawa, Ontario. Electronic resource: www.scienceadvice.ca/en/assessments/completed/groundwater.aspx.

Cox, S. E. and Kahle, S. C., 1999. Hydrogeology, groundwater quality, and sources of nitrate in lowland glacial aquifers of Whatcom County, Washington, and British Columbia, Canada, U.S. Geological Survey Water Resources Investigation Report, 98-4195.

Cox, S.E., Simonds, F.W., Doremus, L., Huffman, R.L. and Defawe, R.M., 2005. Ground and Surface Water Interactions and Quality of Discharging Ground Water, Lower Nooksack River Basin, WA. U.S. Geological Survey Scientific Investigations Report 2005-5255.

CRWR, 2006. Center for Research in Water Resources, University of Texas at Austin ArcHydro Groundwater Toolbar, electronic resource.

Culler, R.C., Hanson, R.L., Myrick, R.M., Turner, R.M. and Kipple, F.P., 1982. Evapotranspiration before and after clearing phreatophytes, Gila River Flood Plain, Graham County, Arizona, U.S. Geological Survey Professional Paper 655-P, 67 pp.

de Vries, J. and Simmers, I., 2002. Groundwater recharge: an overview of processes and challenges. Hydrogeology Journal, 10(1): 5-17.

Devito, K.J., Hill, A.R. and Roulet, N., 1996. Groundwater-surface water interactions in headwater forested wetlands of the Canadian Shield. Journal of Hydrology, 181(1-4): 127-147.

Domenico, P.A. and Schwartz, F.W., 1998. Physical and Chemical Hydrogeology, 2nd Edition. John Wiley & Sons, New York, 528 pp.

Easterbrook, D.J., 1963. Late Pleistocene Glacial Events and Relative Sea-Level Changes in the Northern Puget Lowland, Washington. Geological Society of America Bulletin, 74(12): 1465-1483.

Easterbrook, D.J., Kovanen, D.J., and Slaymaker, O., 2007. New developments in Late Pleistocene and Holocene glaciation and volcanism in the Fraser Lowland and North Cascades, Washington. Geological Association of America, Field Guide No. 9.

Ebel, B.A., Loague, K., VanderKwaak, J.E., Dietrich, W.E., Montgomery, D.R., Torres, R. and Anderson, S.P., 2007. Near-surface hydrologic response for a steep, unchanneled catchment near Coos Bay, Oregon: 2. Physics-based simulations. American Journal of Science, 307(4): 709-748.

Ebel, B.A., Mirus, B.B., Heppner, C.S., VanderKwaak, J.E. and Loague, K., 2009. First-order exchange coefficient coupling for simulating surface water–groundwater interactions: parameter sensitivity and consistency with a physics-based approach. Hydrological Processes, 23(13): 1949-1959.

Engdahl, N.B., Vogler, E.T. and Weissmann, G.S., 2010. Evaluation of aquifer heterogeneity effects on river flow loss using a transition probability framework. Water Resources Research, 46(1): W01506.

Environment Canada, 2009. Canadian Climate Normals Online, Retrieved from: http://www.climate.weatheroffice.ec.gc.ca/climateData/canada_e.html, on November 20, 2009.

Envirowest, 2000. An Assessment of Hydrological Conditions at Naval Radio Station, Aldergrove, 22 pp.

Everest, F.H., Stouder, D.J., Kakoyannis, C., Houston, L., Stankey, G., Kline, J. and Alig, R., 2004. A review of scientific information on issues related to the use and management of water resources in the Pacific Northwest. General Technical Report PNW-GTR-595. Portland, Oregon, U.S. Department of Agriculture, Forest Service, Pacific Northwest Research Station, 128 pp.

Fairbanks, J., Panday, S. and Huyakorn, P.S., 2001. Comparisons of linked and fully coupled approaches to simulating conjunctive surface/subsurface flow and their interactions, In: Seo, B., Poeter, E. and C. Zheng (editors), MODFLOW 2001 and Other Modeling Odysseys, Conference Proceedings, Golden, Colorado, p. 356-361.

Feddes, R.A., Kowalik, P.J. and Zaradny, H., 1978. Simulation of field water use and crop yield. John Wiley and Sons, New York, 188 pp.

Feddes, R.A., Kabat, P., Van Bakel, P.J.T., Bronswijk, J.J.B. and Halbertsma, J., 1988. Modelling soil water dynamics in the unsaturated zone - State of the art. Journal of Hydrology, 100(1-3): 69-111.

Fisheries and Oceans Canada, 2012. Action Plan for the Nooksack Dace (Rhinichthys cataractae) and Salish Sucker (Catostomus sp.) in Canada (Draft). Species at Risk Act Action Plan Series. Fisheries and Oceans Canada, Ottawa. 19 pp.

Fleckenstein, J.H., Niswonger, R.G. and Fogg, G.E., 2006. River-aquifer interactions, geologic heterogeneity, and low-flow management. Ground Water, 44(6): 837-852.

Freeze, R.A., 1972. Role of subsurface flow in generating surface runoff: 1. Base flow contributions to channel flow. Water Resources Research, 8(3): 609-623.

Frei, S., Fleckenstein, J.H., Kollet, S.J. and Maxwell, R.M., 2009. Patterns and dynamics of river-aquifer exchange with variably-saturated flow using a fully-coupled model. Journal of Hydrology, 375(3-4): 383-393.

Gburek, W.J. and Folmar, G.J., 1999. Flow and chemical contributions to streamflow in an upland watershed: a baseflow survey. Journal of Hydrology, 217(1-2): 1-18.

Gleeson, T., Novakowski, K., Cook, P.G. and Kyser, T.K., 2009. Constraining groundwater discharge in a large watershed: Integrated isotopic, hydraulic, and thermal data from the Canadian shield. Water Resources Research, 45(8): W08402.

Goderniaux, P., Brouyère, S., Fowler, H.J., Blenkinsop, S., Therrien, R., Orban, P. and Dassargues, A., 2009. Large scale surface-subsurface hydrological model to assess climate change impacts on groundwater reserves. Journal of Hydrology, 373(1-2): 122-138

Golder Associates Ltd. (Golder), 2005. Comprehensive Groundwater Modelling Assignment, Report to the Township of Langley, 90 pp.

Graham, G., Allen, D.M., Starzyk, C. and Urbanski, I., 2010. Understanding natural variability of nitrate concentrations in a regional groundwater monitoring network. Canadian Water Resources Association Conference. Vancouver, B.C., June, 2010.

Grapes, T.R., Bradley, C. and Petts, G.E., 2005. Dynamics of river-aquifer interactions along a chalk stream: the River Lambourn, UK. Hydrological Processes, 19(10): 2035-2053.

Grayson, R.B., Moore, I.D. and McMahon, T.A., 1992. Physically based hydrologic modeling: 1. A terrain-based model for investigative purposes. Water Resources Research, 28(10): 2639-2658.

Gribovszki, Z., Kalicz, P., Szilágyi, J. and Kucsara, M., 2008. Riparian zone evapotranspiration estimation from diurnal groundwater level fluctuations. Journal of Hydrology, 349(1-2): 6-17.

Halford, K.J. and Mayer, G.C., 2000. Problems associated with estimating ground water discharge and recharge from stream-discharge records. Ground Water, 38(3): 331-342.

Halstead, E.C., 1966. Aldergrove Test Hole, Fraser Valley, B.C., Geological Survey of Canada, Water Supply Paper 64-51, 17 pp.

Halstead, E.C., 1986. Ground-Water Supply – Fraser Lowland, British Columbia. Inland Waters Directorate, Scientific Series No. 145, National Hydrology Research Institute, Paper No. 26, 80 pp.

Hamilton, T.S. and Ricketts, B.D., 1994. Contour map of the sub-Quaternary bedrock surface, Strait of Georgia and Fraser Lowland; In: J.W.H. Monger (editor), Geology and Geological Hazards of the Vancouver Region, Southwestern British Columbia, Geological Survey of Canada, Bulletin 481, p. 193-196.

Harbaugh, A.W., Banta, E.R., Hill, M.C. and McDonald, M.G., 2000. MODFLOW-2000, the U.S. Geological Survey modular ground-water model—User guide to modularization concepts and the Ground-Water Flow Process, U.S. Geological Survey Open-File Report 00-92.

Harvey, J.W. and Bencala, K.E., 1993. The effect of streambed topography on surface-subsurface water exchange in mountain catchments. Water Resources Research, 29(1): 89-98.

Hatch, C.E., Fisher, A.T., Ruehl, C.R. and Stemler, G., 2010. Spatial and temporal variations in streambed hydraulic conductivity quantified with time-series thermal methods. Journal of Hydrology, 389(3-4): 276–288.

Herschy, R.W., 1995. Streamflow Measurement, 2nd Edition. E&FN Spon, London, 524 pp.

Hill, A.R., Labadia, C.F. and Sanmugadas, K., 1998. Hyporheic zone hydrology and nitrogen dynamics in relation to the streambed topography of a N-rich stream. Biogeochemistry, 42(3): 285-310.

Hinton, M.J., Schiff, S.L. and English, M.C., 1993. Physical properties governing groundwater flow in a glacial till catchment. Journal of Hydrology, 142(1-4): 229-249.

Hjerdt, K.N., McDonnell, J.J., Seibert, J. and Rodhe, A., 2004. A new topographic index to quantify downslope controls on local drainage. Water Resources Research, 40(5): W05602.

Hvorslev, M.J., 1951. Time lag and soil permeability in ground-water observations. U.S. Army Corps of Engineers Waterways Experimental Station Bulletin, no.36, 50 pp.

ISO, 1980. Water flow measurements in open channel using weirs and venturi flumes, Part 1. Thin-plate weirs. International Organization for Standardization Technical Report ISO 1438/1–1980(E).

Ivkovic, K.M., 2009. A top-down approach to characterise aquifer-river interaction processes. Journal of Hydrology, 365(3-4): 145-155.

Jakeman, A.J. and Hornberger, G.M., 1993. How much complexity is warranted in a rainfall-runoff model? Water Resources Research, 29(8): 2637-2649.

James, A.L., McDonnell, J.J., Tromp-van Meerveld, I. and Peters, N.E., 2010. Gypsies in the palace: experimentalist's view on the use of 3-D physics-based simulation of hillslope hydrological response. Hydrological Processes, 24(26): 3878-3893.

Johanson, D., 1988. Fishtrap/Pepin/Bertrand Creeks Water Management Basin Plan: Groundwater Component. Province of British Columbia Ministry of Environment and Parks Water Management Branch, 16 pp.

Jones, J.P., Sudicky, E.A. and McLaren, R.G., 2008. Application of a fully-integrated surface subsurface flow model at the watershed-scale: a case study. Water Resources Research, 44: doi:10.1029/2006WR005603.

Juckem, P.F., Hunt, R.J. and Anderson, M.P., 2006. Scale effects of hydrostratigraphy and recharge zonation on base flow. Ground Water, 44(3): 362-370.

Jyrkama, M.I., Sykes, J.F. and Normani, S.D., 2002. Recharge estimation for transient ground water modeling. Ground Water, 40(6): 638-638.

Kalbus, E., Reinstorf, F. and Schirmer, M., 2006. Measuring methods for groundwater-surface water interactions: a review. Hydrology and Earth System Sciences, 10(6): 873-887.

Kerr Wood Leidal Associates Ltd., 2009. Integrated Stormwater Management Plan. Report to the Township of Langley, 258 pp.

Kindsvater, C. E. and R. W. Carter. 1959. Discharge characteristics of rectangular thin-plate weirs. Transactions, American Society of Civil Engineers. v. 24, Paper No. 3001.

Kirby, R.K., 1956. Thermal expansion of polytetrafluoroethylene (Teflon) from -190° to +300°C. Journal of Research of the National Bureau of Standards, 57(2): 91-94.

Kirkby, M.J. and Chorley, R.J., 1967. Throughflow, overland flow and erosion. International Association of Scientific Hydrology. Bulletin, 12(3): 5-21.

Kohut, A.P., Sather, S., Kwong, J. and Chwojka, F., 1989. Nitrate contamination of the Abbotsford Aquifer, British Columbia. British Columbia Ministry of Environment, Water Management Branch, 24 pp.

Kollet, S.J. and Maxwell, R.M., 2006. Integrated surface-groundwater flow modeling: A free-surface overland flow boundary condition in a parallel groundwater flow model. Advances in Water Resources, 29(7): 945-958.

Kollet, S.J. and Maxwell, R.M., 2008. Capturing the influence of groundwater dynamics on land surface processes using an integrated, distributed watershed model. Water Resources Research, 44(2): W02402.

Konrad, C.P., 2006a. Location and timing of river-aquifer exchanges in six tributaries to the Columbia River in the Pacific Northwest of the United States. Journal of Hydrology, 329(3-4): 444-470.

Konrad, C.P., 2006b. Longitudinal hydraulic analysis of river-aquifer exchanges. Water Resources Research, 42(8): W08425.

Kovanen, D.J., 2002. Morphologic and stratigraphic evidence for Allerød and Younger Dryas age glacier fluctuations of the Cordilleran Ice Sheet, British Columbia, Canada and Northwest Washington, U.S.A. Boreas, 31(2): 163-184.

Kovanen, D.J. and Easterbrook, D.J., 2002. Timing and extent of Allerød and Younger Dryas age (ca. 12,500–10,000 14C yr B.P.) oscillations of the Cordilleran Ice Sheet in the Fraser Lowland, Western North America. Quaternary Research, 57(2): 208-224.

Krause, S., Bronstert, A. and Zehe, E., 2007. Groundwater-surface water interactions in a North German lowland floodplain - Implications for the river discharge dynamics and riparian water balance. Journal of Hydrology, 347(3-4): 404-417.

Kreye, R. and Wei, M., 1994. A Proposed Aquifer Classification System for Groundwater Management in British Columbia. Water Management Division, B.C. Ministry of Environment, Lands and Parks, Victoria, 27 pp.

Kristensen, K.J. and Jensen, S.E., 1975. A model for estimating actual evapotranspiration from potential evapotranspiration. Nordic Hydrology, 6(3): 170-188.

LaBolle, E.M. and Fogg, G.E., 2001. A review of California's integrated groundwater and surface-water model (ISGM). In: Seo, B., Poeter, E., and C. Zheng (editors), MODFLOW 2001 and Other Modeling Odysseys, Conference Proceedings, Golden, Colorado, p. 349–355.

Laio, F., D'Odorico, P. and Ridolfi, L., 2006. An analytical model to relate the vertical root distribution to climate and soil properties. Geophysical Research Letters, 33(18): L18401.

Langhoff, J.H., Rasmussen, K.R. and Christensen, S., 2006. Quantification and regionalization of groundwater-surface water interaction along an alluvial stream. Journal of Hydrology, 320(3-4): 342-358.

Langley Environmental Partners Society, 2006. Sensitive habitat inventory and mapping program. Retrieved from: http://www.leps.bc.ca.

Larkin, R.G. and Sharp, J.M., 1992. On the relationship between river-basin geomorphology, aquifer hydraulics, and ground-water flow direction in alluvial aquifers. Geological Society of America Bulletin (December 1992), 104(12): 1608-1620.

Larned, S.T., Hicks, D.M., Schmidt, J., Davey, A.J.H., Dey, K., Scarsbrook, M., Arscott, D.B. and Woods, R.A., 2008. The Selwyn River of New Zealand: a benchmark system for alluvial plain rivers. River Research and Applications, 24(1): 1-21.

Larson, P. and Runyan, C., 2009. Evaluation of a Capacitance Water Level Recorder and Calibration Methods in an Urban Environment. CUERE Technical Memo 2009/003. University of Maryland Baltimore County, Center for Urban Environmental Research and Education, Baltimore, MD, 29 pp.

Li, Q., Unger, A.J.A., Sudicky, E.A., Kassenaar, D., Wexler, E.J. and Shikaze, S., 2008. Simulating the multi-seasonal response of a large-scale watershed with a 3D physically-based hydrologic model. Journal of Hydrology, 357: 317-336.

Liebscher, H., Hii, B. and McNaughton, D., 1992. Nitrates and pesticides in the Abbotsford Aquifer, southwestern British Columbia, Inland Waters Directorate, Environment Canada, North Vancouver, BC, 83 pp.

Livingstone, D.A., 1963. Chemical composition of rivers and lakes. In: M. Fleischer (editor), Data of Geochemistry, 6th ed. U.S. Geological Survey Professional Paper, 440-G.

Loague, K., Heppner, C.S., Abrams, R.H., Carr, A.E., VanderKwaak, J.E. and Ebel, B.A., 2005. Further testing of the Integrated Hydrology Model (InHM): event-based simulations for a small rangeland catchment located near Chickasha, Oklahoma. Hydrological Processes, 19(7): 1373-1398.

Luttmerding, H.A., 1980. Soils of the Langley-Vancouver Map Area; British Columbia Soil Survey Report No. 15.

Mark, D. M. and Ojamaa, P.M., 1979. Late Pleistocene meltwater channels and Sumas deglaciation, Fraser Lowland, British Columbia. In: Brown M.C. and G. Wynn (editors), The Bellingham Collection of Geographical Studies, B.C. Geographic Series No. 27, p. 81-91.

Mathews, W.H., 1972. Geology of Vancouver Area of British Columbia. Field Excursions; 24th International Geological Congress, Guidebook for field excursion 5.

McLaren, R.G., 2009. Gridbuilder: a pre-processor for 2-D, triangular element, finite-element programs. Unpublished User Manual. Groundwater Simulations Group, Waterloo, Ontario. 87 pp.

McLeod, A.I., 1993. Parsimony, model adequacy and periodic correlation in time series forecasting. International Statistical Review / Revue Internationale de Statistique, 61(3): 387-393.

Meigs, L.C. and Bahr, J.M., 1995. Three-dimensional groundwater flow near narrow surface water bodies. Water Resources Research, 31(12): 3299-3307.

Meinzer, O.E., 1923. Outline of groundwater hydrology with definitions, U.S. Geological Survey Water Supply Paper 494.

Meyboom, P., 1966. Unsteady groundwater flow near a willow ring in hummocky moraine. Journal of Hydrology, 4(0): 38-62.

Ministry of Agriculture, Food and Fisheries, 2002. Township of Langley Agricultural Land Use Inventory, 2001, Summary Report, 15 pp.

Mirus, B.B., Ebel, B.A., Heppner, C.S. and Loague, K., 2011. Assessing the detail needed to capture rainfall-runoff dynamics with physics-based hydrologic response simulation. Water Resources Research, 47: W00H10.

Monteith, J.L., 1965. Evaporation and environment. In: G.E. Fogg (editor), Symposia of the Society for Experimental Biology, The State and Movement of Water in Living Organisms. Academic Press Inc., New York, p. 205-234.

Moore, R.D., 2004a. Introduction to salt dilution gauging for streamflow measurement: Part 1. Streamline Watershed Management Bulletin 7(4): 20-23.

Moore, R.D., 2004b. Introduction to salt dilution gauging for streamflow measurement Part II: Constant-rate injection. Streamline Watershed Management Bulletin 8(1): 11-15.

Moore, R.D., Spittlehouse, D.L. and Story, A., 2005. Riparian microclimate and stream temperature response to forest to harvesting: a review. Journal of the American Water Resources Association, 41(4): 813-834.

Nelson, L.M., 1991. Surface-water resources of the Columbia Plateau in parts of Washington, Oregon, and Idaho. U.S. Geological Survey Water-Resources Investigations Report 88-4105, 4 sheets, scale 1:2,000,000.

Niswonger, R.G. and Fogg, G.E., 2008. Influence of perched groundwater on base flow. Water Resources Research, 44(3): W03405.

Panday, S. and Huyakorn, P.S., 2004. A fully coupled physically-based spatially-distributed model for evaluating surface/subsurface flow. Advances in Water Resources, 27(4): 361-382.

Pearson, M.P., 2004. The ecology, status and recovery prospects of Nooksack Dace (rhinichthys cataractae spp.) and Salish Sucker (catostomus sp.) in Canada. Ph.D. thesis, University of British Columbia, Vancouver, B.C.

Penman, H.L., 1948. Natural evaporation from open water, bare soil and grass. Proceedings of the Royal Society of London Series A Mathematical and Physical Sciences, 193(1032): 120-145.

Peters, E. and van Lanen, H.A.J., 2005. Separation of base flow from streamflow using groundwater levels—illustrated for the Pang catchment (UK). Hydrological Processes, 19(4): 921-936.

Piteau Associates Engineering Ltd. (Piteau), 1991. Hydrogeological Assessment of Aldergrove Aquifer. Report to the Corporation of the Township of Langley, January, 55 pp.

Piteau Associates Engineering Ltd. (Piteau), 2004. Construction and Testing of Production Well No. 9 (PW-9) – Aldergrove, B.C., Report to the Corporation of the Township of Langley, March, 15 pp.

Piteau Associates Engineering Ltd. (Piteau), 2005. Construction and Testing of Aldergrove Production Well No. 10. Report to the Corporation of the Township of Langley, November, 11 pp.

Potter, M.C. and Wiggert, D.C., 1997. Mechanics of Fluids, 2nd Edition. Prentice Hall, Inc., Upper Saddle River, New Jersey, 752 pp.

Prudic, D.E., 1989. Documentation of a computer program to simulate stream-aquifer relations using a modular, finite-difference, ground-water flow model, U.S. Geological Survey Open-File Report 88-729, 113 pp.

Pruneda, E.B., Barber, M.E., Allen, D.M. and Wu, J.Q., 2010. Use of stream response functions to determine impacts of replacing surface-water use with groundwater withdrawals. Hydrogeology Journal, 18(5): 1077-1092.

Puckett, L.J., Zamora, C., Essaid, H., Wilson, J.T., Johnson, H.M., Brayton, M.J. and Vogel, J.R., 2008. Transport and Fate of Nitrate at the Ground-Water/Surface-Water Interface. Journal of Environmental Quality, 37(3): 1034-1050.

R Development Core Team, 2008. R: A language and environment for statistical computing. R Foundation for Statistical Computing, Vienna, Austria. Retrieved from: http://www.R-project.org.

Ramireddygari, S.R., Sophocleous, M.A., Koelliker, J.K., Perkins, S.P. and Govindaraju, R.S., 2000. Development and application of a comprehensive simulation model to evaluate impacts of watershed structures and irrigation water use on streamflow and groundwater: the case of Wet Walnut Creek Watershed, Kansas, USA. Journal of Hydrology, 236(3-4): 223-246.

Refsgaard, J.C., 2000. A formal approach to calibration and validation of models using spatial data. In: R.B. Grayson and G. Blöschl (editors), Spatial Patterns in Catchment Hydrology: Observations and Modelling. Cambridge Univ. Press, Cambridge, U.K., p. 355-367.

Ribeiro, P.J, and Diggle P.J., 2001. geoR: a package for geostatistical analysis, R-NEWS, 1(2):15-18.

Ritter, W.F. and Chirnside, A.E.M., 1990. Impact of animal waste lagoons on ground-water quality. Biological Wastes, 34(1): 39-54.

Robertson, W.D., Cherry, J.A. and Sudicky, E.A., 1991. Ground-water contamination from two small septic systems on sand aquifers. Ground Water, 29(1): 82-92.

Ronan, A.D., Prudic, D.E., Thodal, C.E. and Constantz, J., 1998. Field study and simulation of diurnal temperature effects on infiltration and variably saturated flow beneath an ephemeral stream. Water Resources Research, 34(9): 2137-2153

Ruehl, C., Fisher, A.T., Hatch, C., Huertos, M., Stemler, G.and Shennan, C., 2006. Differential gauging and tracer tests resolve seepage fluxes in a strongly-losing stream. Journal of Hydrology, 330(1-2): 235-248.

Ryder, J.M., Fulton, R.J. and Clague, J.J., 1991. The Cordilleran Ice Sheet and the glacial geomorphology of southern and central British Colombia. Géographie physique et Quaternaire, 45(3): 365-377.

Said, A., Stevens, D.K. and Sehlke, G., 2005. Estimating water budget in a regional aquifer using HSPF-MODFLOW Integrated model. Journal of the American Water Resources Association, 41(1): 55-65.

Schaap, M.G., Leij, F.J. and van Genuchten, M.T., 2001. Rosetta: a computer program for estimating soil hydraulic parameters with hierarchical pedotransfer functions. Journal of Hydrology, 251(3-4): 163-176.

Scibek, J. and Allen, D.M., 2005. Numerical groundwater flow model of the Abbotsford-Sumas Aquifer, central Fraser Lowland of BC, Canada, and Washington State, US., Unpublished report prepared for Environment Canada, Vancouver, BC, 203 pp.

Scibek, J. and Allen, D.M., 2006. Modeled impacts of predicted climate change on recharge and groundwater levels. Water Resources Research, 42(11): W11405.

Sciuto, G. and Diekkrüger, B., 2010. Influence of soil heterogeneity and spatial discretization on catchment water balance modeling. Vadose Zone Journal, 9(4): 955-969.

Silliman, S.E. and Booth, D.F., 1993. Analysis of time-series measurements of sediment temperature for identification of gaining vs. losing portions of Juday Creek, Indiana. Journal of Hydrology, 146: 131-148.

Silliman, S.E., Ramirez, J. and McCabe, R.L., 1995. Quantifying downflow through creek sediments using temperature time series: one-dimensional solution incorporating measured surface temperature. Journal of Hydrology, 167(1-4): 99-119.

Smerdon, B.D., Mendoza, C.A. and Devito, K.J., 2007. Simulations of fully coupled lake-groundwater exchange in a subhumid climate with an integrated hydrologic model. Water Resources Research, 43(1): W01416.

Sophocleous, M., 2002. Interactions between groundwater and surface water: the state of the science. Hydrogeology Journal, 10(1): 52-67.

Sophocleous, M. and Perkins, S.P., 2000. Methodology and application of combined watershed and ground-water models in Kansas. Journal of Hydrology, 236(3-4): 185-201.

Speight, J.G., 1974. A parametric approach to landform regions, In: Brown E.H. and R.S. Waters (editors), Progress in Geomorphology, Special Publication Institute British Geographers, 7, 21-230.

Speight, J.G., 1980. The role of topography in controlling throughflow generation: A discussion, Earth Surface Processes, 5, 187– 191.

Stanford, J.A. and Ward, J.V., 1993. An ecosystem perspective of alluvial rivers: connectivity and the hyporheic corridor. Journal of the North American Benthological Society, 12(1): 48-60.

Stephenson, G.R. and Freeze, R.A., 1974. Mathematical simulation of subsurface flow contributions to snowmelt runoff, Reynolds Creek Watershed, Idaho. Water Resources Research, 10(2):284-294.

Stonestrom, D.A. and Constantz, J., 2003. Heat as a tool for studying the movement of ground water near stream, U.S. Geological Circular, 1260, 1-96.284.

Storey, R.G., Howard, K.W.F. and Williams, D.D., 2003. Factors controlling riffle-scale hyporheic exchange flows and their seasonal changes in a gaining stream: A three-dimensional groundwater flow model. Water Resources Research, 39(2): 1034. doi:10.1029/2002WR001367.

Story, A., Moore, R.D. and Macdonald, J.S., 2003. Stream temperatures in two shaded reaches below cutblocks and logging roads: downstream cooling linked to subsurface hydrology. Canadian Journal of Forest Research, 33(8): 1383-1396.

Sudicky, E., Jones, J., Park, Y.-J., Brookfield, A. and Colautti, D., 2008. Simulating complex flow and transport dynamics in an integrated surface-subsurface modeling framework. Geosciences Journal, 12(2): 107-122.

Tallaksen, L.M., 1995. A review of baseflow recession analysis. Journal of Hydrology, 165(1-4): 349-370.

Tesoriero, A.J., Liebscher, H. and Cox, S.E., 2000. Mechanism and rate of denitrification in an agricultural watershed: Electron and mass balance along groundwater flow paths. Water Resources Research, 36(6): 1545-1559.

Tetzlaff, D. and Soulsby, C., 2008. Sources of baseflow in larger catchments - using tracers to develop a holistic understanding of runoff generation. Journal of Hydrology, 359(3-4): 287-302.

Tetzlaff, D., McDonnell, J.J., Uhlenbrook, S., McGuire, K.J., Bogaart, P.W., Naef, F., Baird, A.J., Dunn, S.M. and Soulsby, C., 2008. Conceptualizing catchment processes: simply too complex? Hydrological Processes, 22(11): 1727-1730.

Therrien, R., McLaren, R.G., Sudicky, E.A. and Panday, S.M., 2010. HydroGeoSphere: a three-dimensional numerical model describing fully-integrated subsurface and surface flow and solute transport. Code Documentation and Users Guide. Groundwater Simulations Group, Waterloo, Canada. 457 pp.

Tóth, J., 1963. A theoretical analysis of groundwater flow in small drainage basins. Journal of Geophysical Research, 68(16): 4795-4812.

Troxell, H.C., 1936. The diurnal fluctuations in the groundwater and flow of the Santa Ana River and its meaning, Trans. Amer. Geophys. Union, 496–504.

U.S. Geological Survey (USGS), 2010. Washington Water Science Center, streamflows for Bertrand Creek Station 12212390. Streamflow data provided electronically by the USGS.

van der Gulik, T. and Nyvall, J., 2001. Coefficients for use in irrigation scheduling. Water Conservation Factsheet No. 577.100-5. Abbotsford: Ministry of Agriculture, Food and Fisheries Resource Management Branch.

van Genuchten, M., 1980. A closed-form equation for predicting the hydraulic conductivity of unsaturated soils. Soil Science Society of America Journal, 44(5): 892–898.

VanderKwaak, J.E., 1999. Numerical simulation of flow and chemical transport in integrated surface–subsurface hydrologic systems. Ph.D. thesis, University of Waterloo, Waterloo, Ontario, Canada.

VanderKwaak, J.E. and Loague, K., 2001. Hydrologic-response simulations for the R-5 catchment with a comprehensive physics-based model. Water Resources Research, 37(4): 999-1013.

Vidon, P.G.F. and Hill, A.R., 2004. Landscape controls on the hydrology of stream riparian zones. Journal of Hydrology, 292(1-4): 210-228.

Vivoni, E.R., Ivanov, V.Y., Bras, R.L. and Entekhabi, D., 2005. The effects of triangulated terrain resolution on distributed hydrologic model response. Hydrologic Processes, 19(11): 2101-2122.

Wassenaar, L.I., 1995. Evaluation of the origin and fate of nitrate in the Abbotsford Aquifer using the isotopes of 15N and 18O in NO3-. Applied Geochemistry, 10: 391-405.

Water Survey of Canada (WSC), 2008. Archived Hydrometric Data, Bertrand Creek Station (08MH152). Website: http://www.wsc.ec.gc.ca/applications/H2O/index-eng.cfm Website accessed November 15, 2008.

Water Survey of Canada (WSC), 2009. Archived Hydrometric Data for the Bertrand Creek Station (08MH152). Streamflow data provided electronically by the Water Survey of Canada.

Webb, B.W. and Zhang, Y., 1997. Spatial and seasonal variability in the components of the river heat budget. Hydrological Processes, 11(1): 79-101.

Werner, A.D., Gallagher, M.R. and Weeks, S.W., 2006. Regional-scale, fully coupled modelling of stream-aquifer interaction in a tropical catchment. Journal of Hydrology, 328(3-4): 497-510.

Winter, T.C., 1976. Numerical simulation analysis of the interaction of lakes and ground water, U.S. Geological Survey Professional Paper 1001, 45 pp.

Winter, T.C., 1999. Relation of streams, lakes, and wetlands to groundwater flow systems. Hydrogeology Journal, 7(1): 28-45.

Winter, T.C., Harvey, J.W., Franke, O.L. and Alley, W.M., 1998. Ground water and surface water – a single resource. U.S. Geological Survey Circular 1139.

Wittenberg, H. and Sivapalan, M., 1999. Watershed groundwater balance estimation using streamflow recession analysis and baseflow separation. Journal of Hydrology, 219(1-2): 20-33.

Woessner, W.W., 2000. Stream and fluvial plain ground water interactions: rescaling hydrogeologic thought. Ground Water, 38(3): 423-429.

Wroblicky, G.J., Campana, M.E., Valett, H.M. and Dahm, C.N., 1998. Seasonal variation in surface-subsurface water exchange and lateral hyporheic area of two stream-aquifer systems. Water Resources Research, 34(3): 317-328.

Appendix A Photographs

Figure A1: Bertrand Creek headwater wetland on September 11, 2006.

Figure A2: Bertrand Creek gauge at watershed outlet.

Figure A3: Seasonal differences in flow upstream of km.6.3: low flow (October 4, 2005), dry (August 22, 2006), and overbank flow (March 24, 2007).

Figure A4: Bertrand Creek and riparian zone within the urban area (km.14.2) on July 20, 2006.

Figure A5: Bertrand Creek riparian zone downstream of Reach C (km.10.3) on May 20, 2006.

Figure A6: Spring streamflows at gauging station B4 (km.6.7) on March 14, 2007.

Figure A7: Bertrand Creek riparian zone and hummocky landscape (km.14) on May 20, 2006.

Figure A8: Looking upstream towards station B3 (from km.6.25).

Figure A9: Looking downstream at gauging station B3 weir (km.6.3), secured in place with sand bags.

Figure A10: Weir at station A4 (km.3.2) on August 1, 2007.

Figure A11: Weir at gauging station A1 (km.2.0) on August 14, 2007.

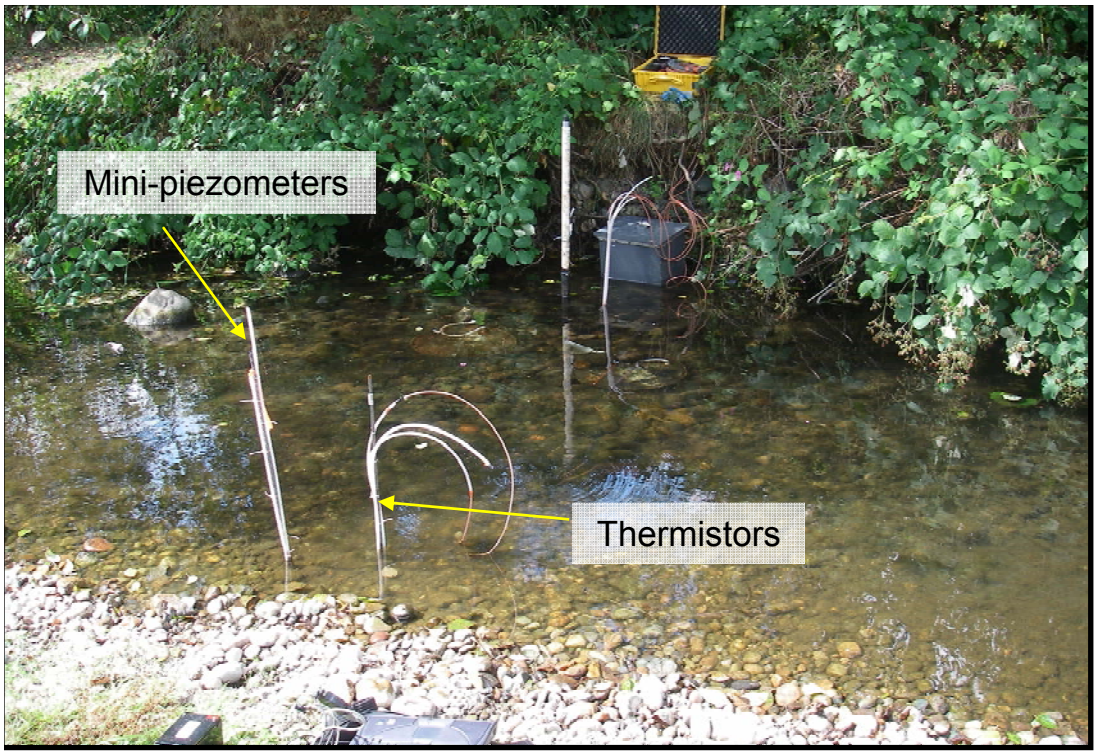

Figure A12: Thermistors [T-B2(1)] and mini-piezometers [transect MP-B2(1)] at station B2 (km.6.2) on August 21, 2007.

Figure A13: Mini-piezometer installation at MP-D2 (km.14.12) on May 10, 2007.

Figure A14: Stream gauging at station A4b (km.3.0) June 13, 2007.

Figure A15: Gauging station A3 (km.2.7) with salt dilution equipment in background on August 30, 2007.

Figure A16: Surface water pond represented in the model. Location of the pond is indicated on Figure 4.1.

Appendix B Streamflow Measurements and Rating Curves

Streamflows and stage-discharge relationships on the following pages include:

2006: Stage-discharge relationship and streamflows at station: B2
Spot streamflow measurements at stations: A1, A2, A3, A4b, B1b, B3, B4

2007: Stage-discharge relationship and streamflows at stations: A1, A4, B1, and B3
Spot streamflow measurements at stations: A2, A3, B2, B4

Theoretically, flow through a weir can be expressed as (Bos, 1989):

$$Q = c\, h^{x} \qquad [B1]$$

where:

Q = discharge (L/s);
c = constant describing the water entry coefficient, which is dependent on weir shape and units of measurement, among other factors;
h = height of water measured from the apex of the V-notch or above the crest of the rectangular weir (m); and
x = power theoretically equal to 2.5 for V-notch and 1.5 for rectangular weirs

Rectangular sharp-crested weirs were designed as 'fully-contracted' – the channel bed and sides were considered sufficiently distant enough as to not influence the flow over the crest; (Bos, 1989). V-notch weirs were designed as 'partially-contracted' due to a limited crest height above the channel (Bos, 1989). Weirs were designed so that a 5% measurement error in streamflow would be less than 0.5 L/s at flows equal to 2006 low flows.

Considering site specific conditions and weir dimensions, the theoretical stage-discharge relations describing flow over each of the installed weirs are:

Station A4: $Q=0.493\ (h+0.001)^{1.5}$ [rectangular crest; Kindsvater-Carter, 1959]
Station A1: $Q=0.558\ (h+0.001)^{1.5}$ [rectangular crest; Kindsvater-Carter, 1959]
Stations B1 and B3: $Q=1.37(h+0.001)^{2.5}$ [V-notch; ISO, 1980]

Actual rating curves at each weir were determined in the field by stream gauging. These equations deviate from the theoretical equations presented above by up to 1.4 L/s at stations A1, A4, and B3. The theoretical and calibrated stage-discharge curves are illustrated on the following figures. The stage-discharge relation describing flow at station B1 is identical to the theoretical equation presented above.

Note: The technique used to measure streamflows is abbreviated in the following pages as:

- CM: current meter (Marsh McBirney Doppler flow sensor)
- Salt: salt dilution
- Cup: streamflow collected in a vessel

References

Bos, M.G.,1989. Discharge Measurement Structures, 3rd edition, International Institute for Land Reclamation and Improvement, Publication 20, Wageningen, The Netherlands.

ISO, 1980. Water flow measurements in open channel using weirs and venturi flumes, Part 1. Thin-plate weirs. International Organization for Standardization Technical Report ISO 1438/1–1980(E).

Kindsvater, C. E. and R. W. Carter., 1959. Discharge characteristics of rectangular thin-plate weirs. Transactions, American Society of Civil Engineers. v. 24, Paper No. 3001.

Station B2 (2006): Natural Control Section

Station B2 streamflow gauging record (2006)

No.	Date	Stage (m)	Q (m^3/s)	Error (m^3/s)	Error (%)	Technique
1a.	25/05/2006	0.331	0.408	0.0220	5%	CM
1b.	25/05/2006	0.331	0.391	0.0586	15%	Salt
2	06/06/2006	0.258	0.126	0.0079	6%	CM
3	21/06/2006	0.230	0.069	0.0055	8%	CM
4a.	30/06/2006	0.189	0.011	0.0015	13%	CM
4b.	30/06/2006	0.189	0.012	0.0018	15%	Salt
5	21/07/2006	0.182	0.010	0.0007	7%	CM
6	03/08/2006	0.188	0.006	0.0005	8%	CM
7a	11/08/2006	0.182	0.008	0.0006	8%	CM
7b	11/08/2006	0.182	0.008	0.0012	15%	Salt
8	17/08/2006	0.183	0.006	0.0006	10%	CM
9	27/08/2006	0.184	0.007	0.0006	8%	CM
10	11/09/2006	0.179	0.006	0.0005	8%	CM

B2 Stage - Discharge Relationship

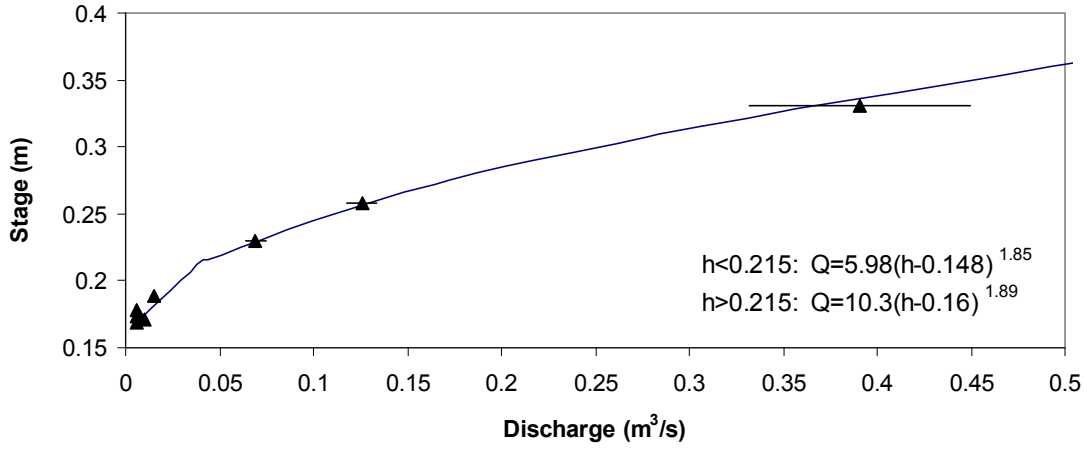

B2 Hydrograph

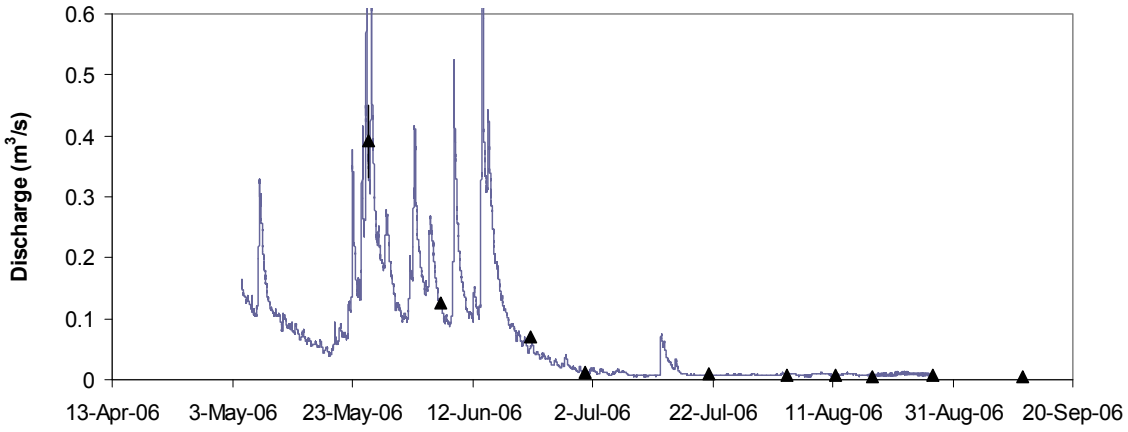

Additional streamflow measurements in 2006

	A1		A2		A3		A4b	
	Q (m^3/s)	Error (%)	Q (m^3/s)	Error (%)	Q (m^3/s)	Error (%)	Q (m^3/s)	Error (%)
07/06/2006	0.125	8%	0.128	7%	--	--	--	--
22/06/2006	--	--	--	--	0.058	5%	--	--
26/06/2006	0.047	5%	0.044	5%	0.036	5%	0.034	5%
02/07/2006	0.037	7%	0.033	6%	0.029	6%	0.024	8%
21/07/2006	--	--	0.027	8%	--	--	--	--
25/07/2006	0.024	8%	0.020	8%	0.018	5%	0.015	9%
28/07/2006	0.020	10%	0.021	8%	0.017	5%	0.015	9%
10/08/2006	0.022	8%	0.019	10%	0.014	6%	--	9%
16/08/2006	0.020	8%	0.019	9%	0.014	6%	0.012	8%
25/08/2006	0.018	8%	0.018	--	0.015	10%	0.012	7%
27/08/2006	--	--	0.018	8%	--	--	--	--
12/09/2006	0.018	7%	0.017	11%	0.016	5%	0.013	9%
13/10/2006	0.017	10%	0.018	10%	--	--	--	--

	B1b		B3		B4	
Date	Q (m^3/s)	Error (%)	Q (m^3/s)	Error (%)	Q (m^3/s)	Error (%)
25/05/2006	0.444	8%	--	--	--	--
06/06/2006	0.140	7%	0.143	6%	--	--
30/06/2006	0.015	10%	0.005	5%	0.004	10%
21/07/2006	0.011	7%	0.001	100%	dry	--
03/08/2006	0.007	7%	0.0002	100%	dry	--
11/08/2006	0.008	7%	0.0002	20%	dry	--
17/08/2006	0.009	7%	0.0001	25%	dry	--
27/08/2006	0.009	8%	4.E-06	100%	dry	--
11/09/2006	0.009	8%	dry	--	dry	--

Station A1 (2007): Rectangular sharp-crested weir

Station A1 streamflow gauging record (2007)

No.	Date	Stage (m)	Q (m^3/s)	Error (m^3/s)	Error (%)	Technique
--	02/06/2007	--	0.063	0.004	7%	CM
--	21/06/2007	--	0.055	0.004	7%	CM
--	06/07/2007	--	0.047	0.002	6%	CM
1	02/08/2007	0.163	0.040	0.001	7%	CM
2	07/08/2007	0.134	0.030	0.001	8%	CM
3	10/08/2007	0.132	0.027	0.002	8%	CM
4	14/08/2007	0.124	0.027	0.001	8%	CM
5	30/08/2007	0.115	0.025	0.001	8%	CM
6	09/09/2007	0.120	0.022	0.002	7%	CM
7	26/09/2007	0.130	0.025	0.003	12%	CM
8	14/09/2007	0.105	0.021	0.001	7%	CM

A1 Stage - Discharge Relationship

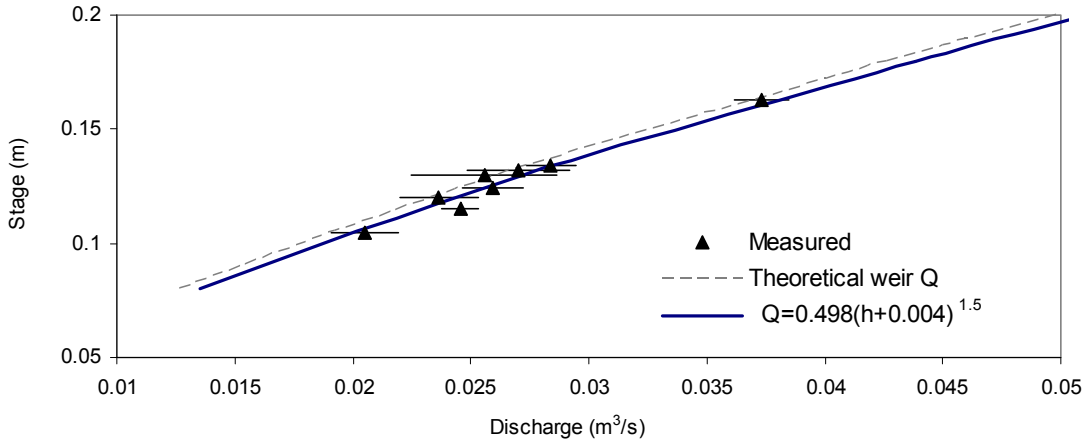

A1 Hydrograph

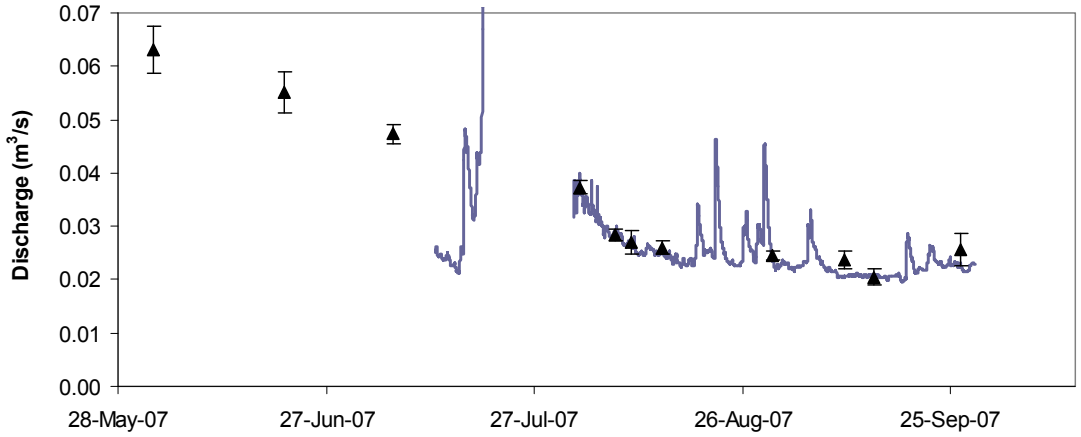

Station A4 (2007): Rectangular sharp-crested weir

Station A4 streamflow gauging record (2007)

No.	Date	Stage	Q	Error		Technique
		(m)	(m^3/s)	(m^3/s)	(%)	
--	02/06/2007	--	0.048	0.004	8%	CM
--	21/06/2007	--	0.041	0.003	8%	CM
1	02/08/2007	0.143	0.031	0.002	6%	CM
2	07/08/2007	0.126	0.021	0.001	5%	CM
3	10/08/2007	0.127	0.020	0.001	5%	CM
4	14/08/2007	0.113	0.019	0.001	6%	CM
5	21/08/2007	0.109	0.019	0.001	7%	CM
6	30/08/2007	0.102	0.016	0.001	5%	CM
7	09/09/2007	0.092	0.015	0.001	5%	CM
8	18/09/2007	0.099	0.017	0.001	5%	CM
9	26/09/2007	0.104	0.017	0.001	5%	CM

A4 Stage - Discharge Relationship

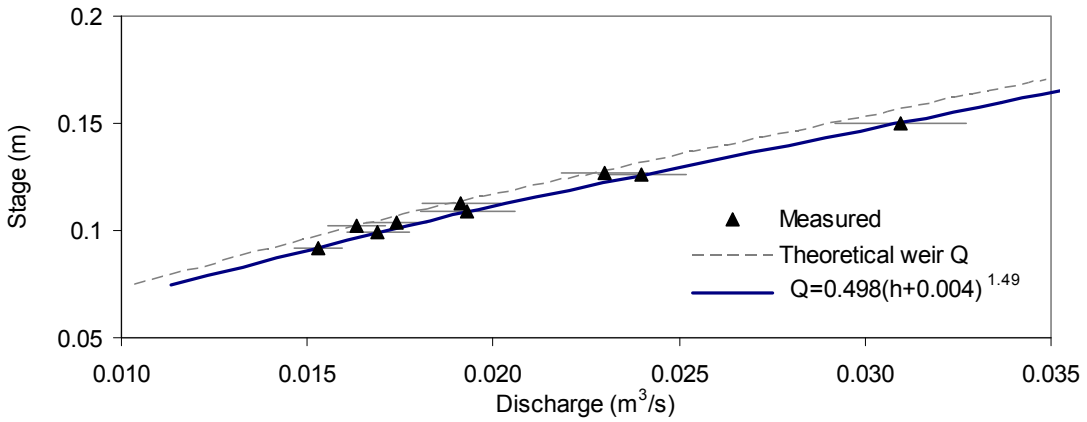

A4 Hydrograph

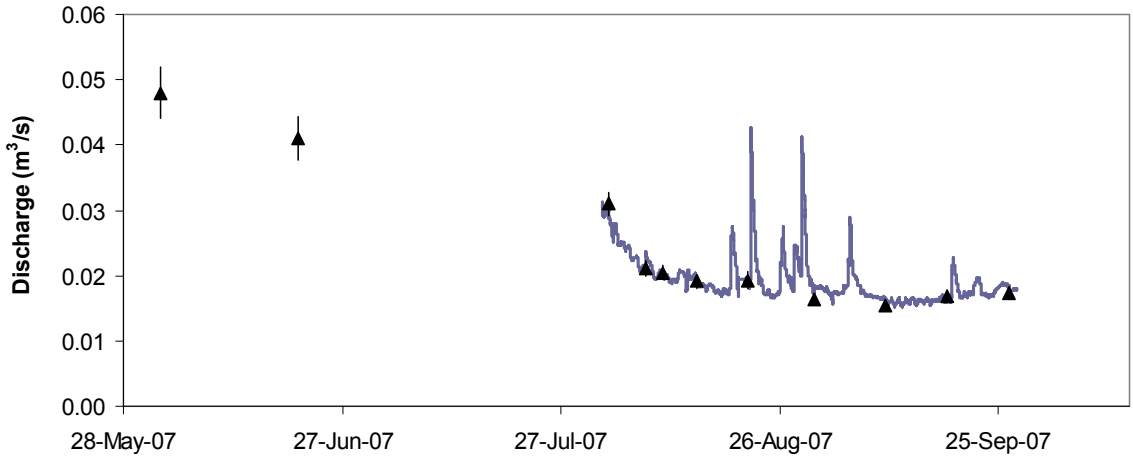

Station B1 (2007): V-notch sharp-crested weir

Station B1 streamflow gauging record (2007)

No.	Date	Stage	Q	Error		Technique
		(m)	(m^3/s)	(m^3/s)	(%)	
--	01/06/2007	--	0.038	0.0057	15%	CM
--	04/07/2007	--	0.030	0.0045	15%	CM
--	18/07/2007	--	0.026	0.0052	20%	CM
1	28/07/2007	0.23	0.032	0.0053	17%	CM
2	02/08/2007	0.17	0.020	0.0025	17%	CM
3	06/08/2007	0.15	0.013	0.0021	16%	Salt
4	10/08/2007	0.13	0.010	0.0016	18%	Salt
5	13/08/2007	0.15	0.012	0.0008	7%	CM
6	17/08/2007	0.14	0.010	0.0007	7%	CM
7	28/08/2007	0.15	0.012	0.0010	7%	CM
8	31/08/2007	0.14	0.010	0.0008	8%	CM
9	05/09/2007	0.14	0.010	0.0006	6%	CM
10	19/09/2007	0.13	0.009	0.0006	7%	CM
11	29/09/2007	0.13	0.009	0.0006	7%	CM

B1 Stage - Discharge Relationship

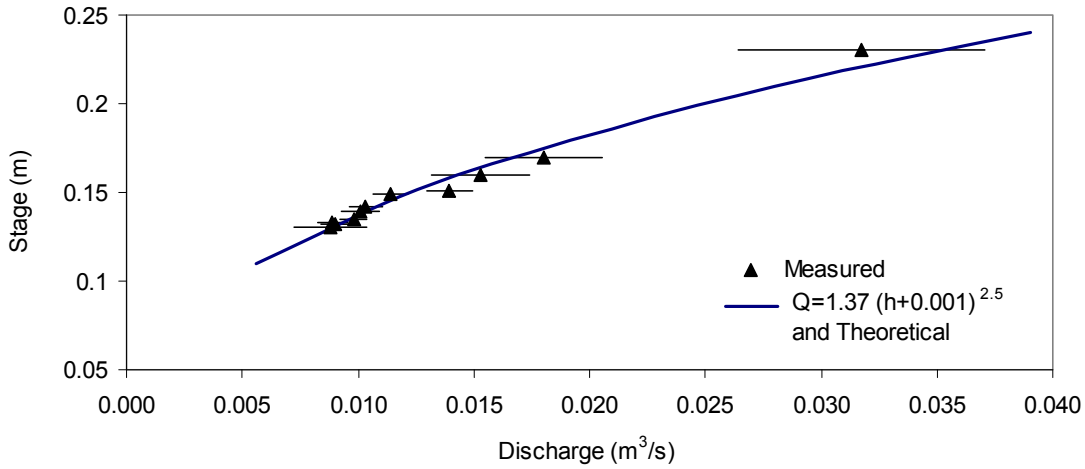

B1 Hydrograph

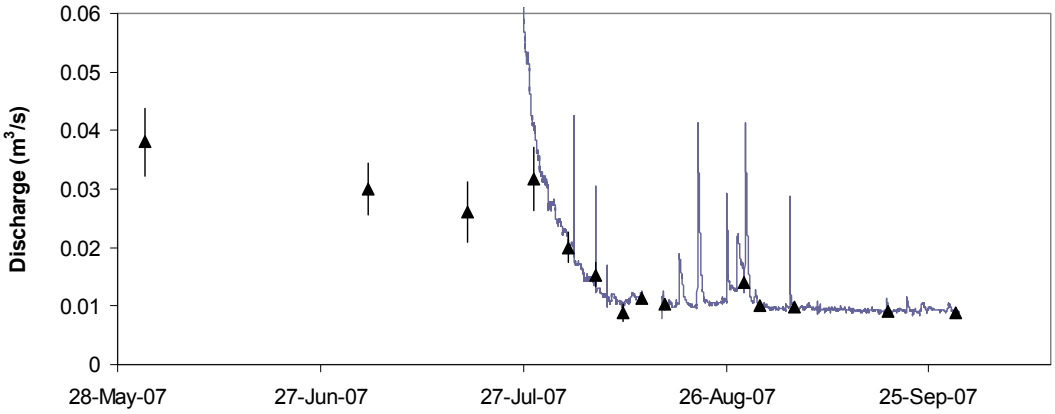

Station B3 (2007): V-notch sharp-crested weir

Station B3 streamflow gauging record (2007)

No.	Date	Stage (m)	Q (m^3/s)	Error (m^3/s)	Error (%)	Technique
--	01/06/2007	--	0.025	0.002	7%	CM
--	04/07/2007	--	0.018	0.002	10%	CM
--	16/07/2007	--	0.028	0.003	11%	CM
--	28/07/2007	--	0.022	0.003	13%	CM
--	30/07/2007	--	0.012	0.002	17%	CM
1	03/08/2007	0.111	0.008	0.0008	10%	CM
2	06/08/2007	0.085	0.003	0.0004	11%	CM
3	13/08/2007	0.070	0.003	0.0003	10%	CM
4	17/08/2007	0.037	0.0005	0.0001	25%	Cup
5	31/08/2007	0.030	0.0006	0.0001	33%	Cup
6	05/09/2007	0.037	0.0005	0.0001	25%	Cup
7	09/09/2007	0.025	0.0002	0.0001	33%	Cup
8	17/09/2007	0.023	0.0002	0.0001	33%	Cup
9	23/09/2007	0.023	0.0002	0.0001	33%	Cup

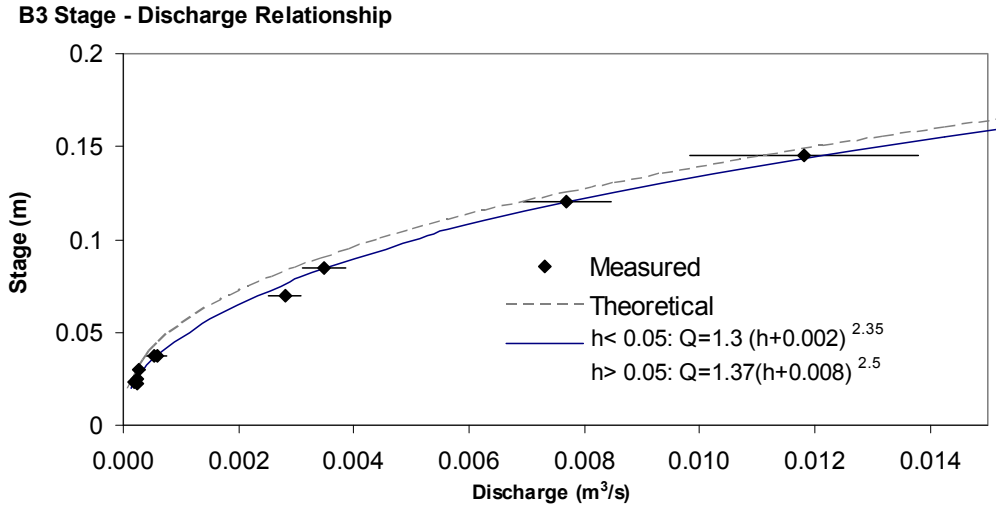

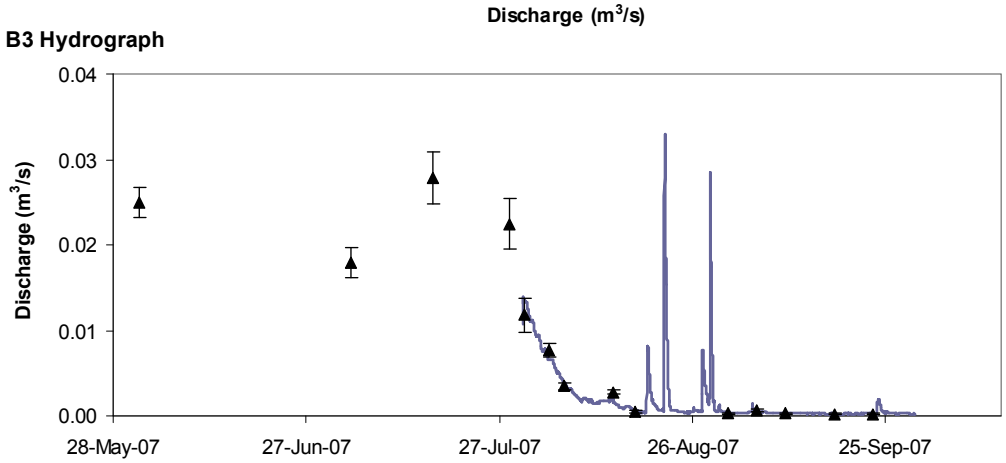

Additional streamflow measurements in 2007

Station A2 streamflow gauging record (2007)

No.	Date	Q (m^3/s)	Error (%)	Technique
1	02/06/2007	0.058	9%	CM
2	21/06/2007	0.052	8%	CM
3	06/07/2007	0.044	5%	CM
4	02/08/2007	0.035	8%	CM
5	07/08/2007	0.025	8%	CM
6	10/08/2007	0.025	8%	CM
7	14/08/2007	0.023	8%	CM
8a	30/08/2007	0.022	8%	CM
8b	30/08/2007	0.025	20%	Salt
9	09/09/2007	0.018	9%	CM

Station A3 streamflow gauging record (2007)

No.	Date	Q (m^3/s)	Error (%)	Technique
1	02/06/2007	0.054	9%	CM
2	21/06/2007	0.047	8%	CM
3	06/07/2007	0.044	7%	CM
4	02/08/2007	0.036	7%	CM
5	07/08/2007	0.028	7%	CM
6	10/08/2007	0.024	6%	CM
7	14/08/2007	0.026	7%	CM
8a	30/08/2007	0.024	6%	CM
8b	30/08/2007	0.023	10%	Salt
9	09/09/2007	0.017	9%	CM

Station B2 streamflow gauging record (2007)

No.	Date	Q (m^3/s)	Error (%)	Technique
1	01/06/2007	0.033	9%	CM
2	04/07/2007	0.027	8%	CM
3	16/07/2007	0.036	7%	CM
4	03/08/2007	0.018	10%	Salt
5	06/08/2007	0.013	10%	Salt
6a	13/08/2007	0.013	10%	Salt
6b	13/08/2007	0.012	10%	CM
7	17/08/2007	0.008	11%	CM
8	31/08/2007	0.008	10%	CM
9	05/09/2007	0.007	11%	CM

Station B4 streamflow gauging record (2007)

No.	Date	Q (m^3/s)	Error (%)	Technique
1	01/06/2007	0.024	9%	CM
2	04/07/2007	0.021	9%	CM
3	16/07/2007	0.034	8%	CM
4	03/08/2007	0.008	8%	CM
5	06/08/2007	0.005	8%	CM
6	08/08/2007	0.008	8%	CM
7a	13/08/2007	0.005	8%	CM
7b	13/08/2007	0.004	12%	Salt
8	17/08/2007	0.0003	14%	CM
9	31/08/2007	<[a]	--	--
10	05/09/2007	<	--	--

[a] surface water height too low to measure streamflow

Appendix C Sensitivity Testing of Odyssey Capacitance Water Level Probes

1. Background

Odyssey capacitance water level probes employ a capacitance method to calculate the height of water in contact with the probe (Dataflow Systems Pty Limited, 2010). Capacitance is the measure of electric field that develops between two conductors separated by a dielectric (non-conducting) material. The Odyssey employs a Teflon strip as the dielectric medium. The Teflon strip surrounds a sensor element, which serves as one conductor, and water serves as the second conductor. The height of water contacting the probe is directly proportional to the variation in capacitance and is recorded by the Odyssey data logger as a raw value in millivolts (mV). Each probe was individually calibrated to correlate the raw reading with height of water contacting the probe. Probes tested in this study were 1.0 m long.

Teflon has a coefficient of linear thermal expansion which behaves in a non-ideal manner between 10 to 30°C (Kirby, 1956). At 19°C there is a conversion in the crystalline grid of the Teflon molecules which causes a fourfold increase in the coefficient of thermal expansion (Kirby, 1956). The coefficient decreases in value by 30°C, returning to a value similar to that before the spike. Considering this behavior, a change in temperature between 10 to 30°C will influence the thickness and density of the Teflon in the Odyssey probe, which will in turn affect the measured capacitance.

2. Objective

Test the sensitivity of the Odyssey capacitance logger to the following variables:

(1) electrical conductivity (EC, at 25°C) of water,
(2) water temperature, and
(3) air temperature.

3. Methods

Sensitivity tests were conducted by immersing the Odyssey water level probe into a plastic column containing tap water (Figure C1). The Odyssey instrument was secured in a manner so that the Teflon strip was free hanging and did not contact the sides of the plastic column. Each logger was calibrated prior to the sensitivity tests to correlate the raw reading (mV) into

a length measurement (mm). On average, a reading of two millivolts was equivalent to approximately 1 mm water height.

Details of each of the three sensitivity tests conducted in this study include:

(1) Electrical conductivity of water: EC was varied by adding table salt. Prior to each reading, the water column was stirred and EC values were allowed to equilibrate through the water column.

(2) Water temperature: Cool water was placed into the plastic column and measurements were taken while the water warmed to room temperature.

(3) Air temperature: A plastic covering was placed over the plastic column and Odyssey instrument, and the surrounding air was heated using an air heater.

To test the sensitivity to the submerged length of the capacitance probe, tests were conducted at a shallow submerged length (20 or 30 cm) and a deep submerged length (~85 cm). Three to four tests were conducted for each variable.

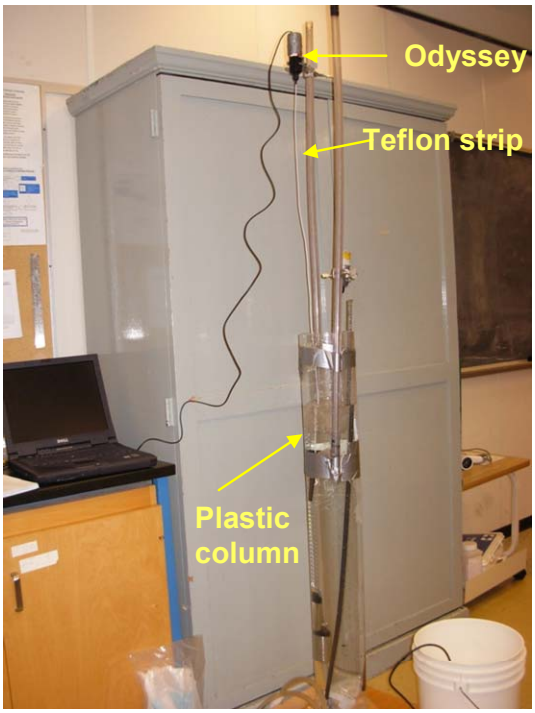

Figure C1. Laboratory testing of Odyssey capacitance water level probe.

Prior to obtaining a measurement, the Teflon strip was tapped several times to release bubbles from the sides of the strip. Bubbles attached to the Teflon strip decreased the raw reading by up to 30 mV (approximately equivalent to 15 mm). In addition to bubbles, the Odyssey demonstrated sensitivity to the strip coming in contract with another object (i.e, the column walls), or proximity to metal objects. Measurements are considered accurate to +/- 3 mV.

4. Results

Results of each test are provided on the following pages. Results of the tests indicate that Odyssey water level probes are sensitive to values of water EC, air temperature, and water temperature. Results are summarized below.

(1) EC: The data logger readings are positively correlated to EC. Below 150 µS/cm, the logger reading displays a non-linear relationship to EC, which is dependent on submerged length. Above 150 µS/cm, a slight linear relationship is apparent (i.e., a change in EC over 30 µS/cm is required for the probe to register a difference of 1 mm).

(2) Water temperature: The logger is sensitive to water temperature and displays a positive linear relationship to water temperature within the range of water temperatures tested (6 to 20°C). The reading is sensitive to the submerged length. An average of 1.7 mm is induced in the Odyssey reading by a 1°C change in temperature per metre of submerged probe length.

(3) Air temperature: The logger reading displays a negative correlation to air temperature within the range of air temperatures tested (20 to 42°C).

5. Discussion and Implication

The results show that the Odyssey data logger is sensitive to electrical conductivity and temperature, and the sensitivity is dependent on the length of probe in contact with water. It is hypothesized that the negative relationship observed between Odyssey readings and air temperature develops owing to the negative slope of the coefficient of thermal expansion between 20 and 30°C, and is not indicative of a different relationship between air and water temperatures.

Larson and Runyan (2009) tested the sensitivity of the Odyssey instrument to water temperature and electrical conductivity. Their results are similar to those presented in this study and demonstrate that Odyssey raw values: (1) have a positive, non-linear relationship to EC at values below 2,000 μS/cm; (2) have a positive relationship with water temperature from 5 to 13°C; and (3) have a negative relationship to water temperature from 13 to 20°C.

Considering the varying amounts of riparian shelter surrounding the gauging stations, differences in microclimate are expected to locally influence the air temperature, water temperature, and humidity within the PVC stilling wells at each station. As a result, location specific corrections to each Odyssey time series record are likely necessary. Water temperature measurements were available at each Odyssey measurement location, but air temperature measurements were unavailable. Stream water EC values were above the range of values (>150 μS/cm) that demonstrated sensitivity on the instrument reading, and influences on the Odyssey reading due to changes in EC can be disregarded. Attempts to compensate the Odyssey time series record presented in Chapter 3 for variations in water and air temperature were unsuccessful.

The results of this study demonstrate that the Odyssey is sensitive to temperature and electrical conductivity. The nature of this relationship varies as EC and temperature change. Furthermore, the relationship is dependent on the length of the probe in contact with water.

References

Dataflow Systems Pty Limited. 2010. Odyssey Water Level Capacitive Probe Handbook. Christchurch, New Zealand. Handbook received by email on June 9, 2010, 9 pp.

Kirby, R.K., 1956. Thermal Expansion of Polytetrafluoroethylene (Teflon) From -190° to +300°C. Journal of Research of the National Bureau of Standards, 57(2): 91-94.

Larson, P. and Runyan, C., 2009. Evaluation of a Capacitance Water Level Recorder and Calibration Methods in an Urban Environment. CUERE Technical Memo 2009/003. University of Maryland Baltimore County, Center for Urban Environmental Research and Education, Baltimore, MD, 29 pp.

Odyssey Sensitivity to Electrical Conductivity in Water

Test No.	Length Submerged	RAW Reading (mv)	Calibrated Depth (mm)	Tw (C)	Tair (C)	EC (µS/cm)	ΔEC/mm error <150 µS/cm	ΔEC/mm error >150 µS/cm
Test 1	20 cm	1462	342	20.3	18	18.9	29	--
		1469	346	19.9	19	70		
		1471.5	347	19.9	19.3	153		
		1472	347	19.9	19.5	244		
Test 2	30 cm	1662	441	19.9	20	68.3	128	--
		1664.5	442	20.1	20.3	156.2		
		1664.5	442	20.1	20	196.4		
		1664	442	20.1	20.1	241		
		1664	442	20.1	20.1	420		
Test 3	85.6 cm	2705	957	19.9	19.6	20.4	3	61
		2771	990	19.9	19.6	66.5		
		2787.5	998	19.9	19.6	128.8		
		2791	1000	19.9	19.6	171.7		
		2790	999	19.4	19.6	203		
		2795	1002	19.4	19.6	270		
		2796	1002	19.4	19.6	323		
Test 4	86.3 cm	2687	956	20.3	18	18.9	3	31
		2756	991	20.3	18	70.4		
		2778	1002	20.3	18	149.1		
		2784.5	1005	20.3	18	243.5		
		2784	1005	20.3	18	243.5		

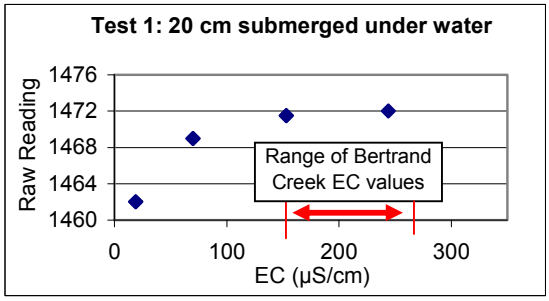

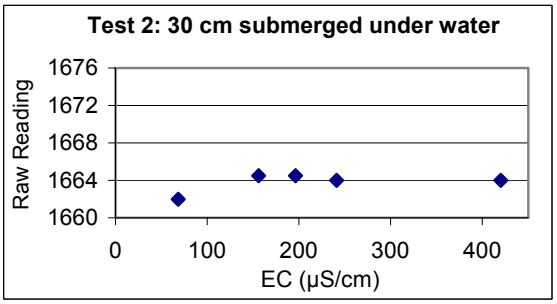

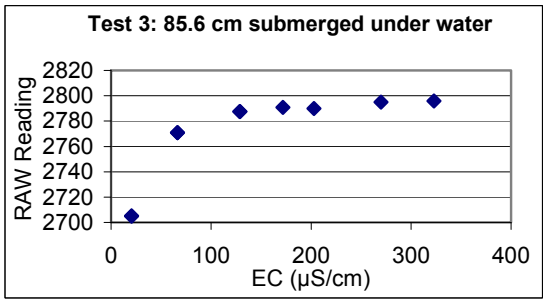

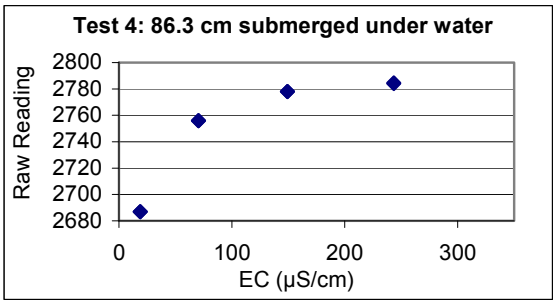

Odyssey Sensitivity to Water Temperature

Test No.	Length Submerged	RAW Reading (mv)	Calibrated Depth (mm)	Tw (°C)	Tair (°C)	EC (µS/cm)		Slope (/°C)	Slope/ m submerged (/°C/m)	ΔT / 1 mm error (°C)
Test 1	0.20	1458	340	6	21	29.1	RAW:	0.7	3.6	
		1460	341	8.8	21	29.1	mm:	0.4	1.8	3
Test 2	0.30	1652.5	436	14	20.2	35.6	RAW:	0.8	2.7	
		1656	438	14.7	19.7	35.6	mm:	0.5	1.8	1.9
		1656	438	15.2	19.7	35.6				
		1657	439	16	19.7	35.6				
		1657	439	16.5	19.7	35.6				
		1657	439	16.7	19.3	35.6				
		1657	439	17.6	20.6	35.6				
		1659	440	20.1	19.9	35.6				
Test 3	0.863	2657.5	942	10.85	20.9	17.9	RAW:	3.1	3.6	
		2687	956	20.3	18	18.9	mm:	1.6	1.8	0.6
Test 4	0.856	2689	949	11.4	19.6	19.6	RAW:	2.7	3.2	
		2689	949	13.15	19.6	19.6	mm:	1.3	1.6	0.7
		2696	953	16.05	19.6	19.6				
		2705	957	18.25	21.1	19.6				
		2706.5	958	19.9	20.2	19.6				
		2711.5	960	19.9	19.6	20.4				
		2711	960	19.5	19.1	20.4				
							Average mm/°C /m submerged		**1.7**	
							Average RAW/°C /m submerged		**3.3**	

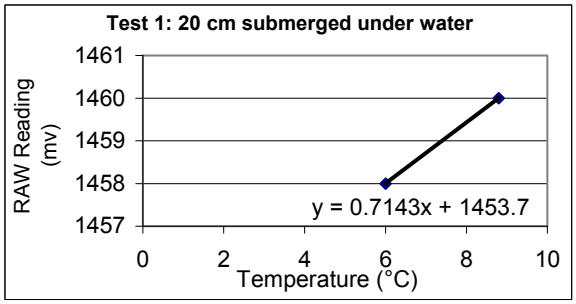

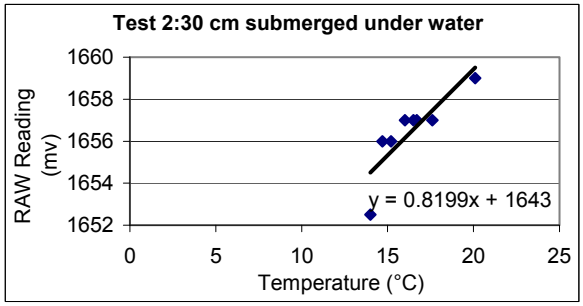

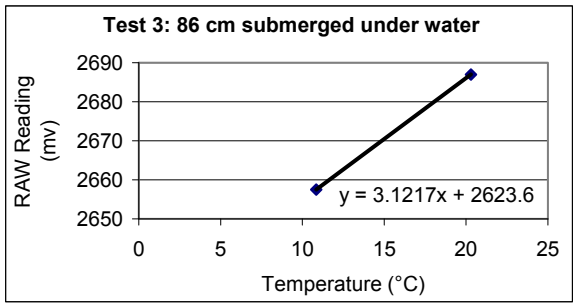

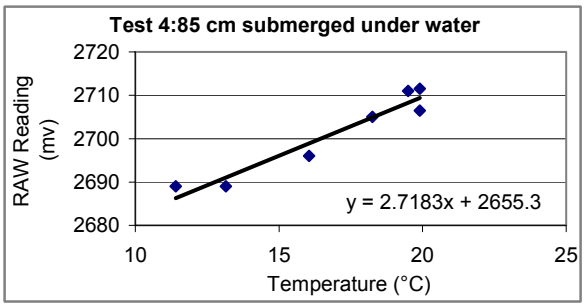

Odyssey Sensitivity to Air Temperature

Test No.	Length Submerged	RAW Reading (mv)	Calibrated Depth (mm)	Tw (°C)	Tair (°C)	EC (µS/cm)		Slope (/°C)	Slope/m exposed (/°C/m)	ΔT / 1 mm error (°C)
Test 1	0.2	1458	340.1	6	21	29.1	RAW:	-0.21	-0.2	
		1456	339.1	7.7	33	29.1	mm:	-0.11	-0.1	9
		1454	338.1	--	37.5	29.1				
		1455	338.6	--	35	29.1				
		1460	341.1	8.5	21	29.1				
Test 2	0.863	2634.5	922.1	6	21	29.1	RAW:	-0.23	-0.7	
		2638	923.8	6	35	29.1	mm:	-0.14	-0.4	7
		2634	921.9	6	42	29.1				
		2631	920.4	7.7	21	29.1				
Test 3	0.856	2711.5	960.2	19.9	19.6	20.4	RAW:	-0.29	-0.8	
		2710	959.5	--	25	20.4	mm:	-0.14	-0.4	7
		2709.5	959.2	--	28	20.4				
		2708.5	958.7	--	29.5	20.4				
		2707.5	958.2	--	33.5	20.4				
		2706	957.5	20.3	34	20.4				
		2705	957.0	20.3	34	20.4				

Average mm / °C **-0.13**
RAW / °C **-0.24**
(does not appear sensitive to length)

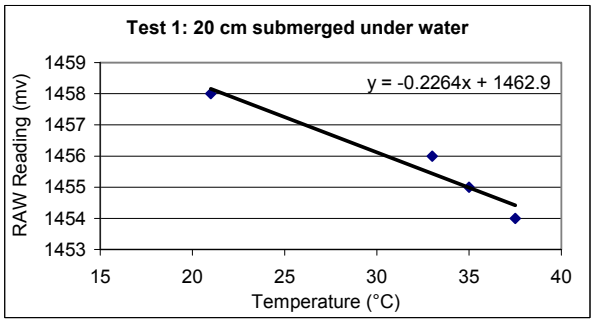

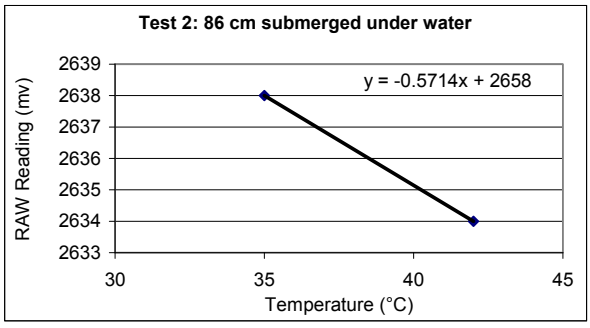

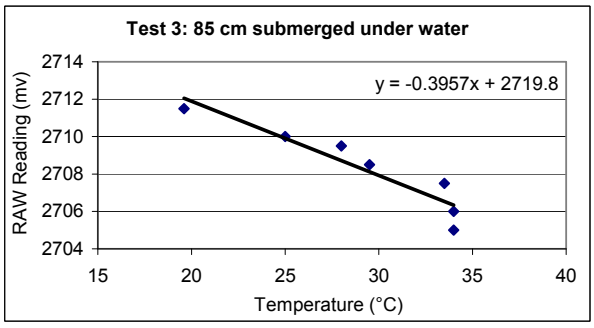

Appendix D Stream Water Chemistry

Surface water chemistry along Bertrand Creek at select locations on August 15, 2007

Upstream Distance	Station/ MP site	HCO_3^- mg/L	Cl^- mg/L	NO_3-N mg/L	SO_4^{2-} mg/L	PO_4^{2-} mg/L	Na^+ mg/L	Ca^{2+} mg/L	Mg^{2+} mg/L	K^+ mg/L	Si mg/L
16.8	MP-D(4)	172	78	0.3	6	0.3	62	22	10.4	8.8	4.3
14.3	MP-D(3)	128	35	0.4	14	0.0	21	26	10.9	8.1	5.3
12.4	MP-D(1)	108	17	4.2	25	0.0	11	29	11.0	8.2	6.2
8.1	--	87	17	0.7	33	0.0	11	26	9.8	9.4	2.8
6.3	B3	58	16	0.4	16	0.4	9	14	5.0	7.1	3.3
6.2	MP-B2(2)	64	15	1.2	15	0.0	11	13	6.2	5.6	7.6
6.1	B2	92	16	4.0	27	0.0	22	16	7.7	8.4	8.4
5.6	B1	90	19	1.8	20	0.0	20	16	8.2	8.4	7.0
3.4	--	76	22	0.8	17	0.0	17	17	6.5	6.8	4.0
3.1	A4	70	21	0.8	15	0.0	14	15	5.5	6.3	3.7
2.4	A2	62	20	0.9	14	0.0	12	15	5.2	5.9	3.8
0	Outlet	42	21	3.7	16	0.0	11	15	5.0	6.5	3.0

Appendix E Equations Governing Flow of Water in HydroGeoSphere

Governing Equations

The equations governing flow of water through the subsurface and surface domains in HydroGeoSphere are discussed below, adopted from Therrien et al. (2010). Each governing equation consists of a term to represent the change in flux (q), the exchange between domains (Γ), and sources or sinks to the domain (Q), which are set equal to a change in water stored in the domain during the time step. The flux term for each governing equation is defined using a conductance term (K), a term to account for reductions to the value of the conductance term (k), and a hydraulic gradient to drive the flow.

Subsurface Flow

Three-dimensional transient flow in a variably-saturated porous medium is described by a modified form of Richards equation:

$$-\nabla\cdot(q)+\Gamma_x \pm Q=\phi\frac{\partial S_w}{\partial t}+S_w S_S\frac{\partial \psi}{\partial t} \qquad \text{[E1]}$$

Where $\nabla = (\partial/\partial x, \partial/\partial y, \partial/\partial z)$; Γ_x [L/L/T^{-1}] is the volumetric fluid exchange rate between the subsurface and surface domain; Q [T^{-1}] represents sources and/or sinks to the subsurface domain; ϕ [–] is the porosity of the porous medium; S_w [–] is the water saturation and is determined by the moisture retention curve as a function of pressure head, ψ [L]; S_s [L^{-1}] is the specific storage of the porous medium; and q [LT^{-1}] is the Darcy flux defined as:

$$q=-K\cdot k_r\nabla(\psi+z) \qquad \text{[E2]}$$

where K [L/T] is the hydraulic conductivity tensor; k_r [–] is the relative permeability of water defined as a function of the pressure head; and z [L] is the elevation.

Permeability-saturation relationships are based on the van Genuchten (1980) model:

$$S_w = S_{wr}+(1-S_{wr})[1+|\alpha\psi|^{\beta}]^{-\nu} \qquad \text{for } \psi < 0$$

$$S_w = 1 \qquad \text{for } \psi \geq 0 \qquad \text{[E3]}$$

with relative permeability given by:

$$k_r = S_e^{(1/2)}[1-(1-S_e^{1/\nu})^{\nu}]^2 \qquad \text{[E4]}$$

where $\left(v = 1 - \frac{1}{\beta}\right)$, for $\beta > 1$

and β [–] and α [L^{-1}] are empirical fitting parameters; S_{wr} [–] is the residual water saturation; and S_e is the effective water saturation defined as $S_e=(S_w - S_{wr})/(1 - S_{wr})$.

The calculation of subsurface flow using Equation E1 assumes that the fluid is incompressible, the porous medium is non-deformable, the system is under isothermal conditions, and the air phase is infinitely mobile.

Surface flow

Surface water flow is represented by the two-dimensional depth averaged diffusion-wave approximation to the Saint Venant equation derived by Gottardi and Venutelli (1993):

$$-\nabla \cdot (d_s q_s) - d_s \Gamma_s \pm Q_s = \frac{\partial \phi_s h_s}{\partial t} \qquad \text{[E5]}$$

Where d_s [L] is the depth of flow; Γ_s [$L/L/T^{-1}$] is the volumetric fluid exchange rate between the surface and subsurface domain, where $\Gamma_s = -\Gamma_x$; Q_s [T^{-1}] is a source/sink term; ϕ [–] is a surface domain 'porosity' that varies between zero at land surface and one at that top of rills and obstructions; h_s [L] is the water surface elevation where $h_s = (z_s+d_s)$ and z_s [L] is the streambed elevation; and q_s is the flux of water [LT^{-1}] defined as:

$$q_s = -K_s \cdot k_{rs} \nabla (d_s + z_s) \qquad \text{[E6]}$$

where k_{rs} [–] is a factor that accounts for a reduction in conductance due to obstruction storage; and K_s [LT^{-1}] is a surface conductance term that results from manipulation of the Saint Venant equations and is given for the Manning equation (Gottardi and Venutelli, 1993) as:

$$K_{si} = \frac{d_s^{2/3}}{n_i} \frac{1}{[\partial h_s / \partial s]^{1/2}} \qquad i = x, y \qquad \text{[E7]}$$

where n_i is Manning's coefficient [$TL^{-1/3}$]; and 's' is the direction of maximum slope.

The calculation of surface flow using Equation E5 assumes a hydrostatic pressure distribution, depth-averaged flow velocities, mild slope, dominant bottom shear stresses, and that frictional resistance forces can be represented by Manning's formula.

References

Gottardi, G. and Venutelli, M.A., 1993. A control-volume finite-element model for two-dimensional overland flow. Advances in Water Resources, 16(5): 277-284.

Therrien, R., McLaren, R.G., Sudicky, E.A. and Panday, S.M., 2010. HydroGeoSphere: a three-dimensional numerical model describing fully-integrated subsurface and surface flow and solute transport. Code Documentation and Users Guide. Groundwater Simulations Group, Waterloo, Canada. 457 pp.

van Genuchten, M., 1980. A closed-form equation for predicting the hydraulic conductivity of unsaturated soils. Soil Science Society of America Journal, 44(5): 892–898.